THE FLORIDA STATE UNIVERSITY

COLLEGE OF ARTS AND SCIENCES

A NUMERICAL MODEL OF COASTAL

UPWELLING OFF PERU - INCLUDING

MIXED LAYER DYNAMICS

by

GEORGE WASHINGTON HEBURN

A Dissertation submitted to the
Department of Meteorology
in partial fulfillment of the
requirements for the degree of
Doctor of Philosophy

Approved:

_____
Professor Directing Dissertation

_____

_____

_____

_____

March, 1981

ABSTRACT

Two versions of a three-dimensional, two-layer, numerical model with realistic coastline and bottom topography on a β-plane are used to study the upwelling system off the Peruvian coast. A hydrodynamic version of the model with two homogeneous layers is used to examine the interaction between the bottom topography and coastal trapped waves.

The fluctuations in the undercurrent off the Peruvian coast have been shown (Smith, 1978) to be uncorrelated with the local winds. The hypothesis proposed by Smith is that these fluctuations are the result of coastal trapped Kelvin waves. A parametrization scheme, based on Kelvin wave dynamics, is introduced to simulate these coastal trapped waves. The relationship between bottom topographic features and the pycnocline height anomalies for a longshore current event is then examined. The principle of conservation of potential vorticity is used to explain the interactions between the waves and the bottom topography. The results of the hydrodynamic model show that the interaction between a propagating wave and the bottom topography can play a significant role in determining the location of the centers of enhanced upwelling.

A thermodynamic version of the model, one in which the layer-averaged densities are predicted variables, is used to extend the information available from the hydrodynamic models. A parameterization scheme for the interfacial mixing is introduced. There is a information available from the hydrodynamic models. A parameterization scheme for the interfacial mixing is introduced. There is a twofold reason for introducing thermodynamics and mixing into the model.

The first is to include physics normally neglected in upwelling models. The second is to provide a physical mechanism to keep the interface from surfacing. The locations of the centers of enhanced upwelling as indicated by the interface displacement and sea surface temperature are examined and compared to observed data. The results of the thermodynamic model show that a positive heat flux is required to balance the large-scale wind-induced upwelling in order to observe the centers of enhanced upwelling due to the interaction between the internal waves and the bottom topography.

The local wind forcing for both versions of the model are derived from meteorological buoy wind observations. The time series of wind observations from Pacific Marine Environmental Laboratory's (PMEL) PSS mooring during March, April, May (MAM) 1977 are used to construct the time-dependent amplitudes for the wind function.

ACKNOWLEDGEMENTS

TABLE OF CONTENTS

LIST OF FIGURES

CHAPTER 1

1. INTRODUCTION

The purpose of this study is to examine the Peruvian upwelling system by means of a numerical model.

The phenomenon of coastal upwelling has been the object of an intensive, multinational, interdisciplinary study over the past decade. This study was undertaken as part of the National Science Foundation funded International Decade of Ocean Exploration (IDOE).

The economic impetus for this effort becomes apparent when we considers the ever increasing world population, the ever decreasing world food supply, and the fact that the upwelling zones, while comprising less than 1% of the world's oceans, account for over half of the world's commercial fish catch (Ryther, 1969). While these narrow bands of upwelled cold water have a disproportionately high biological productivity in relationship to the area covered, there is always the danger of catastrophic failure of these fisheries, such as the Los Niños which periodically appear off the coast of Peru. It is obvious that to manage effectively the fisheries and preserve these regions as food sources, a detailed knowledge of the ecosystem (its biological, chemical and physical stresses) is absolutely necessary.

The Coastal Upwelling Ecosystems Analysis (CUEA) program, composed of meteorologists and (biological, chemical and physical) ocean-ographers from various universities and laboratories from around the posed of meteorologists and (biological, chemical and physical) ocean-ographers from various universities and laboratories from around the world, was chartered under IDOE to obtain the required knowledge, via

field observations, data analysis, and theoretical (both analytical and numerical) studies. One of the mandates of the CUEA program was to emphasize the importance of the interdisciplinary nature of the study, in particular to examine the interactions of the biology, chemistry and physics of the ecosystem. As Dr. Richard Barber, a marine biologist from Duke University, stated in a Research News article by Hartline (1980) - "A (marine) biologist ... with no understanding of the meteorology or currents is just whistling in the dark." One notable recent contribution in this area of interdisciplinary study is Brink et al. (1980) where the biological, chemical, and physical data were synthesized to examine the physical and biological structure and variability of an upwelling center off the coast of Peru in March 1977.

Before discussing the details of the CUEA contribution and our function within CUEA, we will define what is meant by coastal upwelling and present a brief review of the earlier work on the subject. As a working definition of upwelling, we will use the one given by Smith (1968) where upwelling is defined as "ascending motion of some minimum duration and extent by which water from subsurface layers is brought into the surface layer and is removed from the area of upwelling by horizontal flow." Upwelling results from horizontal divergence in the surface layer and usually the upwelled water comes from depths not exceeding a few hundred meters. The coastal upwelling regions have been found to be regions of high biological productivity. In these regions, cold nutrient rich water from the lower layers is brought into the sun-

cold nutrient rich water from the lower layers is brought into the sunlit euphotic zone where plant life flourishes thus providing the first

link in the food chain that ultimately leads to large commercially acceptable fish. Futhermore, the cold sea surface temperatures associated with upwelling have a profound effect on the climate of the adjacent coastal regions. Atmospheric convection and evaporation are usually surpressed in these regions due to the low sea surface temperature thus leading to a semi-arid type climate.

The basis for the study of upwelling lies in the pioneering work by Ekman (1905) when he explained, by means of a balance between vertical friction and earth rotation, the reason for the mass transport in the upper ocean being directed to the right/left of the local winds in the northern/southern hemisphere. Thorade (1909) was the first to apply this reasoning to the upwelling problem, when he showed that winds blowing equatorward parallel to the California coast would cause an off shore transport in the surface layer and thus result in upwelling near the coast.

Over the next six decades, the upwelling problem received relatively little attention. A few of the notable contributions during this period include Sverdrup (1938) and Sverdrup and Fleming (1941). Using data gathered off Southern California, they quantitatively applied Ekman's theory of upwelling to arrive at a dynamical interpretation of coastal upwelling. Hidaka (1954) presented a steady-state theory of upwelling in a homogeneous ocean and Saito (1956) extended this work by considering the transient state which develops in an ocean initially at rest due to impulsively applied winds. Yoshida (1955 a,b) introduced first-order stratification into the upwelling problem when he consid-at rest due to impulsively applied winds. Yoshida (1955 a,b) introduced first-order stratification into the upwelling problem when he considered an ocean model with two homogeneous layers which have a density

difference between the layers of $\Delta\rho$. Yoshida also considered the
effects of time dependent winds.

In a comprehensive theoretical study of upwelling, Yoshida (1967)
used a two-layer quasi-steady model to examine the effects of internal
friction, the effect of the continental shelf, and time variable up-
welling. Smith (1968) presents an in-depth review of these earlier
studies.

During the past decade, considerable research has been dedicated
to the upwelling problem, primarily through the efforts of the CUEA
program. Due to the large volume of work in the various fields in
recent years, we will restrict further discussion primarily to the
physical aspects of the upwelling problem. A number of field experi-
ments have been conducted as part of the CUEA project. In particular,
physical experiments have been conducted off the coasts of Oregon,
Northwest Africa and Peru. The interpretation of the data collected
during these experiments emphasize the fact that the upwelling prob-
lem is highly complex and that factors other than the local winds,
such as bottom topography and internal waves, can have a pronounced
influence on the upwelling circulation.

Energetic low-frequency current fluctuations in the longshore
component of velocity, with periods on the order of several days, are
observed in each of these upwelling regions (Smith, 1974; Mittelstaedt
et al., 1975; Brink et al., 1978). The fluctuations off Oregon and
Northwest Africa show significant correlation with the local winds at
a lag of less than one day (Huyer et al., 1978; Badan-Dangon, 1978).
Northwest Africa show significant correlation with the local winds at
a lag of less than one day (Huyer et al., 1978; Badan-Dangon, 1978).
Off Peru, however, the longshore currents at depth are not significantly

correlated with the local winds (Brink et al., 1978). Smith (1978)
presents observations from the continental shelf and slope off Peru
which demonstrate that the fluctuations on the time scale of days to
weeks are coherent over several hundred kilometers along the coast
(between 12°S and 15°S) but are not correlated with the local winds.
He suggests that the fluctuations in the currents are due to pole-
ward propagating, coastal trapped waves and that the phase speed
and offshore length scale are consistent with that for internal
Kelvin waves.

The idea of coastal trapped waves propagating an upwelling
response into a region has previously been covered by Gill and
Clark (1974). Adamec and O'Brien (1978) have demonstrated by using
a simple numerical model that the seasonal upwelling observed in the
Gulf of Guinea could result from the propagation of internal Kelvin
waves into the region. The Kelvin waves in their model were excited
by changes in the wind stress over the western Atlantic.

The theoretical synthesis of the data collected in these field ex-
periments has primarily taken one of two approaches, numerical or ana-
lytical models. Both of these approaches have their advantages and dis-
advantages. Continuously stratified analytical models (Allen, 1973;
Pedlosky, 1974, 1978a,b; Pietrafesa, 1973) have been successful in pre-
dicting details of steady-state circulation patterns, but due to the
mathematical complexity of the problem, their analysis is restricted to
primarily steady flow with highly idealized geometries and boundary
conditions, and with the exception of Pedlosky (1978a,b), to linear
primarily steady flow with highly idealized geometries and boundary
conditions, and with the exception of Pedlosky (1978a,b), to linear

theory. Some of the difficulties encountered with the analytical models are the modelling of the singular coastal corner region, the consideration of the physical processes introduced by time dependent forcing, turbulent mixing, and the presences of thermocline and pycnoclines. Through careful numerical formulation of the governing equations, application of efficient differencing techniques, and utilization of plausible parameterization schemes for various physical processes such as mixing, etc., numerical models can be effective tools in simulating upwelling circulations. The numerical approach allows us to consider problems where the analytic solution to the problem is untractable, but this is not without cost.

As the models become more sophisticated and realistic, the cost of running the model escalates, and the interpretation of the model results becomes more complex. The optimal approach to the numerical formulation is to start with the simplest model, preferrably one which can be verified analytically. The next step would be to systematically examine the various physical factors and forcing mechanisms which have a bearing on the problem. Then, finally, building on the knowledge gained from these simpler models, develop a model which includes the significant physical parameters and can realistically simulate the observed upwelling events. Ideally, a model which can adequately simulate upwelling events, can be used to provide flow field information to other disciplines, such as biologists, when physical data are not available. This approach has been the method used by the Mesoscale Air/Sea Interaction Group at Florida State University in developing numerical
This approach has been the method used by the Mesoscale Air/Sea Interaction Group at Florida State University in developing numerical models to study the upwelling problem in support of the CUEA program.

The first of these models was the two-layer, time-dependent, nonlinear
f-plane model by O'Brien and Hurlburt (1972). This model successfully
simulated the basic features of the upwelling circulation and the
equatorward coastal surface jet observed in most upwelling regions, but
it failed to reproduce the observed poleward undercurrent. Following
Charney (1955), they attributed the formation of the surface jet to
conservation of potential vorticity. O'Brien et al. (1980) presents
an analytic solution to the linearized version of the O'Brien and
Hurlburt model which demonstrates that solution on a f-plane is dom-
inated by a barotropic equatorward flow. Thompson and O'Brien (1973)
extended the O'Brien and Hurlburt model by considering time-dependent
wind forcing. Since this model was also on a f-plane, it too failed
to find the poleward undercurrent.

Hurlburt and Thompson (1973), using a two-layer x-t β-plane
model which neglected all longshore derivatives except for the long-
shore pressure gradients, successfully removed the barotropic mode
and produced a poleward undercurrent. O'Brien et al. (1980) used
a modified β-plane model to examine the above model analytically.
They found that, as in the full β-plane Hurlburt and Thompson model,
the barotropic mode vanishes identically and both the upper layer
equatorward jet and poleward undercurrent exist. Also, they found
that this equatorward jet is generally stronger than the poleward
undercurrent as found in observations (Mooers, Collins and Smith,
1976). O'Brien et al., also show that, as long as there is no
variation in the longshore bottom topography, the presence of the
1976). O'Brien et al., also show that, as long as there is no
variation in the longshore bottom topography, the presence of the
longshore pressure gradients does not affect the upwelling but, as
shown by Garvine (1971) and Hurlburt and Thompson (1973), is

essential to obtaining a poleward undercurrent.

Hurlburt (1974) used an x-y-t two-layer β-plane model to study the effects of various configurations of bottom topography and coastline geometry on wind driven eastern ocean circulations. He found that the topographic β-effect plays a fundamental role in the dynamics associated with mesoscale longshore topographic variations. All the foregoing numerical models were associated with upwelling along a meridional (N-S) coastline. Kindle and O'Brien (1974) examined upwelling along a zonal (E-W) coastline and found that the β-plane solution for this problem closely resembled the f-plane solution. They concluded that while the β-effect is essential to the upwelling dynamics along a meridional coast, it is of minimal importance along a zonal coast.

The first attempt to introduce realistic shoreline geometry and bottom topography was presented by Peffley and O'Brien (1976). They used a digitized version of the Oregon coast and offshore bottom topography in the Hurlburt (1974) model to simulate the coastal upwelling off Oregon. Peffley and O'Brien found that the topographic variations dominated over coastline irregularities in determining the longshore location of upwelling centers.

Preller and O'Brien (1980) used a version of the Hurlburt (1974) model with an idealized version of the Peruvian bottom topography and straight coastline to study the effects of various topographic features on the Peruvian upwelling system. In their model, Preller and O'Brien were unable to reproduce the poleward undercurrent with features on the Peruvian upwelling system. In their model, Preller and O'Brien were unable to reproduce the poleward undercurrent with just wind stress and β-effect. To induce a steady poleward under-current, Preller and O'Brien introduced an external depth independent

longshore pressure gradient in the form of an atmospheric pressure gradient. O'Brien et al., (1980) used this same model with a digitized version of the Peruvian coastline and bottom topography to simulate the major features of the Peruvian upwelling system.

A comparison of the output data from the O'Brien et al. model with objectively analyzed current meter data (O'Brien, Smith and Heburn, 1980) points out two significant shortcomings of this model. The first is an obvious lack of upper layer onshore flow (induced by horizontal density gradients) during the relaxation of upwelling favorable winds. The second is a rather anemic lower layer flow in the model as contrasted with observed energetic low-frequency current fluctuations. Brink (1978) has shown that these fluctuations are not correlated with the local winds and Smith (1978) suggests that these are the result of remotely forced, coastal trapped waves propagating through the region.

To examine the effects of the interactions of a fluctuating undercurrent and the digitized Peruvian bottom topography, we will use the O'Brien et al. hydrodynamic model with a parameterization, based on coastal trapped Kelvin wave dynamics, for the longshore current. With the passages of one of these coastal trapped waves, we will see a direct relationship between the relative magnitude of the topographically induced upwelling center, as determined by the displacement of the model interface and the strength of the undercurrent.

All of the foregoing models are strictly hydrodynamic and are unable to achieve a realistic steady-state. Furthermore, the interface

All of the foregoing models are strictly hydrodynamic and are unable to achieve a realistic steady-state. Furthermore, the interface is not allowed to intersect the surface, since numerical instabilities

result when the layer thickness approaches zero. Therefore, they
cannot simulate the observed upwelling frontal structure. O'Brien et
al., (1977) have proposed one solution to this problem by allowing the
uppermost layer to entrain mass from the lower layer just before the
layer interface reaches the surface.

Another intrinsic assumption in these models is that the time
scale for vertical advection is much shorter than that for turbulent
vertical diffusion. Thompson (1974) suggests that this is valid
for small departure of the interface from its initial state, but that
the general validity is in question when one considers the studies
of oceanic wind mixing by Kraus and Turner (1967), Denman (1973),
Denman and Miyake (1973), and Pollard and Millard (1970). Thompson
has shown, by using a x-t two-layer model which included thermodynamics
and interfacial mixing, that vertical advection and vertical mixing
may be comparable on a coastal upwelling event time scale. He defined
an upwelling event time scale as "an interval longer than an inertial
period, during which local winds initiate and maintain coastal up-
welling." This particular parameterization of the interfacial mixing
was restricted to the wind-dominated (forced convection) vice heat-
dominated (free convection) regime, since the two-layer formulation
of the model is not readily adaptable to thermocline reformation at
shallower depths under conditions of strong solar heating.

In this study, we will first include a parameterization for the
longshore current fluctuation into the x-y-t two-layer Peru model used
by O'Brien et al., (1980) to examine the interaction of the currents
longshore current fluctuation into the x-y-t two-layer Peru model used
by O'Brien et al., (1980) to examine the interaction of the currents
with the bottom topography. Next, we will add thermodynamics and a

parameterization for interfacial mixing to this model and use time-dependent forcing derived from JOINT II, March, April, and May (MAM) 1977 data to simulate the Peruvian upwelling system.

CHAPTER 2

1. THE COASTAL UPWELLING PROBLEM

a. EKMAN THEORY

The theoretical framework for upwelling is derived from the
pioneering work by Ekman (1905). To explain the reason for the mass
transport in the upper layer of the ocean being directed perpendicular
to the wind stress, Ekman considered a balance between the rotational
and vertical friction terms in the momentum equation.

He assumed steady-state motion in a homogeneous ocean of in-
finite extent, with a steady and uniform wind blowing at the surface.
With this assumption, Ekman found the mass transports M_x and M_y,
(usually referred to as Ekman transports), caused by the wind to be:

$$M_x = \int_{-\infty}^{O} \rho u dz = \frac{\tau_y}{f} \qquad (1)$$

$$M_y = \int_{-\infty}^{O} \rho v dz = \frac{-\tau_x}{f} \qquad (2)$$

where u and v are the meridional and zonal velocity component, ρ is
the sea water density, τ_x and τ_y are the meridional and zonal surface
wind stress components and f is the Coriolis parameter. We can
readily see from equation (1 and 2) that the net mass transports are
directed 90° to the right (left) of the wind stress in the northern
(southern) hemisphere.

Now, as Thorade (1909) has shown, it becomes obvious that for
an equatorward wind blowing along the eastern boundary of the ocean,
Now, as Thorade (1909) has shown, it becomes obvious that for
an equatorward wind blowing along the eastern boundary of the ocean,
the net transport in the surface Ekman layer is offshore. This would

12

result in a one-sided divergence in the upper layer. Mass continuity would require the replacement of the upper layer water along the coast with water from the lower layer (upwelling) and a net onshore transport below the surface Ekman layer.

The exact nature of the onshore flow is still not clearly defined. Smith (1980), in a comparison of upwelling regions off Oregon, Northwest Africa and Peru, shows that the flow patterns derived from moored array current meter observations are in good agreement with the classical conceptual model of coastal upwelling. That is, that the convergence in the horizontal flow beneath the surface layer balances the divergence in the surface layer. Also, Smith does not find any evidence for the two-cell circulation pattern proposed by Mooers, Collins and Smith (1976). However, Johnson and Mooers (1979), by using data from profiling current meters, found that the double-cell circulation does exist in association with a relatively strong coastal upwelling frontal system. Smith states that while his study does not rule out the double-cell patterns, they are "at most, ephemeral and migrant...and play no significant role."

Even the "simple" concept varies from one region to another. Off Peru and Oregon, the observations show that the maximum onshore flow is at mid-depth and clearly not in a bottom Ekman layer. The poleward undercurrent in the Peru and Oregon systems would drive an offshore transport in the bottom Ekman layer. Off Northwest Africa, however, the undercurrent is equatorward and thus drives an onshore bottom Ekman layer. The observation in this region shows the maximum onshore the undercurrent is equatorward and thus drives an onshore bottom Ekman layer. The observation in this region shows the maximum onshore flow is in a bottom layer whose thickness is consistent with a bottom Ekman layer.

b. BOTTOM TOPOGRAPHY EFFECTS

The inclusion of bottom topography into the study of ocean cir-
culations adds considerable difficulty to the analysis and interpre-
tation of the problem. Generally the approach to the solution of
ocean circulation problems is to consider a flat-bottom, stratified
ocean on a β-plane, and then decompose the flow into barotropic and
baroclinic modes. The vertical structure of the horizontal velocities
for these modes can then be determined independently for each mode.
Now with the addition of a sloping bottom, the direct use of the
barotropic and baroclinic modes is no longer possible. The effect
of the bottom topography on this approach is to couple the modes such
that the vertical standing modes are no longer independent. This
coupling makes the problem extremely difficult to interpret.

Rhines (1970) suggests the use of "bottom" and "surface" modes as
the appropriate vertical modes for a two-layer system. The essential
properties of these modes are that the bottom mode is dominated by the
lower layer motion and wave propagation is controlled by both topo-
graphic (β^T) and planetary (β) Beta. The surface mode motion is
isolated away from the bottom and wave propagation is controlled by the
planetary Beta. Suginohara (1980) uses this approach to study quasi-
geostrophic waves in a two-layer system with bottom topography. He
examines, in detail, the coupling between these two modes. Suginohara
finds the coupling, which results from the effect of divergence, tends
to be suppressed by the effect of bottom topography. In fact, he finds
that when $\beta/\beta^T \ll 1$, complete isolation of the surface mode from the
to be suppressed by the effect of bottom topography. In fact, he finds
that when $\beta/\beta^T \ll 1$, complete isolation of the surface mode from the
bottom takes place. Furthermore, he finds that the strength of the

coupling for the lower layer, depends not only on the ratio of planetary to topographic Beta, but also the bottom orientation, and that in some realistic cases, the combined effect of β and β^T give rise to complete decoupling of the upper and lower layers.

Since the observations off Peru tend to suggest that the lower layer is isolated from the local surface forcing and wave propagation is controlled by the topography, we will, for the present, restrict our discussions of the effects of the bottom topography to the lower layer while realizing that the layers are still at least weakly coupled.

We will now consider the lower layer as a homogeneous fluid which conserves potential vorticity on a β-plane with the interface as a free upper surface. Following Pedlosky (1979) we find the conservation of potential vorticity can be expressed as

$$\frac{d}{dt} \left(\frac{f + \beta y - f\, H_B/D + \zeta + f\, \eta/D}{D} \right) = 0 \qquad (3)$$

where the layer thickness is

$$H = D - H_B + \eta \qquad (4)$$

and where D is the mean layer thickness, H_B is the height of the bottom topography from some reference level and η is the displacement of the free surface from its initial position, (see fig. 1), and ζ is the relative vorticity.

For our study, we will consider a case where we have a poleward longshore flow in the southern hemisphere (v<0, f<0) over a mesoscale topographic feature where the magnitude of the topographic Beta $(\beta_T = \frac{\partial H_B}{\partial y})$ is much greater than the planetary Beta. Then we could express the local time rate of change of relative vorticity and free

$(\beta_T = \frac{\partial H_B}{\partial y})$ is much greater than the planetary Beta. Then we could express the local time rate of change of relative vorticity and free
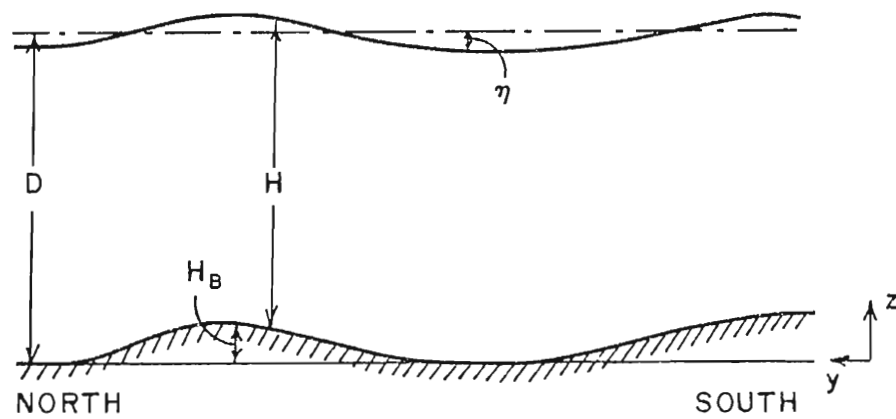
Fig. 1. Schematic of lower layer showing the components which compose the thickness of the layer, i.e., $H = D - H_B + \eta$.

surface displacement as

$$\frac{\partial}{\partial t}(\zeta + f\, \eta/D) = -v\frac{\partial}{\partial y}(\zeta + f\, \eta/D) + v\frac{\partial}{\partial y}\left(\frac{f\, H_B}{D}\right) \tag{5}$$

where the first term on the right-hand side of equation (5) is the change due to wave propagation and the second term is the change due to the topographic Beta effect. If we assume that the wavelength of the wave is much greater than the length scale of the topographic variation, we can, by appropriate scaling, separate the two effects. We will only consider the topographic effects for the present.

For a poleward flow (v<0), if we have $\beta_T = \frac{\partial H_B}{\partial y} > 0$ (i.e., downslope flow) we find that $v\frac{\partial}{\partial y}\left(\frac{f\, H_B}{D}\right) > 0$, which can be compensated for by either an increase in the relative vorticity, a negative free surface displacement or both. Now for v<0 and β_T<0 (upslope flow) we find $v\frac{\partial}{\partial y}\left(\frac{f\, H_B}{D}\right) < 0$, which implies a decrease in the relative vorticity and a positive displacement of the free surface. Similarly for an equatorward flow (v>0), we find that upslope flow (β_T>0) yields $v\frac{\partial}{\partial y}\left(\frac{f\, H_B}{D}\right) < 0$ and downslope flow (β_T<0) yields $v\frac{\partial}{\partial y}\left(\frac{f\, H_B}{D}\right) > 0$.

We can also see the relative magnitude of the local changes are directly proportional to the magnitude of the longshore velocity component.

b.   COASTAL TRAPPED KELVIN WAVES

Smith (1978) in an analysis of the currents in the Peruvian upwelling system found that the primary wave mode seen off Peru has a

phase speed of approximately 200 km/day, a period of approximately 8-10 days and a wavelength of approximately 2000 km.

Basically, a coastal Kelvin wave is a long internal gravity wave constrained by rotation to propagate only alongshore. It is characterized by no cross-shelf flow and has its maximum fluctuations occuring near the coast with an exponential decay offshore. The decay length scale (trapping length scale) is the Rossby radius of deformation. Generally, pure Kelvin waves occur only in the absence of bottom topography. Wang and Mooers (1976) examine the effects of bottom topography on the Kelvin waves and co-existence of Kelvin and topographic Rossby waves.

Now, we will briefly examine the effects of the passage of a Kelvin wave on the upwelling system. First as a wave crest passes, there is a strengthening of the wind driven equatorward flow, a decrease in the poleward undercurrent, and a weak upwarping of the isotherms. Next, as a wave trough passes, there is a weakening of the upper layer flow, a strengthening of the undercurrent, and a weak downwarping of the isotherms.

The primary effect of the wave passage can be seen when we consider the variability of the undercurrent and its interaction with the bottom topography. As discussed in the previous section, with an increase in the magnitude of the poleward undercurrent (trough passage) we would expect larger departures of the relative maxima and minima in the interface displacement which are directly associated with topographic features. Conversely, with a weakening of the poleward undercurrent (crest passage) we would expect a relatively uniform interface dis-reatures. Conversely, with a weakening of the poleward undercurrent (crest passage) we would expect a relatively uniform interface displacement with only minor departures associated with the topography.

One theory (Moore, 1968; Moore and Philander, 1977) as to the

source of the Kelvin waves is that variation in wind stress over the tropical oceans excite equatorially trapped Kelvin waves which propagate eastward along the equator. One property of the equatorial Kelvin waves is that they can only propagate eastward, thus when they encounter the eastern boundary of the ocean basin and are unable to reflect as a westward propagating Kelvin wave, they excite coastal Kelvin waves which propagate poleward along the coast.

Wyrtki (1975) suggests that a relaxation of the trades in the western equatorial Pacific and the resultant Kelvin wave is the mechanism which causes the onset of the El Niño phenomenon off Peru. This hypothesis is supported by the work of Hurlburt et al., (1976), McCreary (1976) and Kindle (1979).

d.   VERTICAL MIXING

With the exception of Yoshida (1967), Thompson (1974) and more recently Clancy et al., (1979), the role of turbulent vertical mixing and thermodynamics has been ignored in coastal upwelling models. The basis for the neglection of vertical mixing in most of the upwelling models has been the assumption that the time scale for vertical advection is much shorter than that for turbulent vertical diffusion. The general validity of this assumption is in question when we consider the studies of oceanic wind mixing by Kraus and Turner (1967), Denman (1973), Denman and Miyake (1973), and Pollard and Millard (1970). Thompson (1974) demonstrated that the vertical advection and vertical mixing may be comparable on a coastal upwelling event time scale, where an upwelling event time scale is defined as "an interval longer than mixing may be comparable on a coastal upwelling event time scale, where an upwelling event time scale is defined as "an interval longer than an intertial period, during which local winds initiate and maintain coastal upwelling."

The major obstacle in including mixing into the upwelling problem is in the nature of mixing, in that, mixing is basically turbulent. Within the present "state-of-the art", turbulence is not well understood and the turbulence problem is unsolved. For that matter the methods to solve the problem are diversified and are the subject of much controversy within the research community. Niiler and Kraus (1977) examine the basic approaches to the problem of one-dimensional mixing in the upper ocean. They discuss the advantages and disadvantages of each of the most popular techniques and show that solutions to even the simplified one-dimensional problem are complex. Thompson (1978) presents a comprehensive review of the role of mixing in the upwelling systems and the problems involved in incorporating mixing into numerical models.

Most of the recent work rely on the theoretical models developed by Kraus and Turner (KT) (1967) or Pollard, Rhines and Thompson (PRT) (1973). The KT model considers the energy balance between the rate of turbulent kinetic energy produced by the surface wind stress and the rate of increase in potential energy due to mixing layer depth deepening, but does not consider the wind effects on the mean velocities. The PRT model on the other hand, considers the balance between the rate of work done by the wind stress on the mean motions and the rate of increase of kinetic and potential energies of the mean field. Niiler (1975) has shown that the potential energy increase in the PRT model is due to the shear production by the entrainment stress at the base of the mixed layer. deSzoeke and Rhines (1976) demonstrate that these ~~ due to the shear production by the entrainment stress at the base of the mixed layer. deSzoeke and Rhines (1976) demonstrate that these two models are two asymptotic limits to the general balance of the turbulent kinetic energy equations.

Zilitinkevich, Chalikov and Resnyansky, 1979, present sample cal-
culations (based on real data) for a number of the one dimensional

models, and compare the predicted depth and temperatures of the homo-

geneous upper layer.

Thompson (1974) introduced simple thermodynamics and interfacial

mixing into the upwelling problem in an x-t two-layer time-dependent

upwelling model. The interfacial mixing parameterization for this

model was prescribed as a function of the Richardson number, Ri, based

on the laboratory work of Kato and Phillips (1969). Kato and Phillips,

by examining a fluid with a linear density gradient subjected to an

applied surface stress, found that a turbulent homogeneous layer

bounded below by a sharp interface quickly formed. Their observations

of the rate deepening of the homogeneous layer yield a relationship

$$Q = u_* f(Ri) \tag{6}$$

Where Q is the deepening rate, u_* is the friction velocity and is

related to the applied stress, τ, as

$$\tau = \rho_0 u_*^2 \tag{7}$$

and ρ_0 is the mean density. The Richardson number is given by

$$Ri = \frac{g \Delta \rho D}{\rho_0 u_*^2} \tag{8}$$

where $\Delta \rho$ is the density jump across the interface, D is the depth of

the homogeneous layer, and g is the gravitational acceleration.

By dimensional analysis arguments, Turner (1973) found that

$$g \Delta \rho Q D \approx \rho_0 u_*^3 \tag{9}$$

By dimensional analysis arguments, Turner (1973) found that

$$g \Delta \rho Q D \approx \rho_0 u_*^3 \tag{9}$$

or

$$Q \propto u_* Ri^{-1}. \tag{10}$$

Which gives the same energy balance as the KT model.

Similar relationships between Q and Ri have been used by Pollard, Rhines and Thompson (1973), Denman (1973), and Niiler (1975).

The form used by Thompson (1974) for entrainment of lower layer fluid into the upper layer was

$$Q_1 = \phi u_* Ri^{-1} = \frac{\rho_o \phi u_*^3}{g \Delta \rho h}. \tag{11}$$

where Q_1 is the entrainment rate of lower layer fluid to the upper layer and h_1 is the thickness of the upper layer. He used the value of the proportionality constant, $\phi = 2$, suggested by Denman (1973). Thompson also assumed that the entrainment of upper layer fluid into the lower layer by bottom generated turbulence could be expressed as

$$Q_2 = \frac{\rho_o \phi \bar{u}_*^3}{y \Delta \rho h_2} \tag{12}$$

where h_2 is the thickness of the lower layer,

$$\bar{u}_*^2 = \frac{|\vec{\tau}_B|}{\rho_o}, \tag{13}$$

is the bottom friction velocity and $|\vec{\tau}_B|$ is the bottom stress. He found that $Q_2 \ll Q_1$ except when the interface is very near the bottom.

found that $Q_2 \ll Q_1$ except when the interface is very near the bottom.

Based on the Mellor-Yamada (1974) level 2 (MYL2) turbulence closure scheme, Martin and Thompson (1977) have developed a bulk model

of the upper mixed layer which is compatable with a layered
formulation for a numerical ocean model.

In this model the mixed layer depth was parameterized for each of
two distinct regimes:

1) stratification limited - limited by the density stratification
underlying the mixed layer.

2) heat flux limited - limited by the rate of surface heating due
to a positive net surface heat flux.

In the stratification regime, as the mixed layer deepens through
a stable density stratification, the stratification at the base of the
layer will increase, while the velocity shear available to generate
turbulent kinetic energy will decrease. Thus for a given stratifica-
tion and wind stress, the mixed layer depth will stabilize when the
turbulence at the base of the mixed layer becomes too weak to erode
the stratified region below. To predict the layer depth for this
regime Martin and Thompson used the PRT bulk mixed layer model to
approximate the MYL2 model. For the PRT model, it is assumed that
during mixed layer deepening into a stably stratified region, the
bulk Richardson number, Ri_B, is equal to one:

$$Ri_B = \frac{\kappa g h \Delta T}{(\Delta u)^2 + (\Delta v)^2} = 1, \tag{14}$$

where h is mixed layer depth, ΔT, Δu, and Δv are temperature and
velocity differentials across the base of the mixed layer and κ is
the coefficient of thermal expansion. Then letting $Ri_B = 1$ and
rearranging, h becomes:
the coefficient of thermal expansion. Then letting $Ri_B = 1$ and
rearranging, h becomes:

$$h = \frac{(\Delta u)^2 + (\Delta v)^2}{\kappa g \Delta T} . \tag{15}$$

In the heat flux limited regime, as the layer deepens, more work has to be done by turbulence to mix the surface heat flux throughout the layer. Thus for a given surface flux and wind stress, the mixed layer depth become established at a depth where a balance between production of kinetic and potential energy and dissipation is reached.

The layer depth predicted by the MYL2 model can be expressed as a function of dimensionless parameter ϕ as

$$h = \frac{u_*}{f} h' (\phi) \tag{16}$$

where ϕ is the ratio of the Monin-Obukov and Ekman layer length scales and is defined as

$$\phi = gH/fu_*^2 , \tag{17}$$

where H is the heat flux.

Briefly, when the mixed layer is limited by 1) underlying stratification, the depth is determined by the PRT bulk model with the bulk Richardson number equal to one, 2) surface heat flux, the depth is determined as a function of the dimensionless parameter ϕ. When both wind deepening and surface heating are present, the mixed layer depth is taken to be the shallower of the two depths.

The next step is to couple the one-dimensional mixing models to a three-dimensional ocean circulation model which include the effects of advection. One approach to this problem would be to compare the upper layer thickness (ULT) predicted by a 1-D mixed layer model (MLM) to that predicted by an advective 3-D model where the entrainment rate upper layer thickness (ULT) predicted by a 1-D mixed layer model (MLM) to that predicted by an advective 3-D model where the entrainment rate is predicted from a previous time step. If the ULT predicted by the

1-D MLM is greater than that predicted by the advection model then a new entrainment rate is calculated. If the ULT from the 1-D MLM is less than that for the advection model then we assume that the wind stress input is just mechanically stirring the upper layer and is not entraining mass across the interface (i.e. no interfacial mixing).

CHAPTER 3

1. MODEL

For this study, we consider a two-layer vertically integrated,
stably stratified, rotating, incompressible, hydrostatic, primitive
equation model on a β-plane with a rotated coordinate system which
is forced by local winds and externally excited coastal trapped waves.
The latter forcing mechanism is new to coastal upwelling models.
To study the effects of this forcing, a hydrodynamic version of the
model with two homogeneous layers, which neglects interfacial mixing
and thermodynamics, is used.

A thermodynamic version of the model, which assumes the fluid
to be Boussinesq, is used to introduce the effects of thermodynamics
and interfacial mixing.

Before discussing the specifics of these models, we will first
describe the model geometry, basin orientation and location.

a. MODEL GEOMETRY

As can be seen in Fig. 2, the Peru coastline in the JOINT II
region is oriented northwest-southeast. In order to maximize the
basin size and resolution within the eastern boundary region
(upwelling zone), the model basin, (Fig. 3), is rotated 45° such
that the righthand boundary approximates the coastline. The basin
dimensions are 300 km in the y-direction (with y = 0 approximately
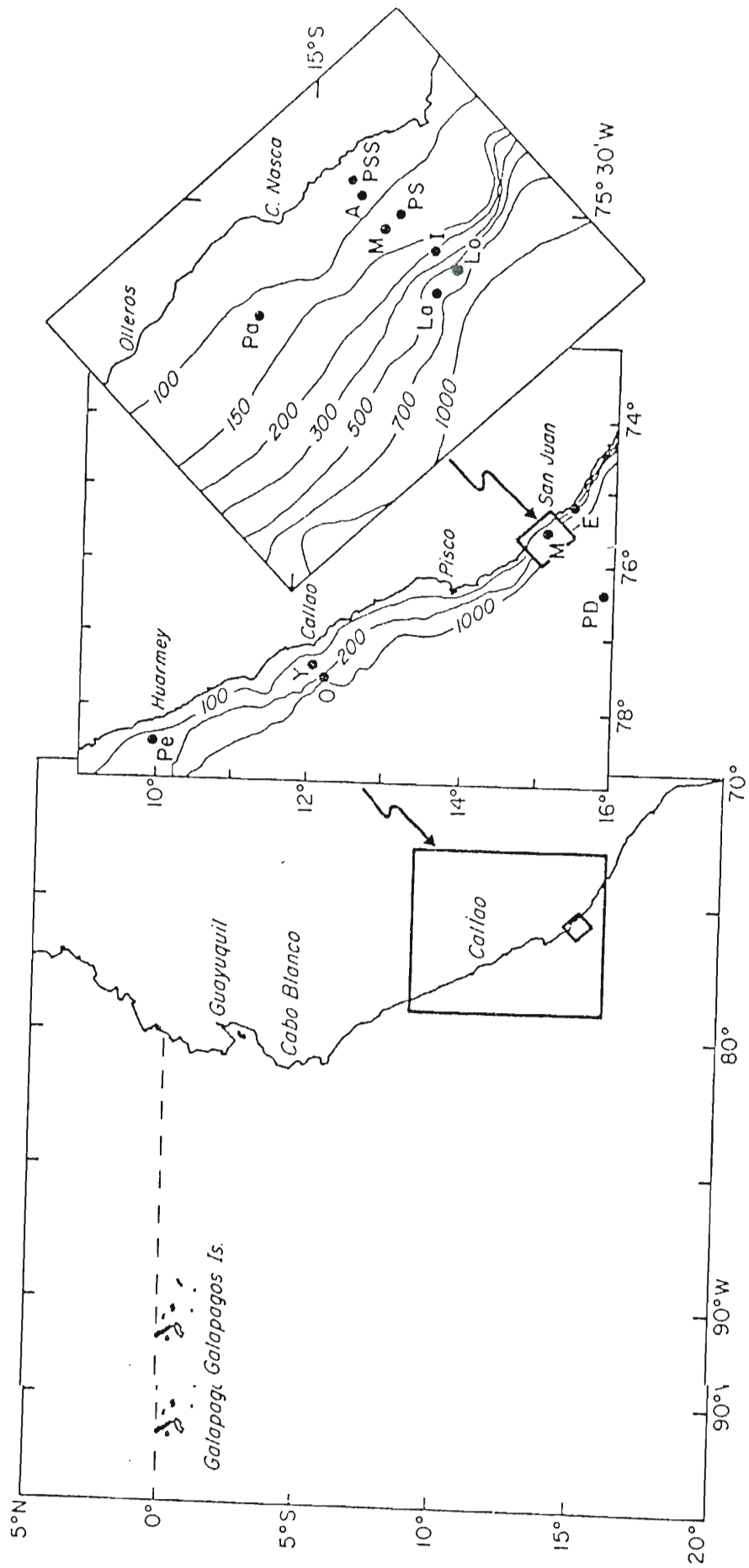along the C-line) and 1500 km in the x-direction.

26

Fig. 2. Site, Bathymetry and Current meter arrays for the JOINT II region, (from Brink, Brink, Smith and Halpern, 1978).
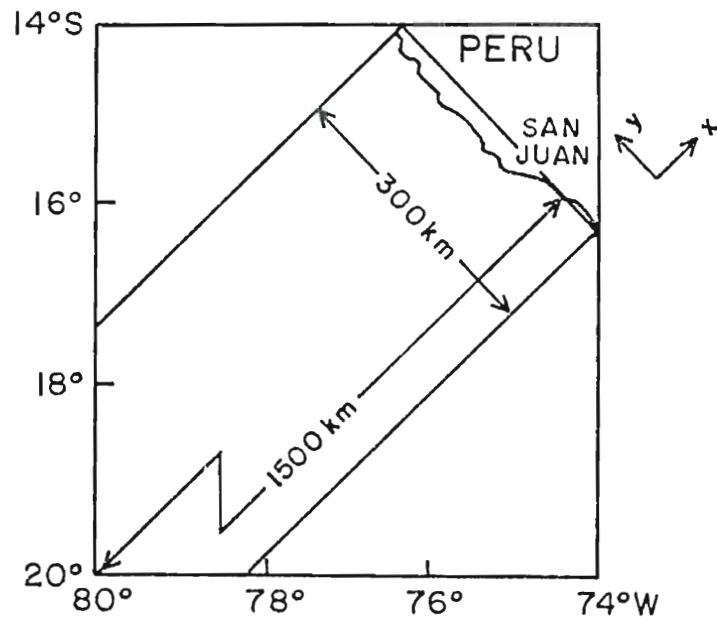
Fig. 3. Model basin orientation. The model dimensions are 300 km in the y-direction and 1500 km in the x-direction. Note that the basin is rotated 45° from a North-South orientation.

Hurlburt and Thompson (1973) have demonstrated that the solution in the upwelling zone is independent of that for the far-field boundary region providing the zonal extent of the basin is such that a Sverdrup interior flow can be established. The barotropic Sverdrup balance for this flow is given by

$$\int_{-L}^{0} \beta v_1 \, dx = \frac{\tau_{sy}}{o(h_1 + h_2)} \tag{18}$$

where v_1 is the upper layer longshore velocity component, τ_{sy} is the longshore component of the surface wind stress, and h_1 and h_2 are the upper and lower layer thicknesses respectively. For $\beta \sim 1.56 \times 10^{-13}$ $cm^{-1} \ sec^{-1}$ and $v_1 \sim 6 \ cm \ sec^{-1}$, this requires a width greater than 1000 km. Therefore, to meet the requirements for a Sverdrup interior, we have used a basin width of 1500 km.

A schematic of the model geometry, Fig. 4, shows the relative location of the vertically averaged variables u_i, v_i, ρ_i and the layer thicknesses h_i. The height of the bottom topography above the base of the model is represented by $D(x, y)$.

In order to resolve the solution in the upwelling zone (generally on the order of 20 km in width), a fine resolution grid (on the order of 2 km) is needed. Since a grid of this resolution applied to a basin of this size is not economically feasible, and the solution in the western part is of no interest for this problem, the model uses a variable resolution grid which varies discretely in the x-direction and is analytically stretched in the y-direction. The grid spacing in the x-direction, Δx, varies from 2 km in the coastal region to 100 km in the western part of the basin, and the grid spacing in the x-direction, Δx, varies from 2 km in the coastal region to 100 km in the western part of the basin, and the grid spacing in the y-direction, Δy, varies from approximately 4 km near y = 0 to approximately 13 km near the northwestern and southeastern boundaries.
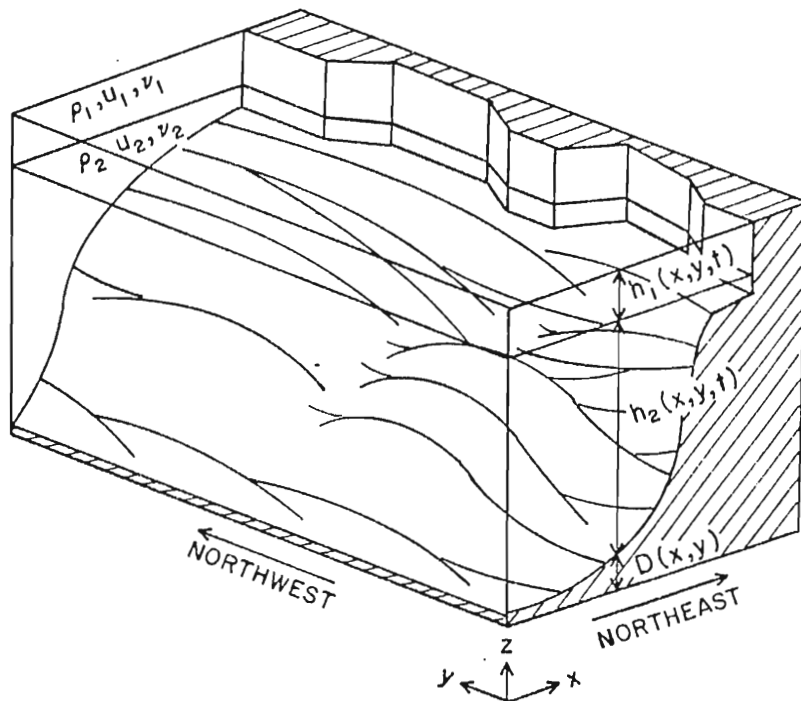
Fig. 4. Model geometry. This schematic of the model geometry shows the relative location of the layer averaged variables, u_i, v_i, ρ_i, layer thicknesses, h_1, h_2, and height of the topography, D, above a reference height.

The bottom topography (Fig. 5) used in this model, is a rotated, digitized version of the Preller-O'Brien (1977) Peruvian near shore bottom topography and coastline map, (Fig. 6). Some of the salient features of this bottom topography are a broad shelf (approximately 20 km) in the north, a narrow shelf (approximately 6 km) in the south, and a shelf slope which is variable in the longshore as well as the offshore direction. Of particular note in the longshore variability is the steep shelf slopes south of Punta Santa Ana and Punta San Juan, and the presence of mesoscale seamounts, which appear to play a significant role in the anchoring of the centers of enhanced upwelling, (Preller and O'Brien, 1980; O'Brien et al., 1980).

b. GOVERNING EQUATIONS

Hydrodynamic Model

The numerical model used for the first part of this study is a modified version of the Hurlburt (1974) model. Since the derivation and numerical formulation of this model are well documented, (see O'Brien and Hurlburt, 1972; Thompson and O'Brien, 1973; Hurlburt, 1974; Preller and O'Brien, 1980; and O'Brien et al., 1980). The model equations will be presented without a detailed explanation.

The governing equations for the model consist of the momentum and continuity equations for each layer. For an x-y-t two-layer model on a rotated β-plane, we have:

$$\frac{\partial \vec{V}_1}{\partial t} + \vec{V}_1 \cdot \nabla \vec{V}_1 + \hat{k} \times f\vec{V}_1 = -g\nabla(h_1 + h_2 + D) + \frac{\vec{\tau}_s - \vec{\tau}_I}{\rho h_1} + A\nabla^2 \vec{V}_1 + \vec{F}_1 \qquad (19)$$

$$\frac{\partial h_1}{\partial t} + V_1 \cdot \nabla \dot{V}_1 + k \times f\dot{V}_1 = -g\nabla(h_1 + h_2 + D) + \frac{\vec{\tau}_s - \vec{\tau}_I}{\rho h_1} + A\nabla^2 \dot{V}_1 + \acute{F}_1 \qquad (19)$$

$$\frac{\partial h_1}{\partial t} + \nabla \cdot (h_1 \vec{V}_1) = 0 \qquad (20)$$
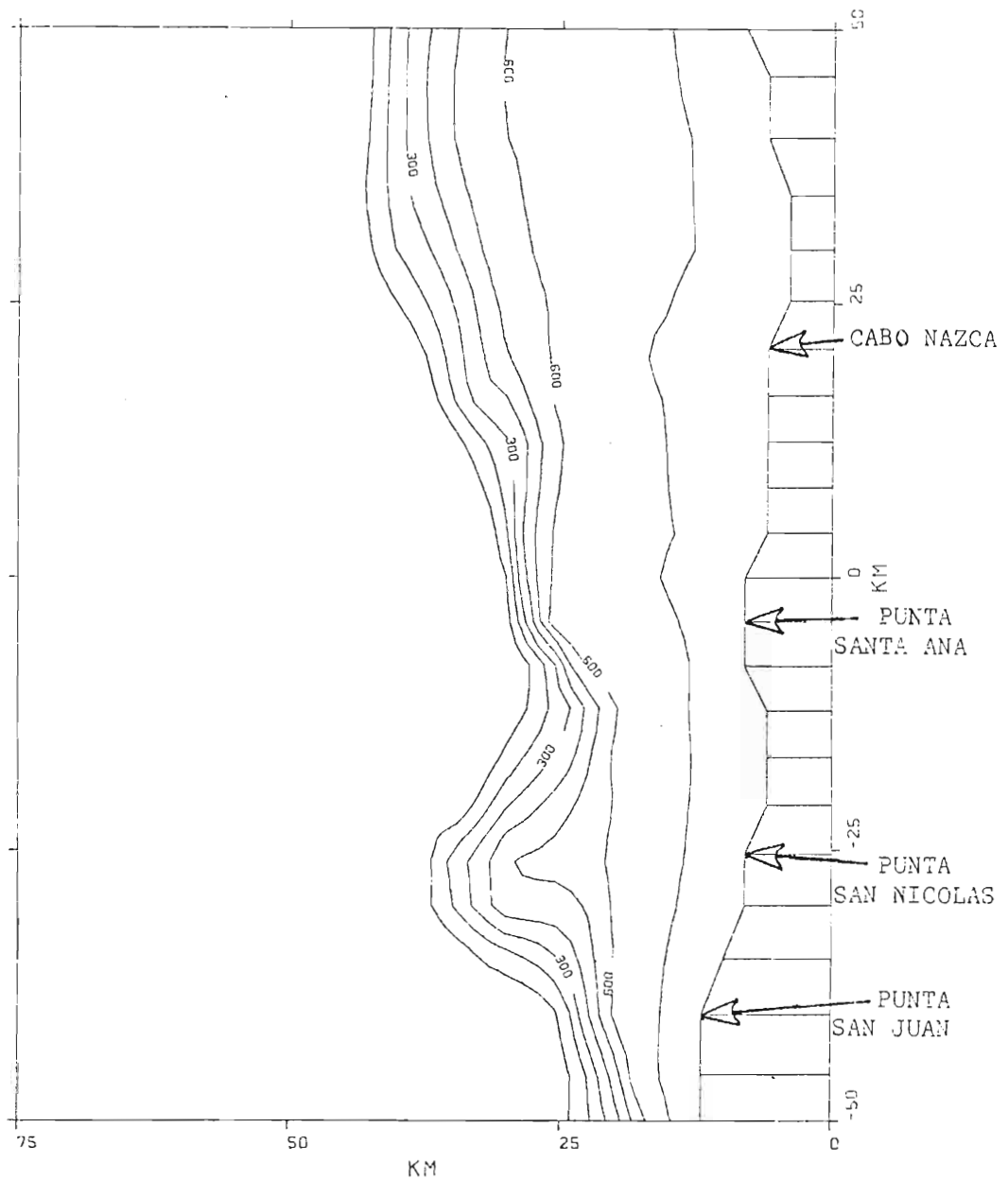
Fig. 5. Digitized bottom topography. The bottom topography is digitized from the Preller and O'Brien, 1977, Peruvian Near Shore Bottom Topography and Coastline. The contour interval is 100 meters.
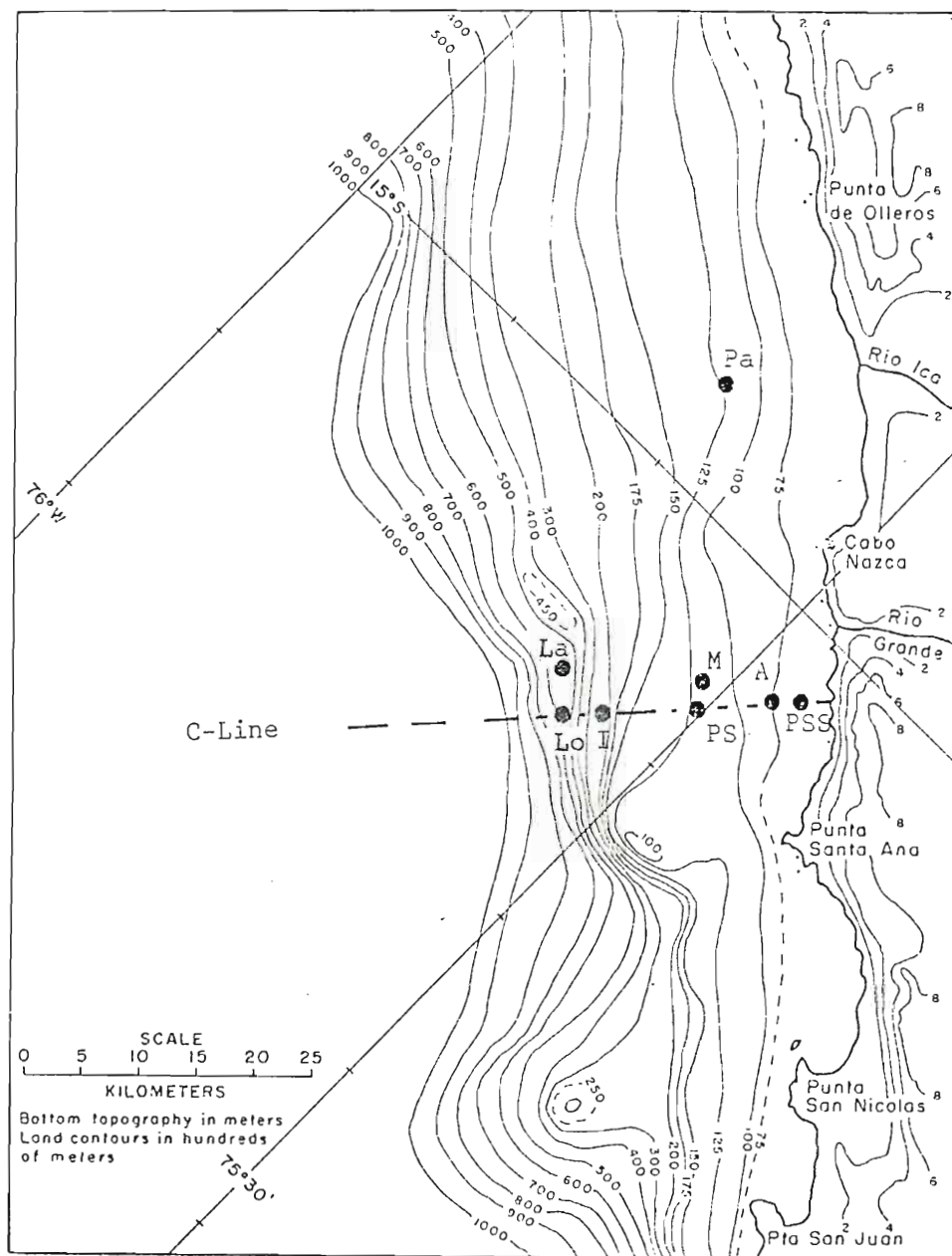
Fig. 6. Peruvian Near Shore Bottom Topography and Coastline -
Preller and O'Brien, 1977. The location of the C-Line (y = 0 for
the model) is indicated by the dashed line. The location of current
meter arrays are plotted.

$$\frac{\partial \vec{V}_2}{\partial t} + \vec{V}_2 \cdot \nabla \vec{V}_2 + \hat{k} \times f\vec{V}_2 = -g\nabla(h_1 + h_2 + D) + g'\nabla h_1 + \frac{\vec{\tau}_I - \vec{\tau}_B}{\rho h_2} + A\nabla^2 \vec{V}_2 + \vec{F}_2 \quad (21)$$

$$\frac{\partial h_2}{\partial t} + \nabla \cdot (h_2 \vec{V}_2) = 0 \tag{22}$$

where

$$\nabla = \frac{\partial}{\partial x} \hat{i} + \frac{\partial}{\partial y} \hat{j} \tag{23}$$

$$\vec{V}_i = u_i \hat{i} + v_i \hat{j} \tag{24}$$

$$f(x, y) = f_o + \beta(y - y_o) + \beta(x - x_o) \tag{25}$$

$$g' = g(\rho_2 - \rho_1)/\rho_2 \tag{26}$$

$$\vec{\tau}_s = \tau_{sx} \hat{i} + \tau_{sy} \hat{j} \tag{27}$$

$$\vec{\tau}_I = \rho C_I |\vec{V}_1 - \vec{V}_2|(\vec{V}_1 - \vec{V}_2) \tag{28}$$

$$\vec{\tau}_B = \rho C_B |\vec{V}_2| \vec{V}_2 \tag{29}$$

and $i = 1, 2$. The external remote forcing function is represented by F_i. Equations (19) and (21) are the conservation . of momentum equations, and (20) and (22) are the vertically integrated mass continuity equations. The interfacial and bottom stresses are formulated following O'Brien and Hurlburt (1972) and modified by Hurlburt (1974) to be invariant under coordinate transformations. The height of the bottom topography above the base of the model is given by D. Also note, that since the model is on a rotated β-plane, the Coriolis parameter, f, is a function of both x and y.

Thermodynamic Model

Thermodynamic Model

To form the governing equations for the thermodynamic model, we

need to reformulate the mass continuity and momentum equations to con-
sider horizontal variations in the layer averaged densities, ρ_i, and
add the equations of state for each layer as well as the heat or energy
equations. Furthermore, we also need to consider the parameterization
of the interfacial mixing.

To start, we will assume that the fluid is Boussinesq, which allows
us to neglect density variations in the momentum equations except when
coupled with gravitational acceleration and to assume fluctuations in
density are the result of thermal effects (Spiegel and Veronis, 1960).

Further, we will assume that in the equation of state, density is
a linear function of termperature only. Brink et al., (1979) has shown,
that for the region which we are modelling off Peru, the density varia-
tions are significantly correlated with the temperature variations and
shows little correlation to the salinity variations. Therefore, for this
region, density can be considered a function of temperature only.

With these additional assumptions, we now express the governing
equations as:

$$\frac{\partial \vec{V}_1}{\partial t} + V_1 \cdot \nabla \vec{V}_1 + \hat{k} \times f \vec{V}_1 = -g\nabla(h_1+h_2+D) + \frac{gh_1}{2\rho_o}\nabla\rho_1 + \frac{\vec{\tau}_s - \vec{\tau}_I}{\rho_o h_1} + \vec{S}_1 + \vec{F}_1$$

$$+ \frac{(\nabla \cdot (\rho_1 h_1 A_H \nabla))\vec{V}_1}{\rho_o h_1} \qquad (30)$$

$$\frac{\partial h_1}{\partial t} + \nabla \cdot (h_1 \vec{V}_1) = Q_1 - Q_2 + \frac{\gamma H}{\rho^2 c} \qquad (31)$$

$$\frac{\partial h_1}{\partial t} + \nabla \cdot (h_1 \vec{V}_1) = Q_1 - Q_2 + \frac{\gamma H}{\rho_1^2 c_p} \qquad (31)$$

$$\frac{\partial \rho_1}{\partial t} + \vec{V}_1 \cdot \nabla \rho_1 = \frac{\Delta \rho Q_1}{h_1} + \frac{1}{h} \nabla \cdot (K_H h_1 \nabla \rho_1) - \frac{\gamma H}{\rho_1 C_p h_1} \tag{32}$$

$$\rho_1 = \rho_0 - \gamma T_1 \tag{33}$$

$$\frac{\partial \vec{V}_2}{\partial t} + \vec{V}_2 \cdot \nabla \vec{V}_2 + \hat{k} \times f \vec{V}_2 = -g\nabla(h_1 + h_2 + D) + g'\nabla h_1 - \frac{gh_1}{\rho_0} \nabla \rho_1 - \frac{gh_2}{2\rho_0} \nabla \rho_2 + \vec{S}_2 +$$

$$\vec{F}_2 + \frac{\vec{\tau}_I - \vec{\tau}_B}{\rho_0 h_1} + \frac{(\nabla \cdot (\rho_2 h_2 A_H \nabla)) \vec{V}_2}{\rho_0 h_2} \tag{34}$$

$$\frac{\partial h_2}{\partial t} + \nabla \cdot (h_2 \vec{V}_2) = Q_2 - Q_1 \tag{35}$$

$$\frac{\partial \rho_2}{\partial t} + \vec{V}_2 \cdot \nabla \rho_2 = -\frac{\Delta \rho Q_2}{h_2} + \frac{1}{h_2} \nabla \cdot (K_H h_2 \nabla \rho_2) \tag{36}$$

$$\rho_2 = \rho_0 - \gamma T_2 \tag{37}$$

where ϕ is a constant of proportionality and $\Delta \rho = \rho_* - \rho_1$ with ρ_* determined from a density function to be discussed in the mixing parameterization section.

The entrainment terms are given by:

$$\vec{S}_1 = \rho_* \frac{Q_1(\vec{V}_2 - \vec{V}_1)}{\rho_1 h_1} \tag{38}$$

$$\vec{S}_2 = -\rho_1 \frac{Q_2(\vec{V}_2 - \vec{V}_1)}{\rho_2 h_2} \tag{39}$$

$$Q_1 = \begin{cases} 0 & : \quad h_1 > h_{MLD} \\[2mm] \dfrac{\rho_o \phi u_*^3}{g \Delta \rho h_1} & : \quad h_{MIN} < h_1 < h_{MLD} \\[3mm] \overline{u}_* \left(\dfrac{\partial D}{\partial x} + \dfrac{\partial D}{\partial y} \right) - h_2 \left(\dfrac{\partial u_2}{\partial x} + \dfrac{\partial v_2}{\partial y} \right) & : \quad h_1 = h_{MIN} \end{cases} \qquad (40)$$

$$Q_2 = \begin{cases} \dfrac{\rho_o \phi \overline{u}_*^3}{g \Delta \rho h_2} & : \quad h_2 < h_{BLD} \\[4mm] 0 & : \quad h_2 > h_{BLD} \end{cases} \qquad (41)$$

where

$$u_*^2 = \frac{|\vec{\tau}_s|}{\rho_o} \qquad (42)$$

$$\overline{u}_*^2 = \frac{|\vec{\tau}_B|}{\rho_o} \qquad (43)$$

and h_{MIN} is the minimum layer thickness for the model, h_{MLD} is the stabilized mixed layer depth, and h_{BLD} is the depth of the bottom mixed layer.

Equations (30) and (34) are the momentum equations where the additional terms involve the horizontal gradients of density and the entrainment ($\vec{S}_i$) of momentum from one layer to the other by some mixing process (Q_i). The density of the lower layer fluid which is entrained into the upper layer is represented by ρ_*. This is the mixing process (Q_i). The density of the lower layer fluid which is entrained into the upper layer is represented by ρ_*. This is the density just below the interface and is determined from a density

function which will be discussed in the mixing parameterization section. Equations (31), (32), (35) and (36) are derived from a combination of the mass continuity and energy equations for each layer. Equations (31) and (35) have the same form as the continuity equations in the hydrodynamic formulization except for a non-zero right-hand side. For ease of comparison between the two systems, we will refer to these as the continuity equations for this system and equations (32) and (36) as the thermodynamics equations. The term, H, represents a heating function, which we will discuss later.

Equations (33) and (37) are the equations of state for this system, where ρ_o is a reference density and γ is the product of the reference density, and the coefficient of thermal expansion for sea water.

Q_i represents an entrainment process due to mixing which we will discuss in detail in a later section.

c. BOUNDARY CONDITIONS

The boundary conditions applied at the coast are the no-slip and kinematic boundary conditions.

Hurlburt and Thompson (1973) have demonstrated that the solution in the upwelling zone is independent of that for the far-field boundary region providing the zonal extent of the model basin is at least 1000 km. Thus, the no-slip and kinematic boundary conditions can also be applied to the southwestern boundary without significantly affecting the solution within the upwelling zone since the zonal extent of this model is 1500 km.

The "quasi-symmetric" open boundary condition (Hurlburt, 1974) is used on the northwestern and southeastern boundaries. Basically this boundary condition is a modification of the Hurlburt and Thompson (1973) x-z model. Hurlburt and Thompson in their x-z model assumed all longshore variations to be negligible except for β and the longshore pressure gradient which can be derived from the Sverdrup balance,

$$\beta(v_1 h_1 + v_2 h_2) = \frac{1}{\rho} \operatorname{curl}_z \vec{\tau} \tag{44}$$

and shown to be given by, for the upper layer

$$g \frac{\partial}{\partial y} (h_1 + h_2 + D)\Big|_x = \int_{-L_x}^{x} \beta v_1 \, dx + g \frac{\partial}{\partial y} (h_1 + h_2 + D)\Big|_{-L_x} \tag{45}$$

and, for the lower layer,

$$g \frac{\partial}{\partial y} (h_1 + h_2 + D)\Big|_x - g' \frac{\partial h'}{\partial y}\Big|_x = \int_{-L_x}^{x} \beta v_2 \, dx + g \frac{\partial}{\partial y} (h_1 + h_2 + D)\Big|_{-L_x}$$
$$- g' \frac{\partial h'}{\partial y}\Big|_{-L_x} \tag{46}$$

Hurlburt (1974) demonstrated that the application of the Hurlburt and Thompson x-z model as an open boundary condition allows the development of a Sverdrup interior flow even when the longshore portion of the basin is of mesoscale extent, provided the longshore flow is nearly geostrophic and that

$$\left| \int_{-L_x}^{x} f \frac{\partial v_i}{\partial y} \, dx \right| << \left| \int_{-L_x}^{x} \beta v_i \, dx \right| \quad ; \quad i = 1, 2 \tag{47}$$

near the open boundary.

The modifications to the Hurlburt and Thompson model for the boundary conditions are that the $\frac{\partial h_i v_i}{\partial y}$ terms are retained in the continuity equations and the longshore pressure gradients are given boundary conditions are that the $\frac{\partial h_i v_i}{\partial y}$ terms are retained in the continuity equations and the longshore pressure gradients are given by:

$$g \frac{\partial}{\partial y} (h_1 + h_2 + D) = \int_{-L_x}^{x} \beta (v_1 - v_A)\, dx + g \frac{\partial}{\partial y} (h_1 + h_2 + D)\Big|_{-L_x} \qquad (48)$$

$$g \frac{\partial}{\partial y} (h_1 + h_2 + D) - g' \frac{\partial h_1}{\partial y} = \int_{-L_x}^{x} \beta \left(v_2 + \frac{h_1}{h_2} v_A\right) dx + g \frac{\partial}{\partial y} (h_1 + h_2 + D)\Big|_{-L_x}$$

$$- g' \frac{\partial h_1}{\partial y}\Big|_{-L_x} \qquad (49)$$

where

$$v_A = v_1 - v_1 h_1 + \left(v_2 + \frac{g'}{f} \frac{\partial h_1}{\partial x}\right) h_2 \Big/ (h_1 + h_2) \qquad (50)$$

The term v_A represents the ageostrophic part of the depth averaged flow. Hurlburt (1974) tested various techniques for removing the ageostrophic component and found this method to effectively remove the inertial oscillations and Ekman drift while suppressing the excitation of Kelvin waves.

Preller and O'Brien (1980) discuss in detail the development of the formulation of this method of removing the ageostrophic component by means of a modal analysis of the two-layer system.

The bottom boundary condition is kinematic and the upper surface is free.

d.   INITIAL CONDITIONS

The model is initially at rest and impulsively started at time zero by application of the local and remote forcing mechanisms to be discussed in a later section. The inertial oscillations, Rossby waves and gravity waves excited by the impulsive application of the forcing mechanisms quickly propagate out of the upwelling region. Since the basin width is chosen to be greater than 1000 km, they have no signi-
mechanisms quickly propagate out of the upwelling region. Since the basin width is chosen to be greater than 1000 km, they have no signi-
ficant effect on the upwelling solution after approximately two and one

half days.

The upper layer, h_1, is initially 50m thick and the maximum basin depth, H_{TOT}, is 800m. The lower layer thickness, h_2, is given by

$$h_2 = H_{TOT} - h_1 - D(x, y) \tag{51}$$

where $D(x, y)$ is the height of the bottom topography above the base of the model.

The upper layer density, in the thermodynamic model, is given by $\rho_1 = \rho_I(x)$ where $\rho_I(x)$ in constant over most of the basin and has a slight gradient in the coastal region. The lower layer density is estimated using

$$\rho_2 = \rho_I(x) + \alpha(\rho_B(x) - \rho_I(x)). \tag{52}$$

Unlike his atmospheric counterpart, the ocean modeller does not have a dense synoptic data network available from which he can derive an objectively adjusted initial state, and therefore must use relatively simple, straightforward estimates for the initial fields.

e. FORCING MECHANISMS

Local   Time dependent surface wind stresses, derived from filtered meteorological buoy wind observations, are used as a local forcing mechanism. The wind function used in this model is designed to simulate the low frequency large scale and diurnal land/sea-breeze wind fluctuations.

To simulate the time dependent amplitude of the large scale wind forcing, the wind observations from Pacific Marine Environmental Laboratory's PSS Mooring (15°03'S, 76°27'W, see fig. (2) and (6)), are

lowpass filtered such that periods greater than 36 hrs. are retained. Surface wind stresses calculated from the filtered observations are then applied such that the curl of the wind stress over the first 300 km is equal to the mean interior longshore flow (i.e. Sverdrup balance) estimated from current meter observations.

The offshore profile for this is given by

$$\frac{\partial \tau_y(x, t)}{\partial x} = \beta V_m (h_1(x, 0) + h_2(x, 0)) \tag{53}$$

and

$$\tau_x(x, t) = F(t) \tag{54}$$

for x from 0 to 300 km offshore. The wind stress is then allowed to slowly decay to zero over the remainder of the basin.

In fig. (7), we have a sample of the cross-shelf profile of the mean wind stress components where $|\tau_y| = 1$ dyne/cm^2 and $|\tau_x| = .5$ dyne/cm^2 at the coast. In this figure, we see that the offshore curl required to drive the mean longshore current (V_m) on the shelf is relatively small (on the order 10^{-9}dyne/cm^2).

The diurnal land/sea-breeze regime is simulated by band-pass filtering the PSS wind observations to allow periods between 12 and 36 hours to be retained. The wind stress amplitudes calculated from these are then superimposed on the large scale wind stresses such that they decay exponentially from a maximum at the coast to the large scale at approximately 20 km off the coast.

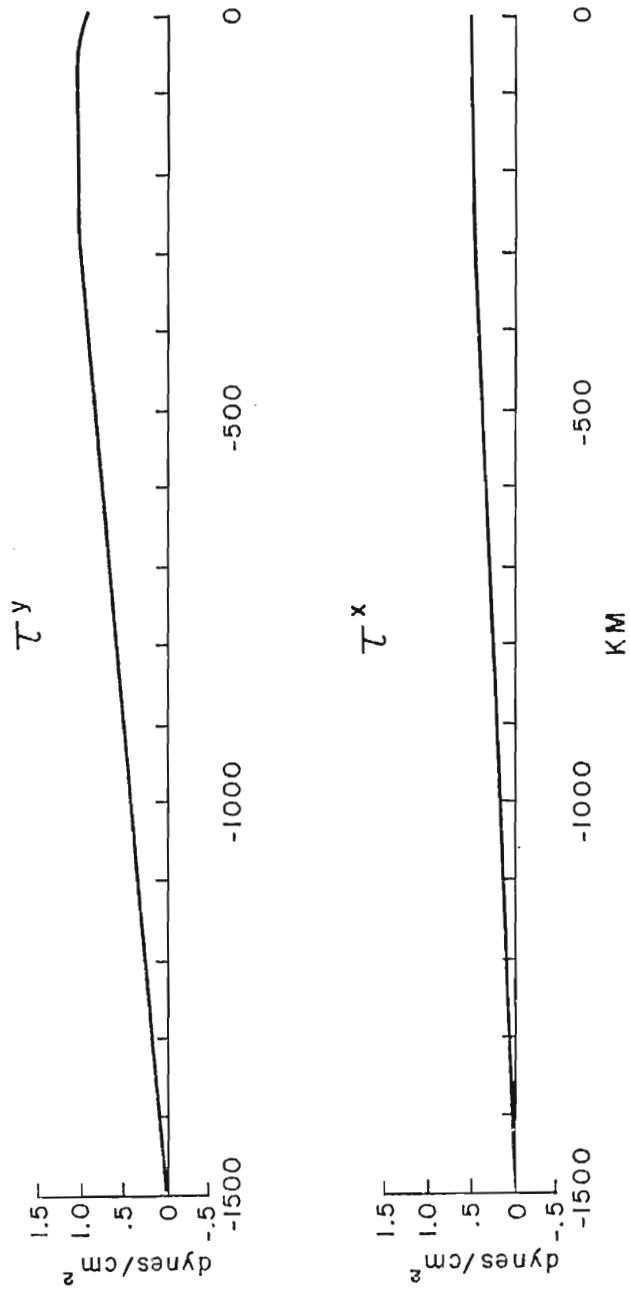The offshore profile for the total wind stress is given by

$$\vec{\tau}(x, t) = \vec{\tau}_L(x, t) + \vec{\tau}_D(t)e^{\delta x} \qquad \text{for } x<0 \tag{55}$$

where the e-folding distance is on the order of 20 km. The large

$$\vec{\tau}(x, t) = \vec{\tau}_L(x, t) + \vec{\tau}_D(t)e^{\delta x} \qquad \text{for } x<0 \tag{55}$$

where the e-folding distance is on the order of 20 km. The large scale wind stress profile is given by $\vec{\tau}_L(x, t)$ and $\vec{\tau}_D(t)$ is the diurnal wind stress amplitude.

WIND STRESS OFFSHORE PROFILES

Fig. 7. Wind Stress Offshore Profiles. Note that there is a slight curl in the τ^y offshore profile within the first 300 km from the coast.

Figure (8) presents time series plots of the large scale wind stress amplitudes, the diurnal wind stress amplitudes, and combined (large scale plus diurnal) wind stress amplitudes for the longshore and cross-shelf components used to drive the model. Day zero in the model integration corresponds to 0000Z on 22 March, 1977.

In this version of the model, no attempt is made to simulate the longshore wind structure due to a lack of a detailed knowledge of the horizontal longshore variability of the wind field and the time evolution of the horizontal structure. The best available source of information on the near shore horizontal structure are the 500 ft. aircraft wind charts (Watson, 1978; and Moody, 1979). These charts which are from flights centered on local noon for selected days, give a good indication of the horizontal structure during the sea-breeze portion of the diurnal land/sea-breeze cycle. However, to adequately parameterize the effects of the longshore variability, we need to know what the horizontal structure is during the land-breeze portion of the diurnal cycle and have some indication as to the time evolution of this structure. These latter data are not available.

Remote   A parameterization scheme based on coastal trapped wave dynamics is employed to simulate the longshore current variability.

From the simplest set of equations which contain coastal trapped Kelvin waves, (for any given mode);

$$fv = g \frac{\partial h}{\partial x} \tag{56}$$

$$\frac{\partial v}{\partial t} = -g \frac{\partial h}{\partial y} \tag{57}$$

$$\frac{\partial v}{\partial t} = -g \frac{\partial h}{\partial y} \tag{57}$$

$$\frac{\partial h}{\partial t} = -H_o \frac{\partial v}{\partial y} \quad . \tag{58}$$
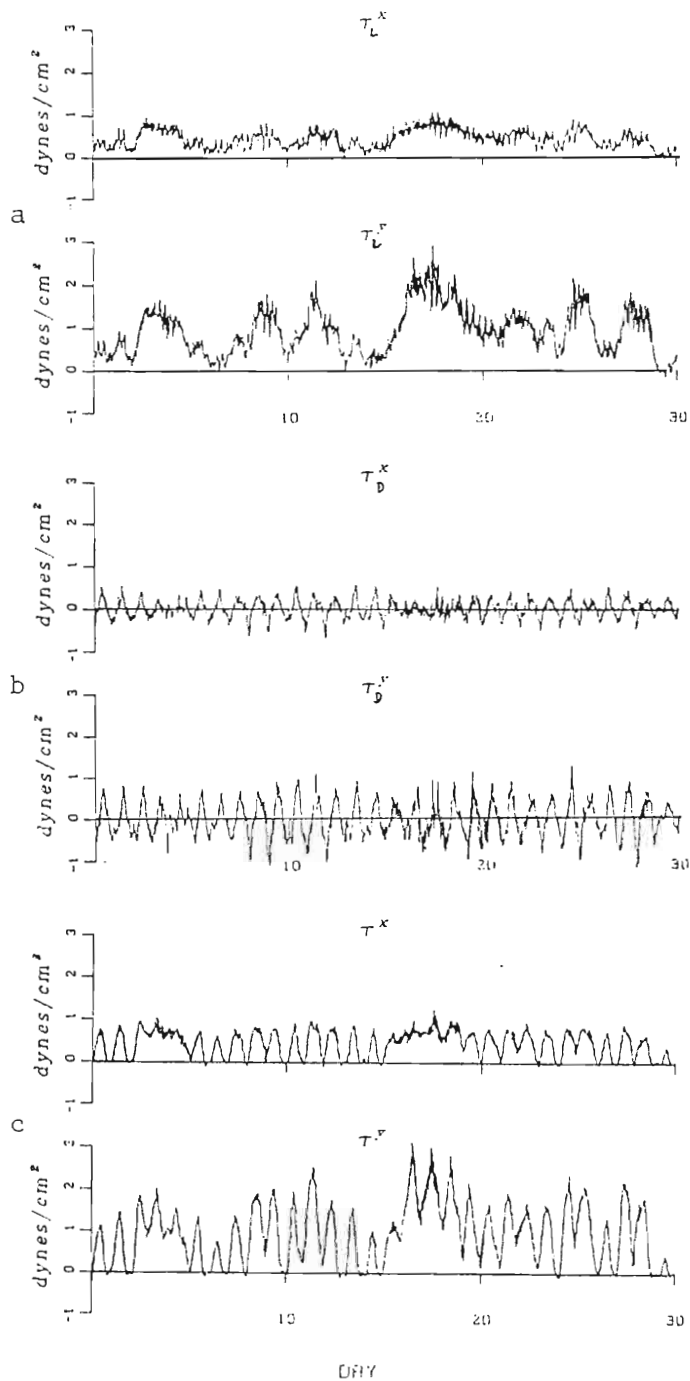
WIND STRESS

Fig. 8 . Wind Stress. This figure shows the time series of the wind stress amplitudes used to drive the model. a) The large scale forcing, b) the diurnal component and c) the total wind stress at the

it can be seen that the local time rate of change of the longshore velocity component is proportional to the local longshore pressure gradient. Therefore, by using the appropriate equivalent depth, phase speeds and wave lengths estimated from observations, it is possible to parameterize the longshore pressure gradients induced by the Kelvin waves using a time series of the longshore currents. For this purpose, the time series of low-pass filtered, longshore velocity components from Oregon State University's current meter mooring, Yucca-Too (12°05'S, 77°20'W, see Fig. (2)) located on the continental shelf equatorward (upstream) of the model basin, are decomposed into their first and second empirical orthogonal vertical modes.

Smith (1978) has shown that the primary Kelvin wave mode has an equivalent depth of around 400 m, a phase speed of around 200 km/d and a trapping scale of about 70 km. This mode will appear as depth independent motions over most of the shelf.

The amplitudes of the first empirical orthogonal mode are time differenced, converted to local longshore pressure gradients and then applied, with the appropriate phase shift (based on 200 km/d phase speed and assuming long wave lengths) as a depth independent body force within the trapping length scale along the northeastern boundary. Similarly, the second mode amplitudes (which have an equivalent depth corresponding to the upper layer thickness) are time differenced, converted to longshore pressure gradients, and applied as a layer dependent force within the appropriate trapping length scale (approximately 20-25 km).

f. MIXING PARAMETERIZATION

The purpose for adding thermodynamics and interfacial mixing to the model is twofold. The first reason is to include the potentially important physics which has been neglected in most upwelling models. The second is to provide a physical mechanism to keep the interface from surfacing and thereby allow the integrations to proceed further than the five to ten-day limitation in the hydrodynamic models.

This second objective cannot be achieved by wind mixing alone in a model which includes forcing mechanisms other than a constant wind stress. Under the influence of variable winds and propagating internal waves, there are times when the pycnocline (which is represented in the model by the interface) will intersect the surface. This condition cannot be modelled directly with a layered model where the interface represent a Lagrangian (material) surface. To model this situation, we must at some point in the vertical replace the Lagrangian vertical coordinate with an Eulerian or fixed level vertical coordinate.

We will for this model consider three regions in the vertical. In the first region, where $h_1 > h_{MLD}$ and h_{MLD} is the upper layer thickness determined from a mixed layer model, we will assume that the wind stress is strong enough to only mechanically stir the upper layer and that no interfacial mixing is occurring.

For the second region, where $h_{MIN} < h_1 < h_{MLD}$, we will assume that the wind stress is sufficient to erode the pycnocline and that the entrainment rate is a function of the Richardson number. Finally in the last region, where $h_1 < h_{MIN}$, we will set h_1 equal to h_{MIN} and entrainment rate is a function of the Richardson number. Finally in the last region, where $h_1 < h_{MIN}$, we will set h_1 equal to h_{MIN} and calculate the mass flux through the interface from the vertically inte-grated three dimensional mass continuity equation.

Following the lead of Martin and Thompson (1977), we will use the Pollard, Rhines, and Thompson, PRT, (1973) model to calculate the h_{MLD} (which we will refer to as the stabilized mixed layer depth) for a given wind stress and stratification.

In the PRT model, it is assumed that the bulk Richardson number,

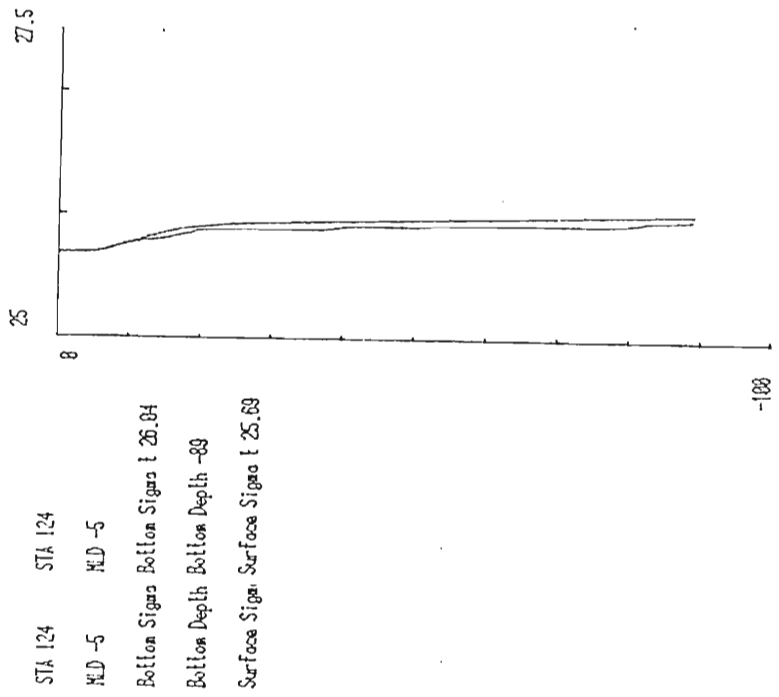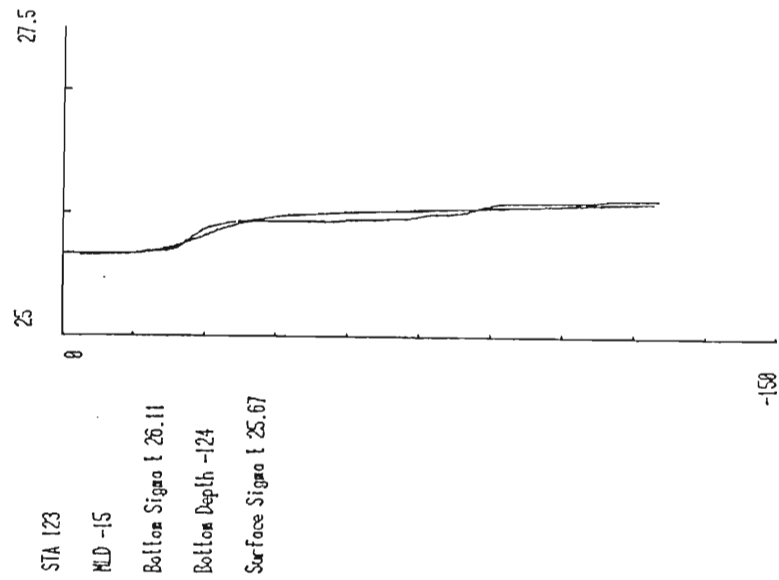$$R_{i_B} = \frac{g\Delta\rho h_{MLD}}{((\Delta u)^2 + (\Delta v)^2)\rho_o} \tag{59}$$

(where $\Delta\rho$, Δu and Δv are the density and velocity differences, across the base of the mixed layer) is equal to one for complete wind mixing. Then by setting $R_{i_B} = 1$, we get for the stabilized mixed layer depth,

$$h_{MLD} = \frac{((\Delta u)^2 + (\Delta v)^2)\rho_o}{g\Delta\rho} \tag{60}$$

To calculate the stratification, Martin and Thompson stored the perturbation temperatures at discrete grid points below the surface layer. In order to save storage space, instead of retaining the density at a series of grids points below the upper layer, we use an analytic density function which was derived by fitting CTD profiles, from the JOINT II area taken during MAM '77, to a hyperbolic tangent function. Fig. 9 is example of the data fit using profiles picked at random. The profiles displayed were not used in the data fitting routine. The density function has the form
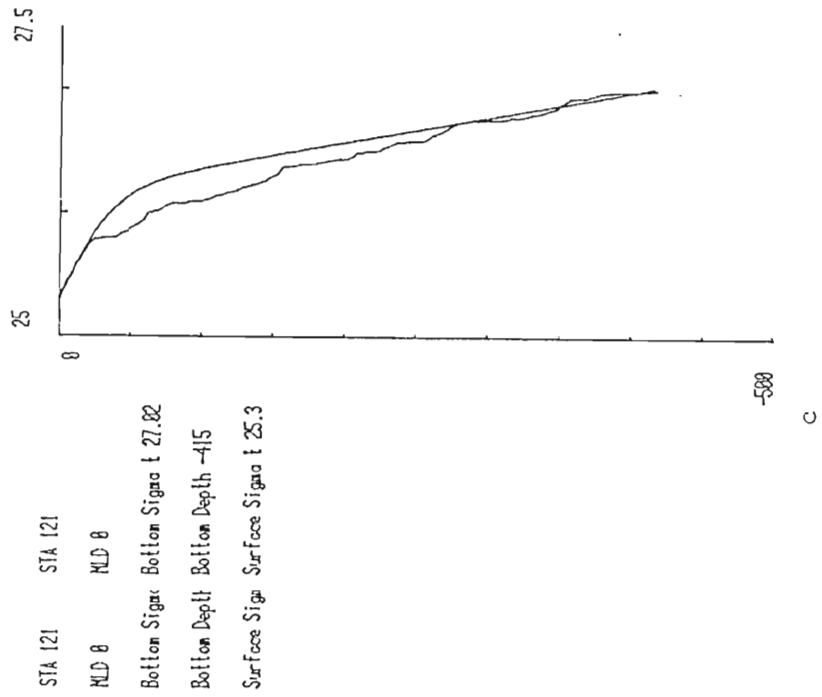
$$\rho(z) = \rho_B + C(\alpha z + \tanh\left(\frac{z - z_o}{s}\right) + b) \tag{61}$$

Fig. 9. Examples of CTD data fit to the analytic density function.

STA 121   STA 121

MLD 0   MLD 0

Bottom Sigma Bottom Sigma t 27.82

Bottom Depth Bottom Depth -415

Surface Sigma Surface Sigma t 25.3

STA 119

MLD -2.5

Bottom Sigma t 27.29

Bottom Depth -824

Surface Sigma t 24.92

Fi   Fig. 9c and d.

$$b = \tanh\left(\frac{z_o}{s}\right) \tag{62}$$

$$c = \left(\rho_T - \rho_B\right) \Big/ \left(\alpha + \tanh\left(\frac{1-z_o}{s}\right) + b\right) \tag{63}$$
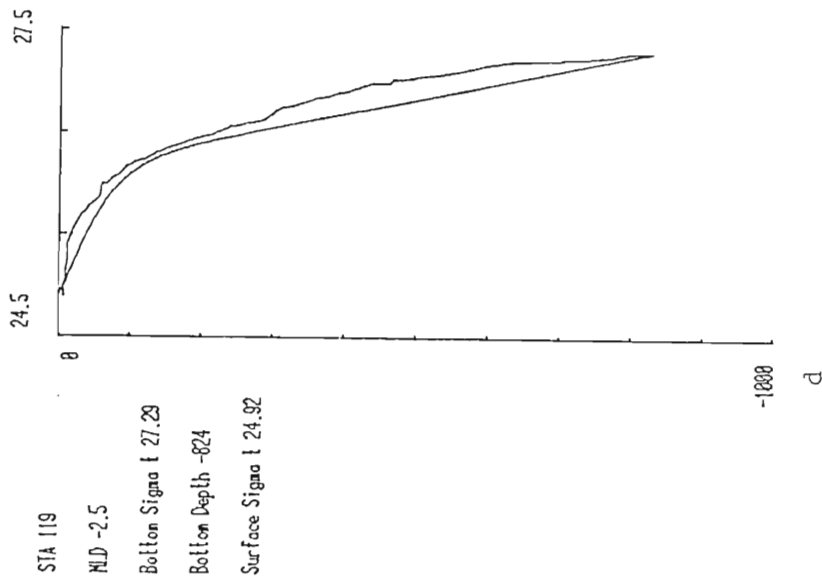
where ρ_T and ρ_B are top and bottom densities respectively, z is the non-dimensional vertical coordinate, which is scaled by the total fluid depth, and z_o is the scaled height of the pycnocline above the bottom. The parameters α and s determine the shape of the profile and are determined empirically from the CTD profiles.

After the mixed layer depth is determined in this manner, it is then compared with the thickness of the upper layer, h_1. If $h_1 > h_{MLD}$ no mixing occurs. If $h_1 < h_{MLD}$ and $h_1 > h_{MIN}$, where h_{MIN} is the minimum allowable upper layer thickness, then the entrainment rate is specified as

$$Q_1 = \phi \, u_* \, R_i^{-1} \tag{64}$$

where

$$R_i = \frac{g\Delta\rho h_1}{u_*^2} \tag{65}$$

or

$$Q_1 = \frac{\phi \, u_*^3}{g\Delta\rho h_1} \tag{66}$$

where ϕ is a constant of proportionality. Finally, if $h_1 < h_{MIN}$, then we let

then we let

$$Q_1 = \bar{u}_* \left(\frac{\partial D}{\partial x} + \frac{\partial D}{\partial y}\right) - h_2 \left(\frac{\partial u_2}{\partial x} + \frac{\partial v_2}{\partial y}\right) \tag{67}$$

where $\bar{u}_*$ is the bottom friction velocity, D is the height of the bottom topography, h_2 is the thickness of the lower layer and u_2 and v_2 are the vertically averaged lower layer velocity components.

g. HEATING

Thompson (1974) examined both heated, and non-heated versions of his x-z mixing model. He found that the primary effects of heating was to strengthen the zonal sea surface temperature (SST) contrast and enhance frontal intensification. His formulation of the heating function included diurnal variations, but he found that the effects of these diurnal variations were minimal. To keep an already complex model as simple as possible, we will use a simple approach to the heating, i.e., we will use a constant heating rate. In particular, we will use an estimate based on the observations from the JOINT II region.

h. CROSS-SHELF PHYSICS

The primary premise for this model is that Ekman dynamics are important to the vertical structure of the flow field. Invoking this premise, and using a method developed by Thompson (1974), continuous analytical solutions can be obtained for the departures from the vertically integrated layer velocity fields, and thereby introduce boundary layers near the internal and external fluid interfaces. Defining $\vec{V}'_j$ as the departure from the vertically integrated velocity, $\vec{V}_j$, within each layer we can then determine the total velocity field,

$$\vec{V}_{Ti} = \vec{V}'_i + \vec{V}_i \qquad (68)$$

$$\vec{V}_{Tj} = \vec{V}'_j + \vec{V}_j \qquad (68)$$

The departures can be calculated from the Ekman equations

$$k \times f\vec{V}_j' = A_v \frac{\partial^2 \vec{V}_j}{\partial z^2} \quad ; \quad j = 1,2 \tag{69}$$

Then by letting $z = 0$ be the sea surface, $z = b$ be the layer interface, $z = c$ be the bottom, and defining the complex velocities as

$$w_j = u_j' + iv_j' \quad ; \quad i = \sqrt{-1} \tag{70}$$

the problem becomes

$$\frac{\partial^3 w_1}{\partial z^3} - s^2 \frac{\partial w_1}{\partial z} = G_1 \qquad b \leq z \leq 0 \tag{71}$$

$$\frac{\partial^3 w_2}{\partial z^3} - s^2 \frac{\partial w_2}{\partial z} = G_2 \qquad c \leq z \leq b \tag{72}$$

where

$$s = (1 + i)(f/2 \, Av)^{\frac{1}{2}} \tag{73}$$

$$G_j = -\frac{g}{\rho_o Av} \left[\frac{\partial p_j}{\partial x} + i \frac{\partial p_j}{\partial y} \right] \quad ; \quad j = 1,2 \tag{74}$$

with the integral constraint on the system that the vertically inte grated perturbation velocities in each layer are zero, i.e.

grated perturbation velocities in each layer are zero, i.e.

$$\int_o^b w_1 dz = \int_o^c w_2 dz = 0 . \tag{75}$$

The boundary condition required to close the problem are; (1) at the surface, $z = 0$, the perturbation velocity shear stress is set equal to the wind stress,

$$\frac{\partial w_1}{\partial z} = \frac{\tau_{sx}}{Av} + i\frac{\tau_{sy}}{Av} \quad ; \tag{76}$$

(2) at the interface, $z = b$, the total velocity is continuous and the perturbation shears are set equal,

$$w_1 = w_2 - [(u_1-u_2) + i(v_1-v_2)] \tag{77}$$

and

$$\frac{\partial w_1}{\partial z} = \frac{\partial w_2}{\partial z} \quad ; \tag{78}$$

and (3) at the bottom, $z = c$, the total velocity is set equal to zero (no slip),

$$w_2 = -(u_2 + i\, v_2) \tag{79}$$

The total velocity for any point in the vertical therefore can be determined by adding the perturbation velocity to the vertically integrated layer velocity.

integrated layer velocity.

CHAPTER 4

1. MODEL RESULTS

a. HYDRODYNAMIC MODEL

Since a numerical model of this complexity generates a considerable amount of data, which is almost as difficult to interpret as observational data, we will restrict our discussion of the interaction between undercurrents and the bottom topography to the flow in the lower layer and the displacement of the interface.

For this case study the model is started at 0000Z 22 March, 1977, and run for ten days. March 22nd was selected as the starting date because the lower layer currents along the C-line (y = 0 in the model) and the winds closely approximated the model's quiescent initial conditions (i.e., winds and currents equal to zero). Furthermore, starting on the 22nd we can observe the passage of a wave with approximately a ten-day period.

The model run is restricted to ten days because, as with all the hydrodynamic upwelling models, the interface will eventually surface. With this particular case the interface will surface around day 12 and the upper layer motion becomes physically unrealistic the last day or two as the upper layer thickness approaches zero.

The scenario we will see in this case study is first the passage

The scenario we will see in this case study is first the passage of a trough with its associated strengthening of the poleward undercurrent followed by a crest and subsequent weakening of the undercurrent.

55

This can be seen graphically in Fig. 10. This figure shows the lower layer flow in a vector plot for days 1 through 10. As can be seen, the poleward flow first increases, then decreases and finally reverses by day 10.

The longshore component of the flow is forced primarily by two factors, the wind stress curl and the externally forced Kelvin wave. The mean poleward flow is the result of the cross-shelf curl of the wind stress as specified in Eq. (53). The variability in the longshore component is induced by the Kelvin wave parameterization and the interaction with the bottom topography.

The cross-shelf component is primarily the result of: (1) the interaction of the Kelvin wave and the bottom topography, and (2) the required onshore flow to compensate for the offshore mass transport in the upper Ekman layer. The horizontal and vertical structure of the flow is dependent on the phase of the Kelvin wave.

To examine the interaction between the Kelvin wave and the topography in detail, we will first consider the large scale effect due to the wave propagation. From Eq. 4 we can obtain,

$$\frac{\partial}{\partial t}\left(\zeta + \frac{f\eta}{D}\right) \propto -v\frac{\partial}{\partial y}\left(\zeta + \frac{f\eta}{D}\right) . \tag{80}$$

Now as a trough passes with its resultant increase in the poleward flow, we would expect a large scale increase in relative vorticity and a large scale negative displacement in the upper surface (interface). Also, as a crest passes, we would expect a large scale decrease in

Also, as a crest passes, we would expect a large scale decrease in

Fig. 10. Lower Layer velocity vectors (VVL) for days one through ten of a ten day model run.
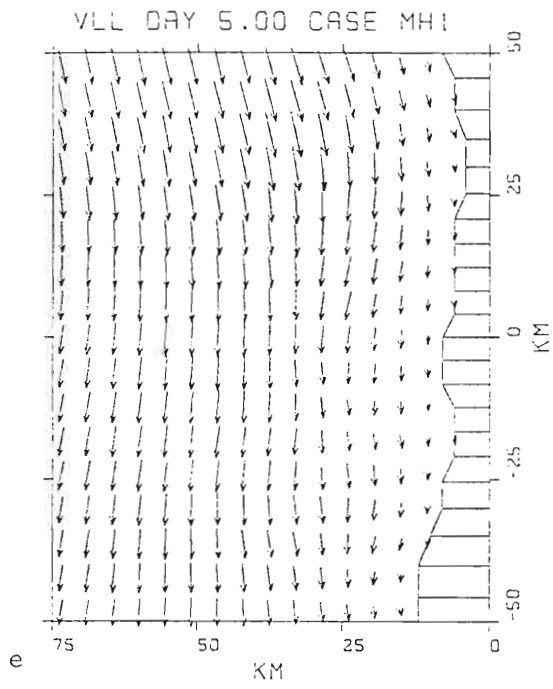
Fig. 10. Lower Layer velocity vectors (VVL) for days one through ten of a ten day model run.

VLL DAY 5.00 CASE MH1

VLL DAY 6.00 CASE MH1

VLL DAY 7.00 CASE MH1

VLL DAY 8.00 CASE MH1
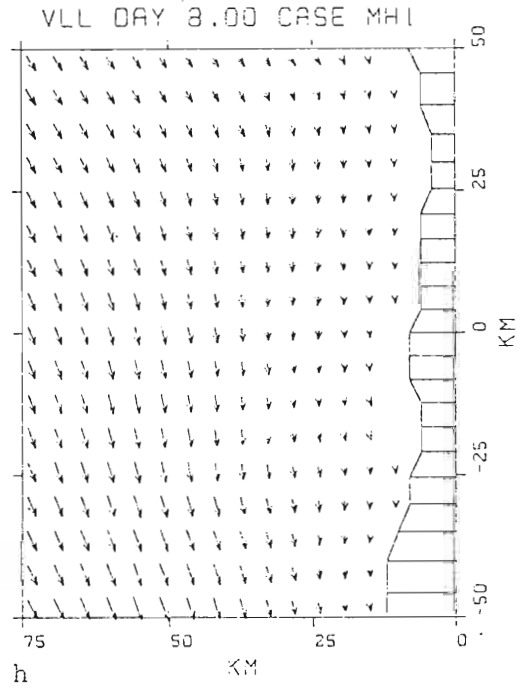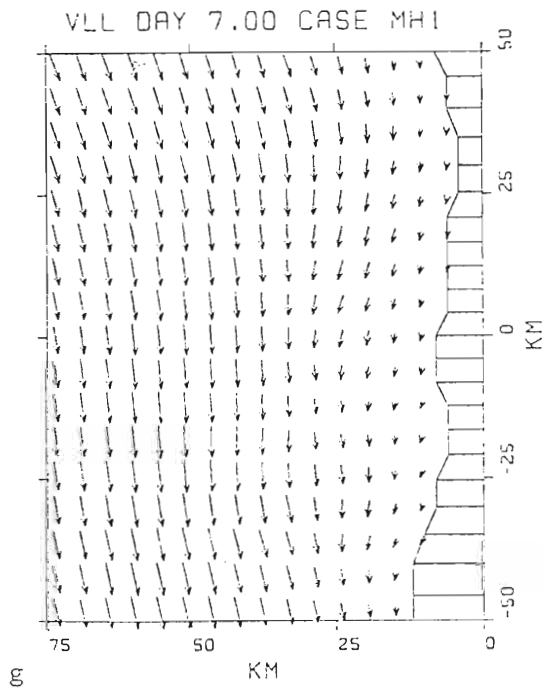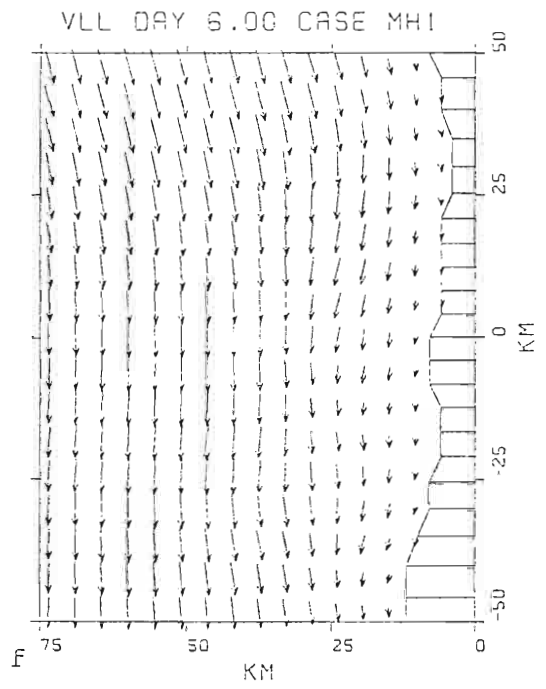
Fig. 10e, f, g, and h.

Fig. 10e, f, g, and h.

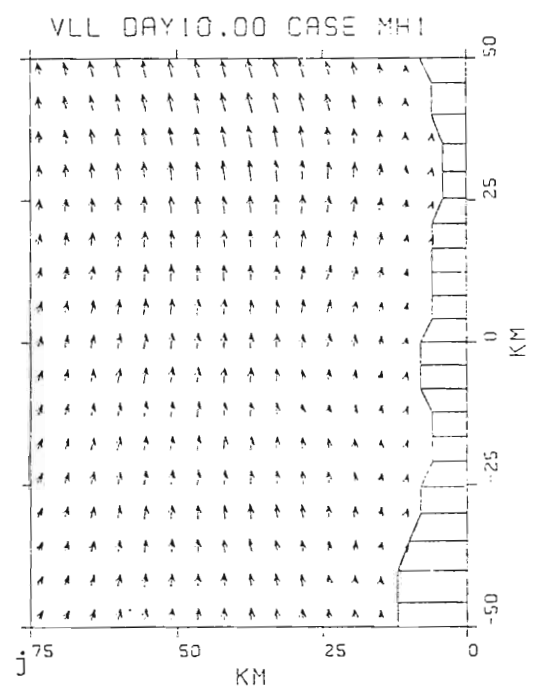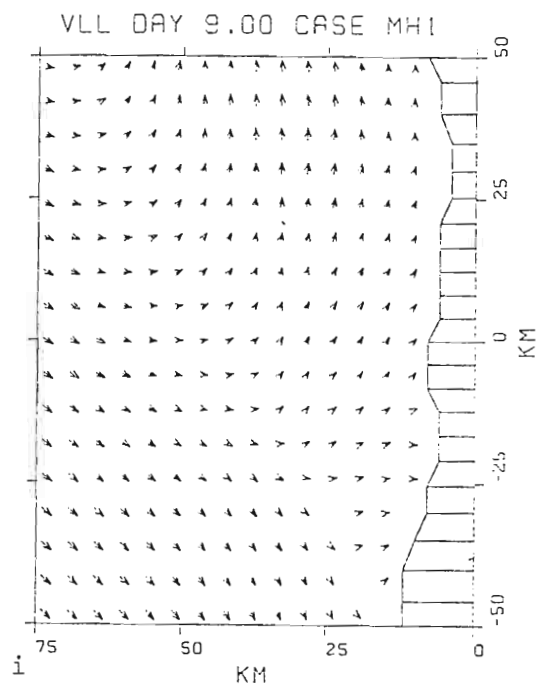VLL DAY 9.00 CASE MH1

VLL DAY 10.00 CASE MH1

Fig. 10i and j.

relative vorticity and a large scale positive displacement in the upper surface (interface). From Fig. 11, which shows the lower layer long-shore velocity component for days 3, 5, 7 and 9, we can see that the large scale relative vorticity increases with the trough passage, (day 1 through 5), and decreases with the passage of the crest,(day 6 through 10). The large scale effect on the interface displacement is not as readily evident since the interface displacement due to the upwelling favorable wind stress tends to mask the displacement due to the wave propagation. The effect due to the wave propagation is to retard the upward displacement due to the wind stress during the passage of a trough and to aid the upward displacement when a crest passes. This can be seen in Fig. 12 by comparing the mean interface displacement between days 5 to 7 and 7 to 9. Also, this effect became more evident by comparing the interface displacement for this case and the March 1977 case presented in O'Brien et al., (1980). The model parameters and wind forcing for these two cases are the same. The only difference between these cases is the parameterization of the poleward undercur-rent. O'Brien et al., used a constant atmospheric pressure gradient to force the poleward undercurrent. This parameterization yielded only a weak steady undercurrent. The O'Brien et al., case yielded a steady rise in the interface of over 50m of mean upwelling within ten days, whereas the present case yields a variable rate of rise in the interface with only approximately 30m of mean upwelling by day 10.

Next, we will examine the localized effects due to the bottom day 10.

Next, we will examine the localized effects due to the bottom topography where we have
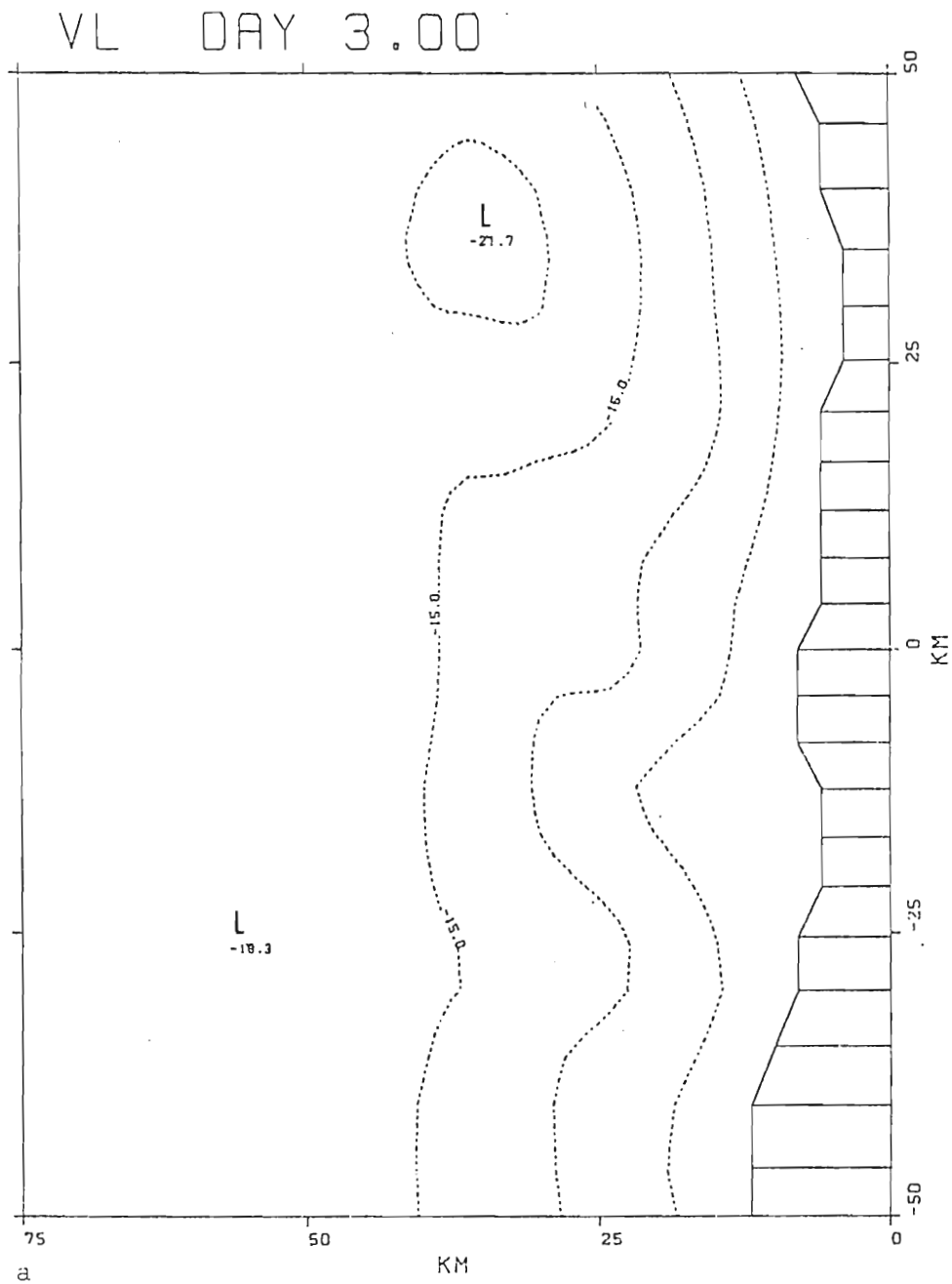
VL DAY 3.00

a

Fig. 11. Lower layer longshore velocity component (VL) in cm/sec for
model days 3, 5, 7 and 9 of a ten day model run. The contour interval
is 5 cm/sec. Dashed contours represent negative values.
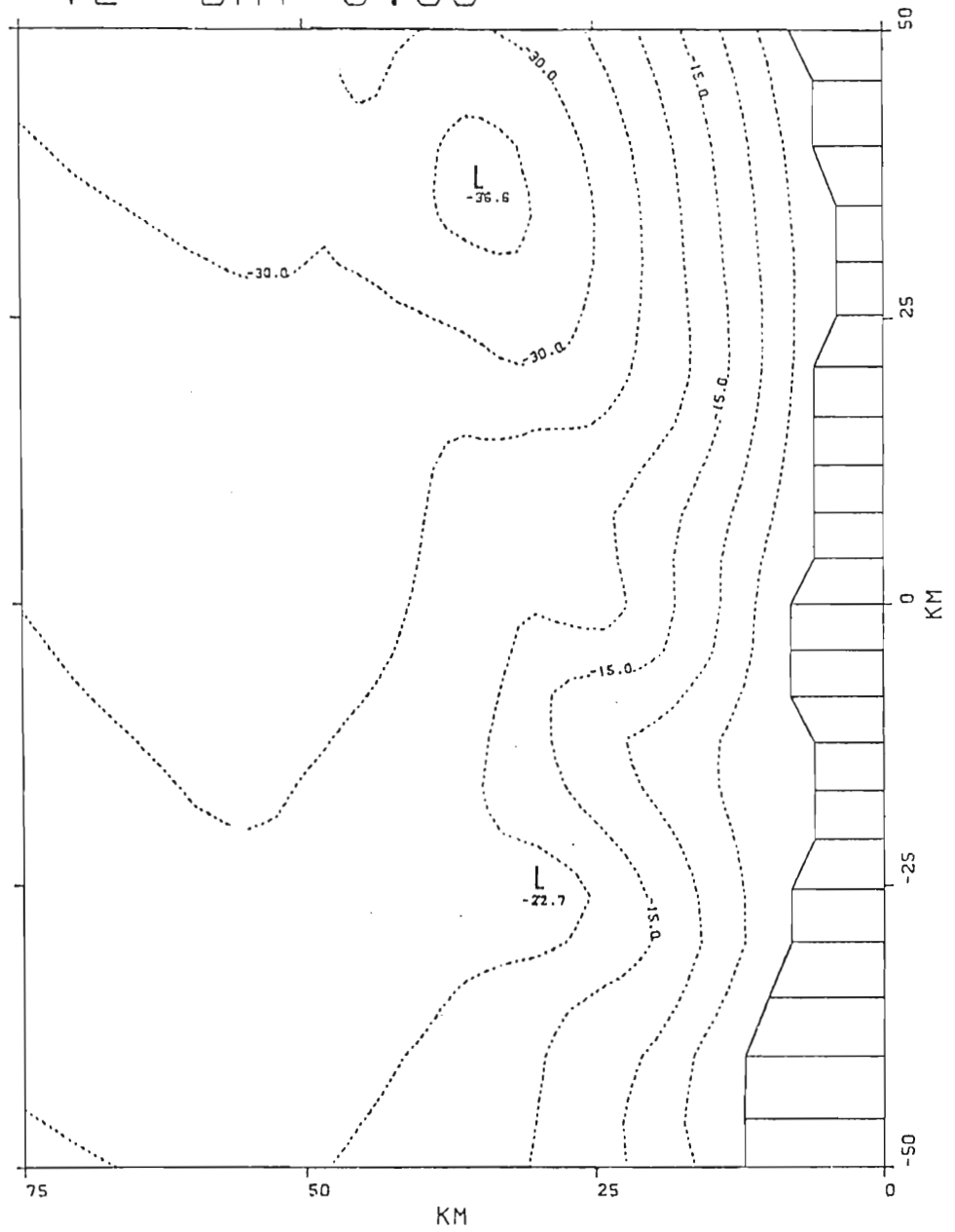
model days 3, 5, 7 and 9 of a ten day model run. The contour interval
is 5 cm/sec. Dashed contours represent negative values.

VL DAY 5.00

Fig. 11b

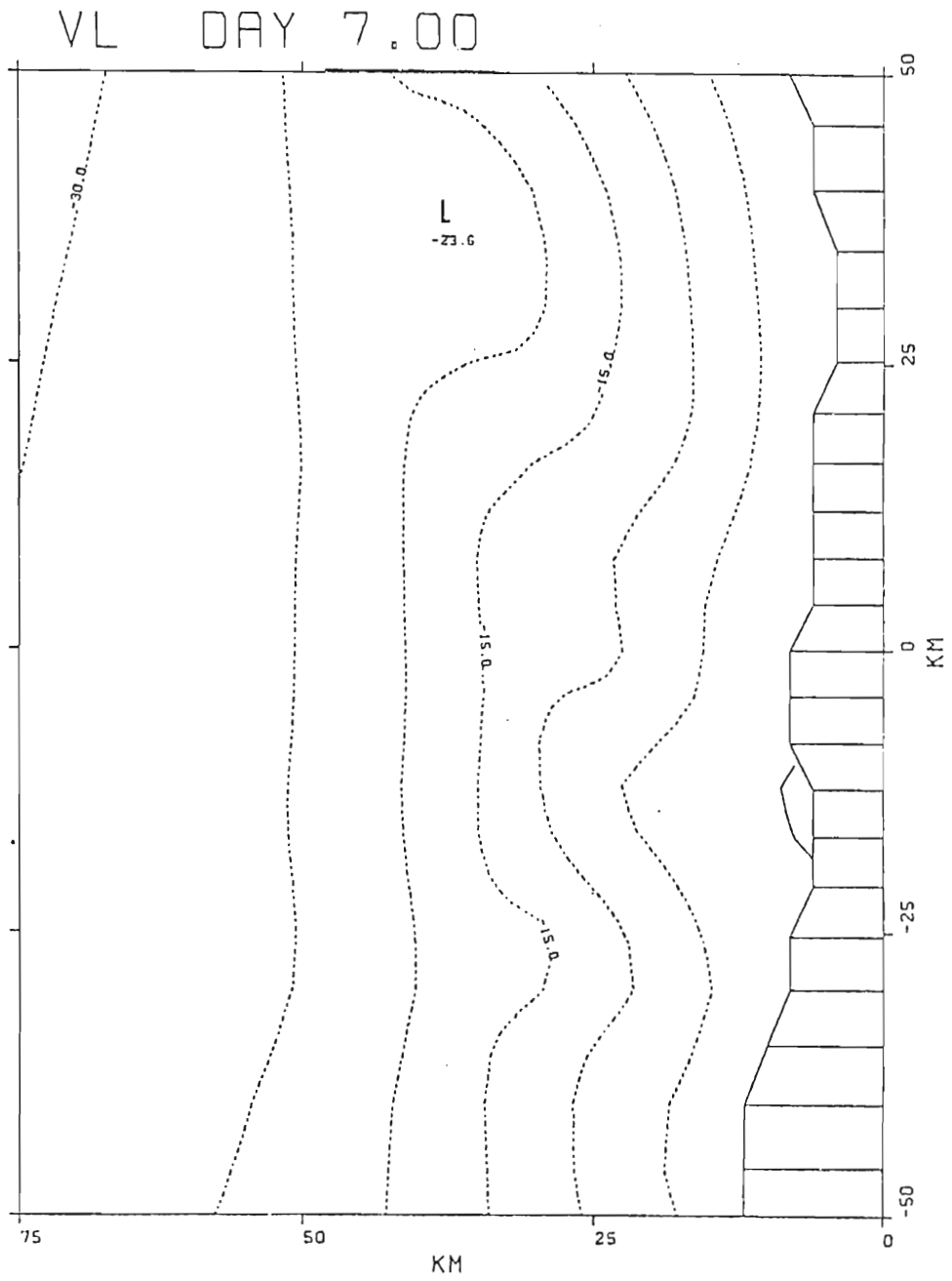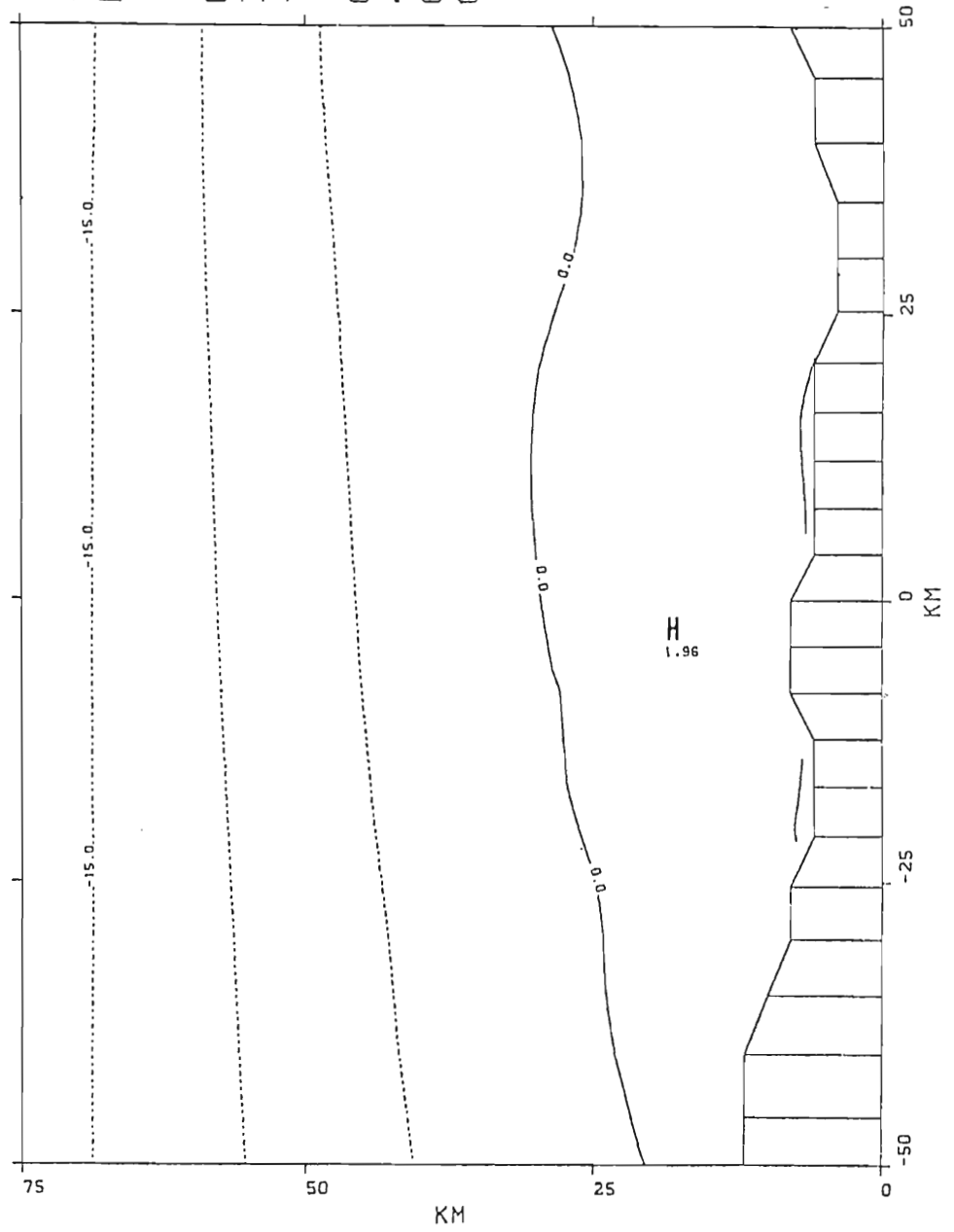VL   DAY 7.00

Fig. 11c.

VL DAY 9.00

Fig. 11d.

PA DAY 3.00

a
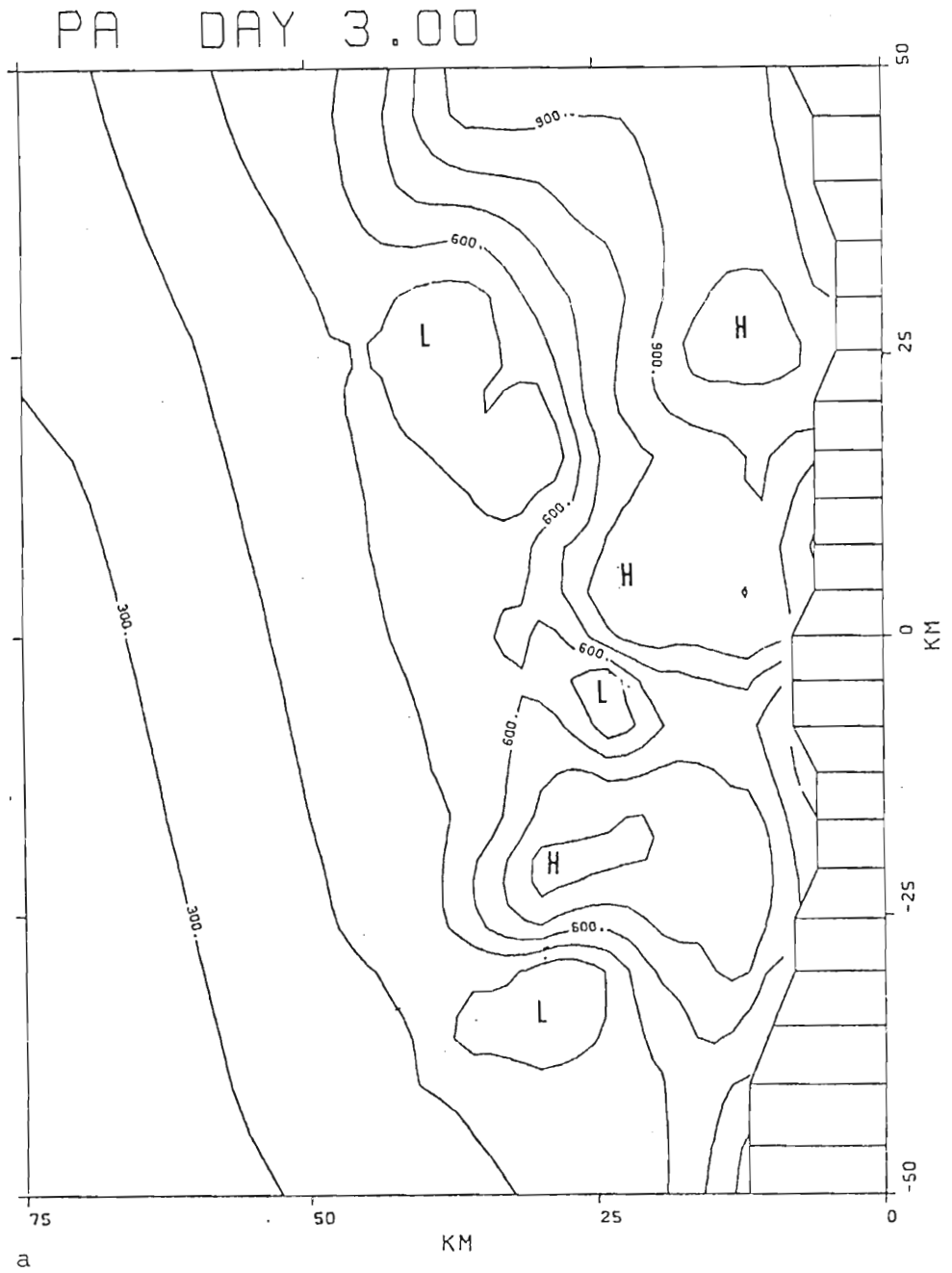
Fig. 12. Pycnocline height anomaly (PA) for model days 3, 5, 7 and 9 of a ten-day model run. Contour interval is 100 cm.

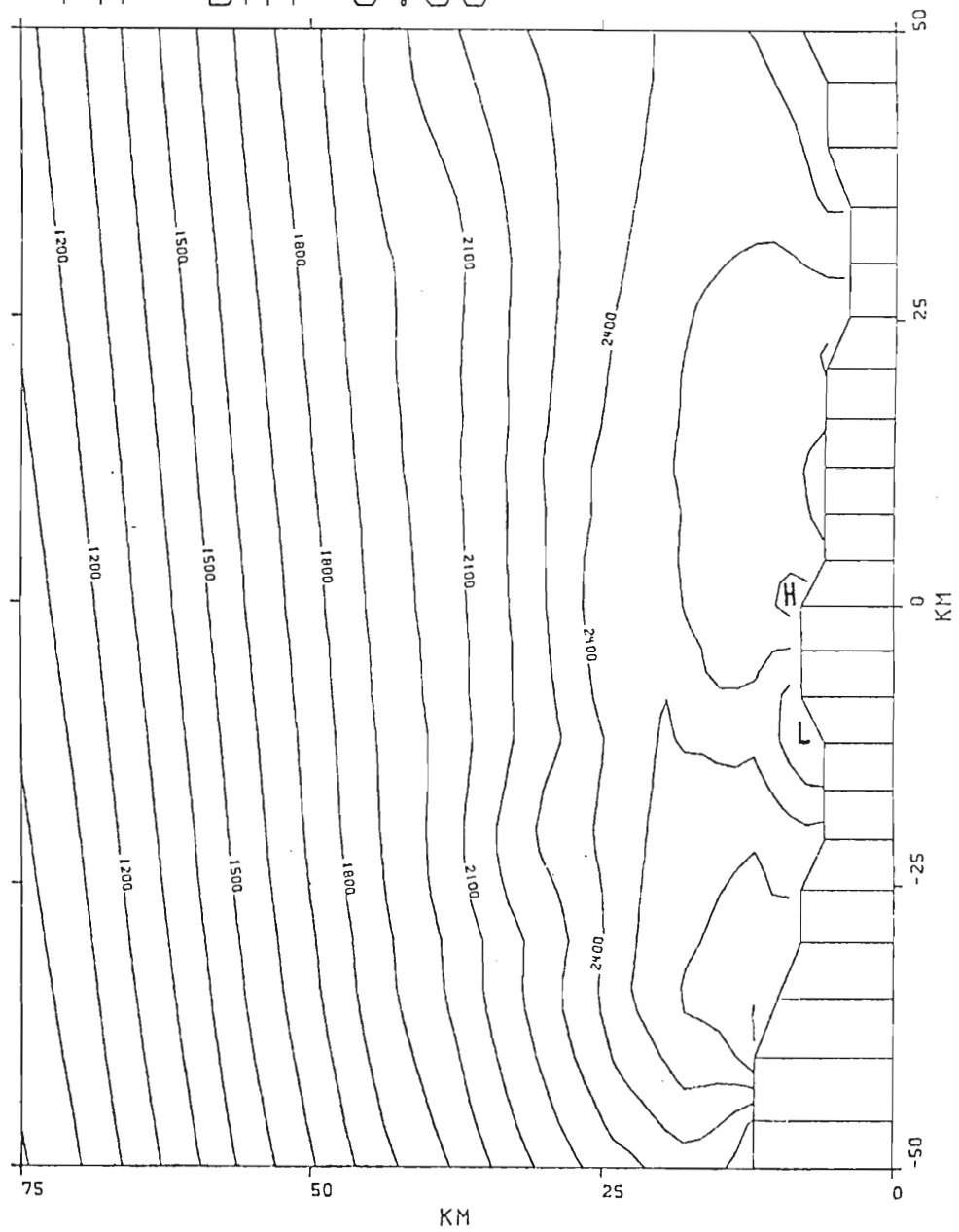PA   DAY 5.00
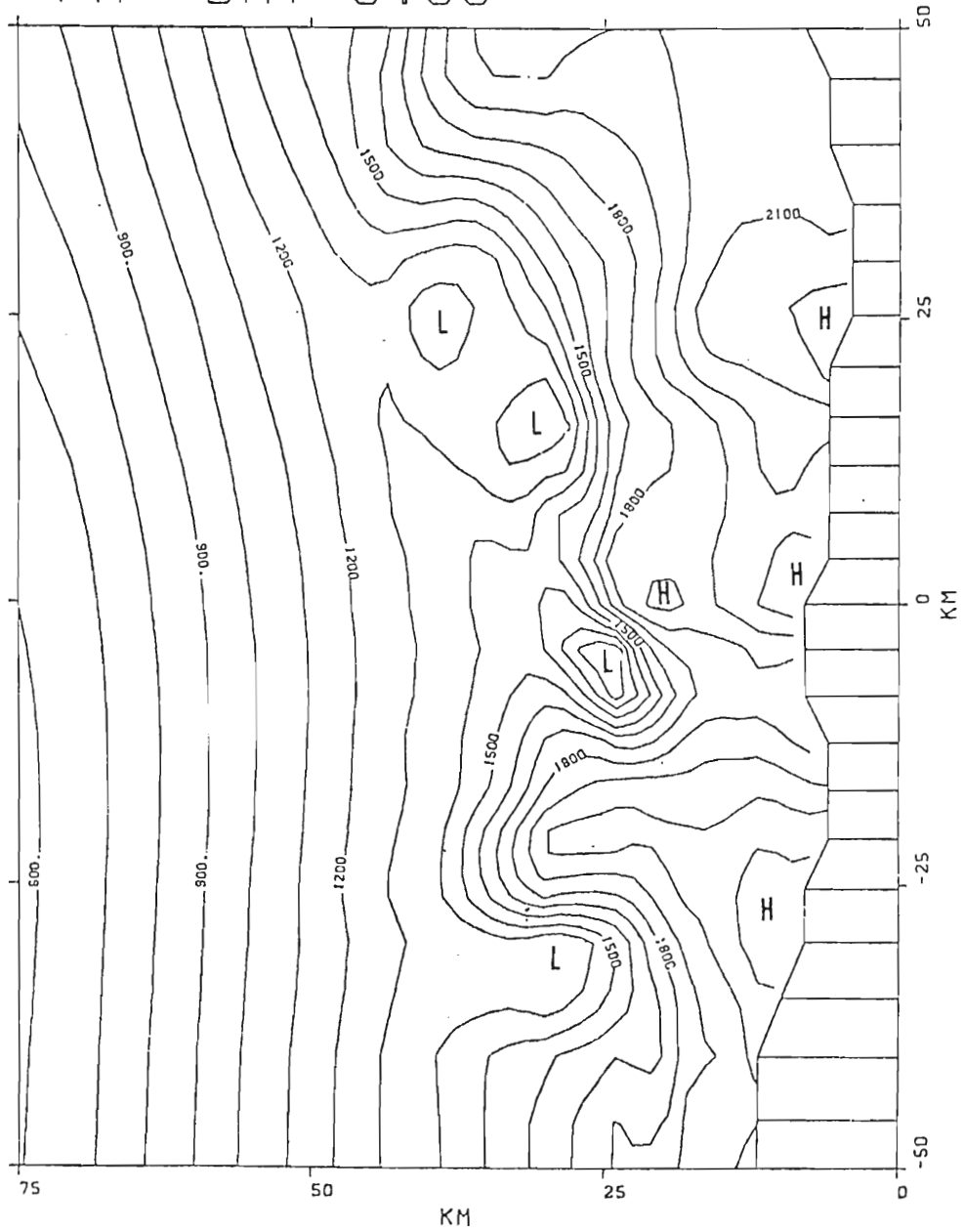
Fig. 12b.

PA DAY 7.00
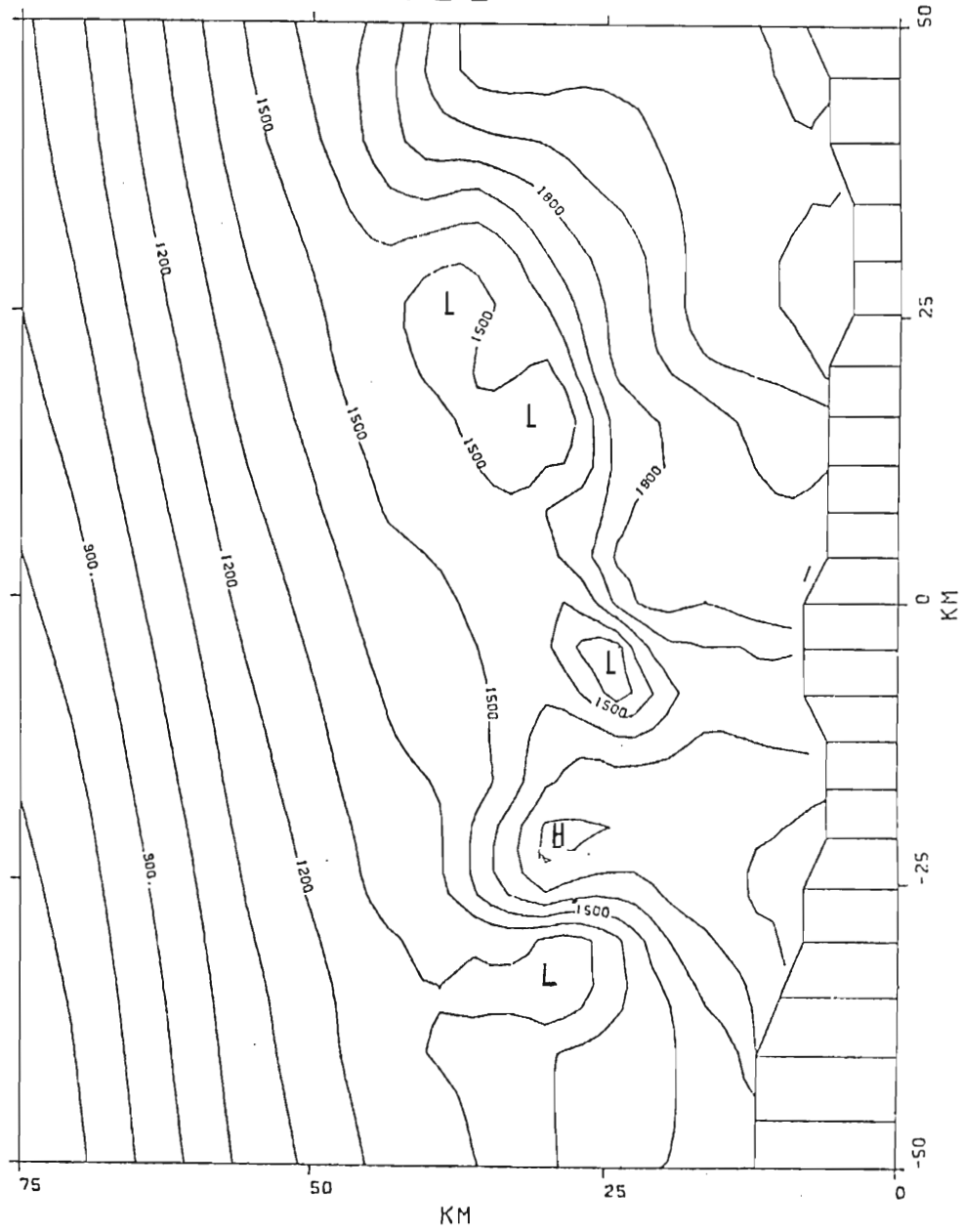
Fig. 12c.

PA   DAY 9.00

Fig. 12d.

Fig. 12d.

$$\frac{\partial}{\partial t}\left(\zeta + \frac{f\eta}{D}\right) \propto v \frac{\partial}{\partial y}\left(\frac{f H_B}{D}\right) \quad . \tag{81}$$

The longshore structure of the lower layer u (Fig. 13) and the v

(Fig. 11) velocity components can be directly related to relative

vorticity changes induced by the interaction of the longshore flow and

the bottom topography. In Fig. 11 we can see that for a strong pole-

ward flow we have a weakening of the offshore gradient in the longshore

component (implying a decrease in relative vorticity) where we have

downslope flow and a strengthening of the offshore gradient associated

with upslope flow. As the poleward flow weakens, we see a general

weakening of the offshore gradient of the longshore velocity component

and a reduced influence due to the topography (i.e., the gradients

become more zonal). In Fig. 13, we see that the longshore structure

in the cross-shelf can also be directly related to the relative vor-

ticity changes. Again we see for a strong poleward flow the structure

is strongly influenced by the topography and as the flow weakens, the

flow loses its longshore structure. By day 10, we see that the lower

layer cross-shelf flow is basically the result of onshore flow to com-

pensate for the offshore mass transport in the upper layer due to the

wind stress. Figure 14 shows the vertical structure of the longshore

and cross-shelf velocity components along the C-line (y = 0) for day

5 and 10. The technique for determining the total velocity

from the layer averaged velocities using Ekman dynamics is presented

in Thompson (1974), Preller and O'Brien (1980) and O'Brien et al.,

(1980). We can see in Fig. 14 that for day five with a strong poleward

in Thompson (1974), Preller and O'Brien (1980) and O'Brien et al.,

(1980). We can see in Fig. 14 that for day five with a strong poleward

undercurrent the onshore return flow is located at mid-depth with
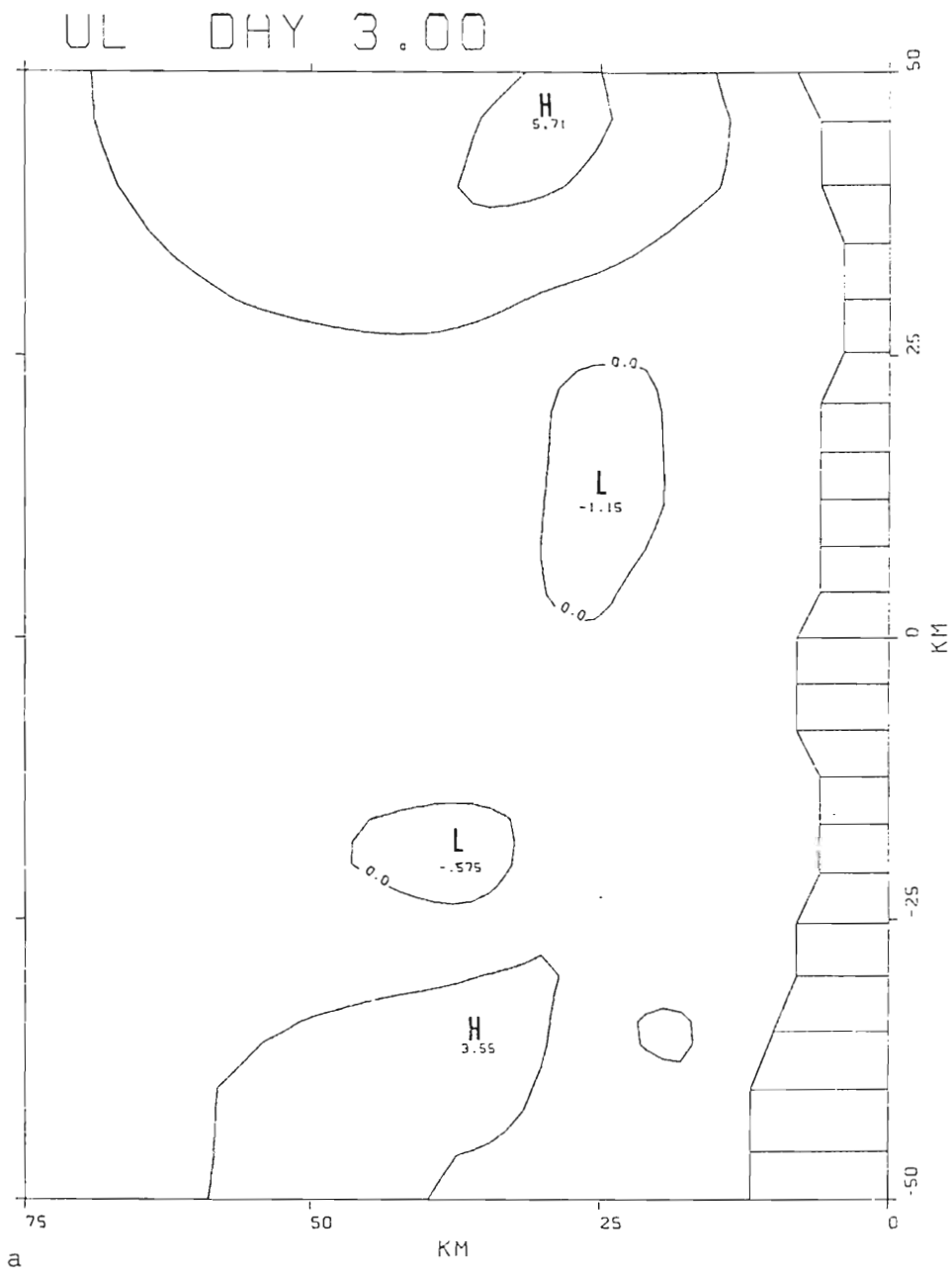
UL   DHY 3.00

a

Fig. 13.   Lower layer cross-shelf velocity component (UL) for
model days 3, 5, 7 and 9 of a ten-day model run. The contour interval
is 2.5 cm/sec and dashed contours represent negative values.

model days 3, 5, 7 and 9 of a ten-day model run. The contour interval
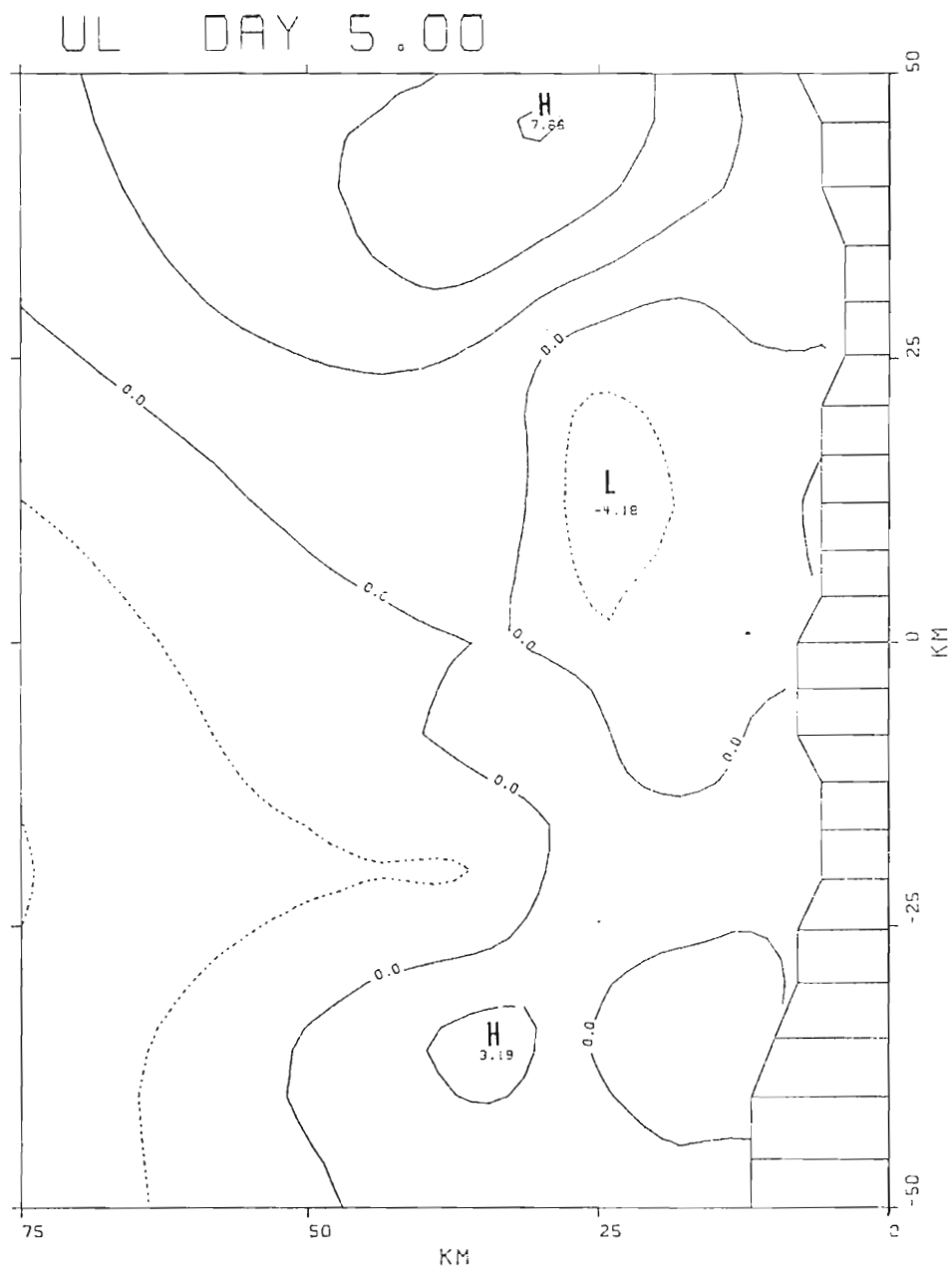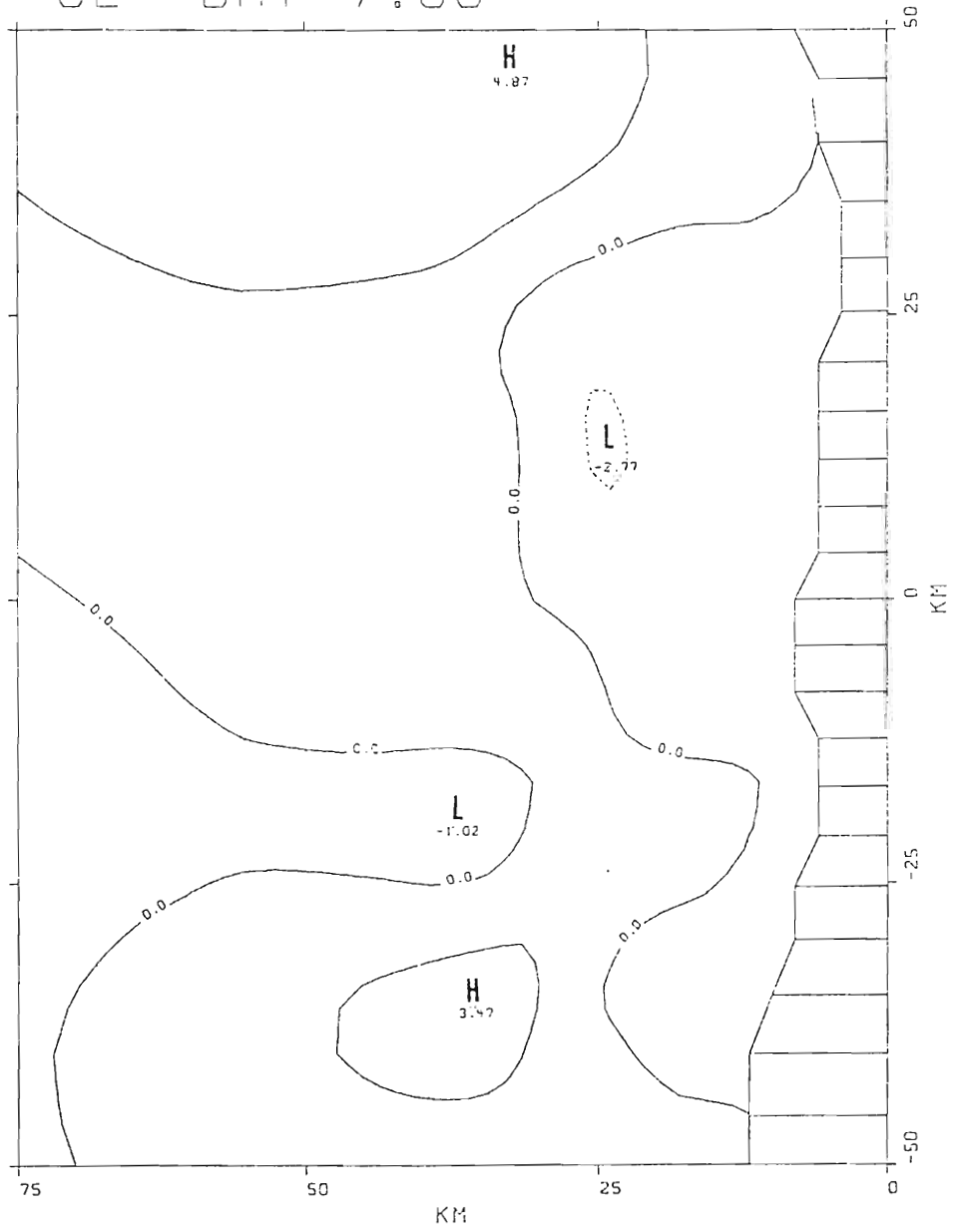is 2.5 cm/sec and dashed contours represent negative values.

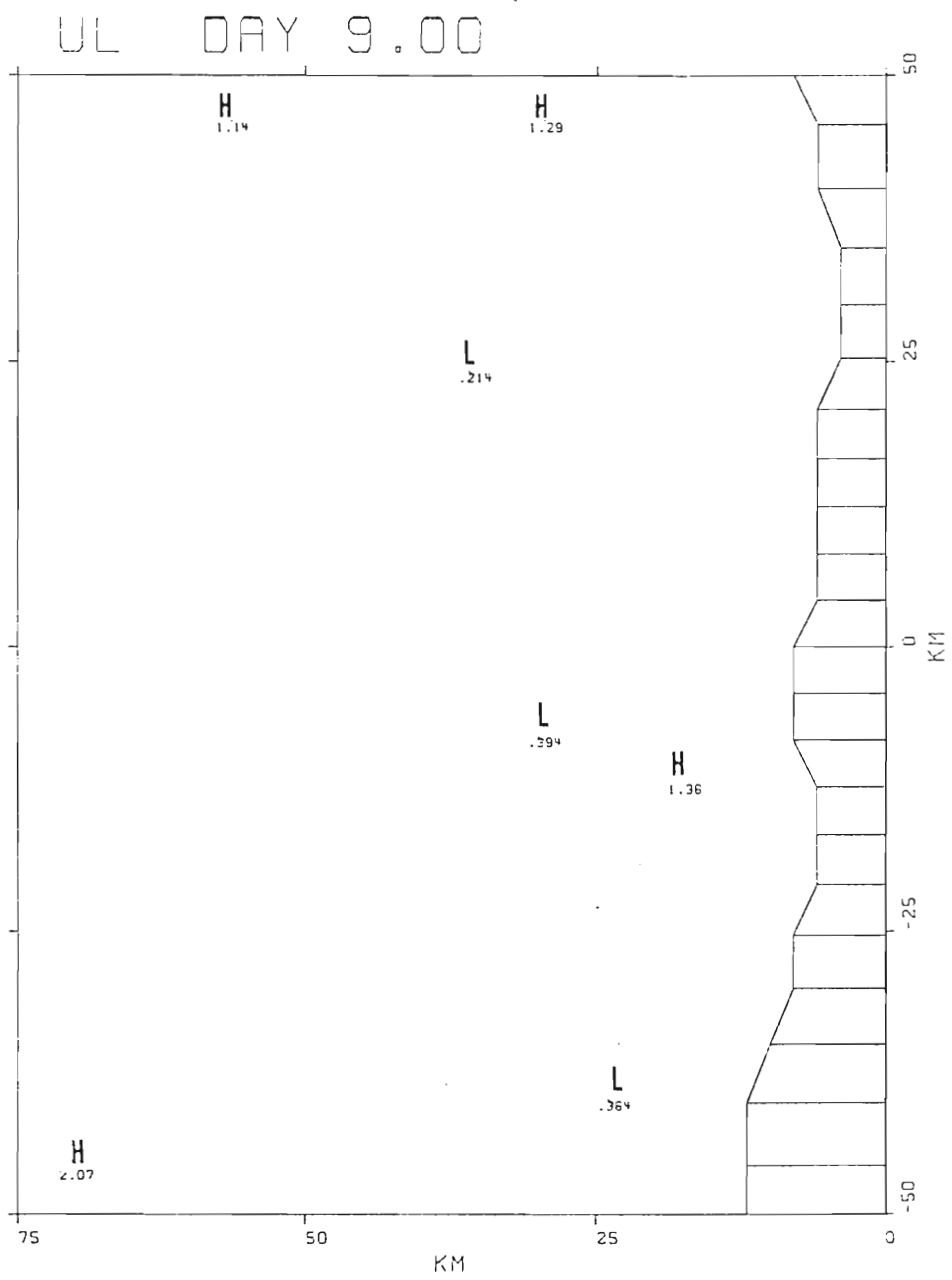Fig. 13b.

UL DAY 7.00

Fig. 13c.
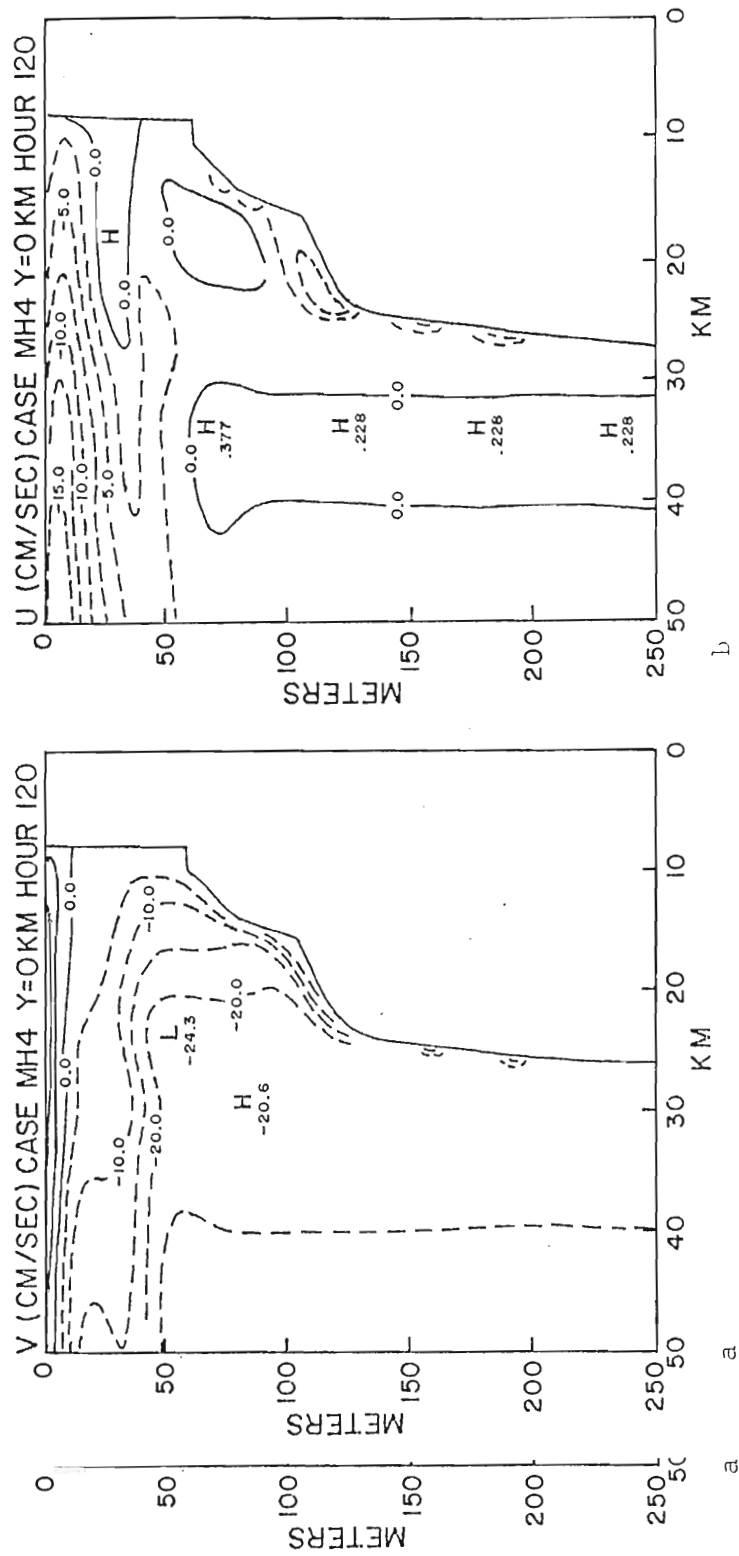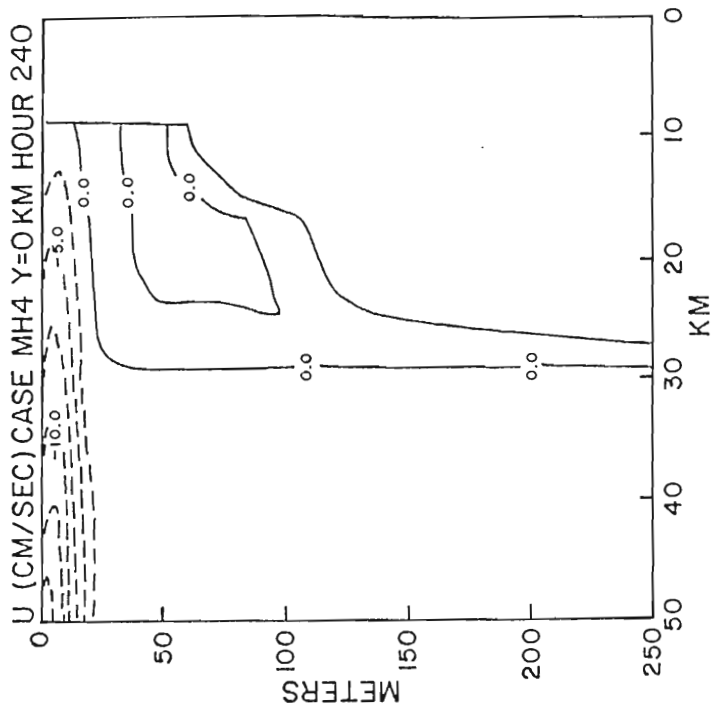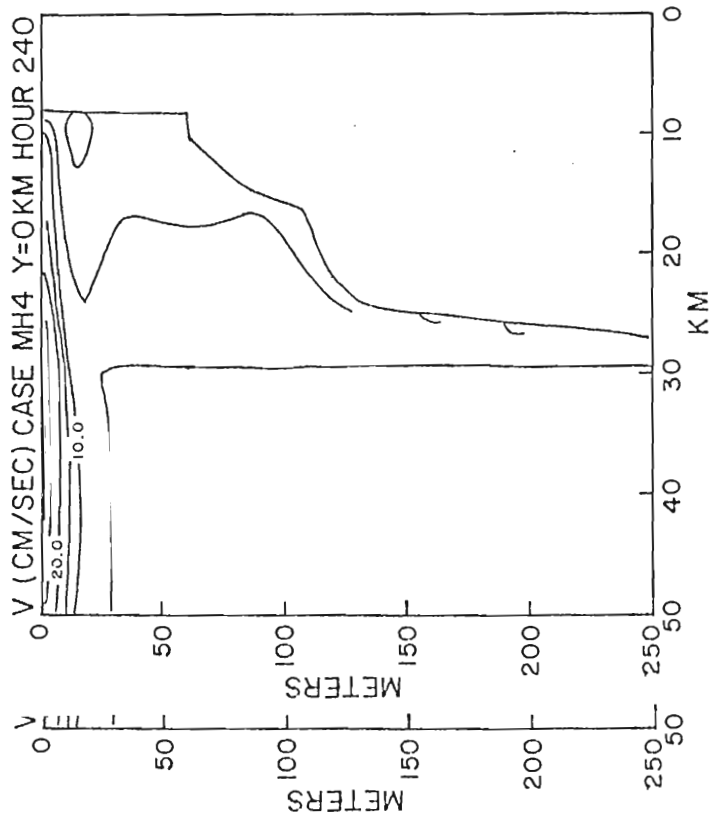
UL   DAY 9.00

Fig. 13d.

Fig. Fig. 14. Cross-shelf (x-z) sections along the C-line (y = 0 in model) of the longshore (v) and cross- cross-shelf (u) velocity components for model days five and ten. The contour interval for the u-compo u-component is 2.5 cm/sec and v-component is 5 cm/sec. Dashed contours represent negative values. ues.

Fig. 14c and d.

offshore flow in both the upper and lower Ekman layers. For day 10 with a weak equatorward flow in the undercurrent, we see that the onshore flow is basically in a bottom Ekman layer.

Now if we turn our attention to the interface displacement (Fig. 12), we see that with a strengthening of the poleward flow we have strong gradients in the interface displacements. The relative maxima and minima are fixed by the bottom topography consistent with the conservation of potential vorticity. Again, as with the velocity components, with a weakening of the poleward undercurrent, we see a reduction of the influence of the bottom topography (i.e., a reduction in the strength of the gradients between the relative maxima and minima) and a more zonal structure to the upwelling field. As can be see at day 9, we still have an area of increased upwelling off Punta Santa Ana which is caused by the upwelling induced by the interaction of the onshore bottom Ekman flow and the ridge located off Punta Santa Ana.

Figure 15 presents a side by side comparison of the bottom topography and the pycnocline height anomaly which can be contrasted with Fig. 16 to obtain a qualitative comparison of the upwelling field inferred from a more traditional indicator of upwelling. A direct quantitative comparison is not possible since the model neglects thermodynamics and vertical mixing processes. Fig. 16 is a sea surface temperature chart (from Moody, 1979) near the time simulated by day four of the model run. Contrasting these two figures, we see that the area of enhanced upwelling of Punta Santa Anna associated with the ridge in the bottom topography is in good agreement.

ridge in the bottom topography is in good agreement.

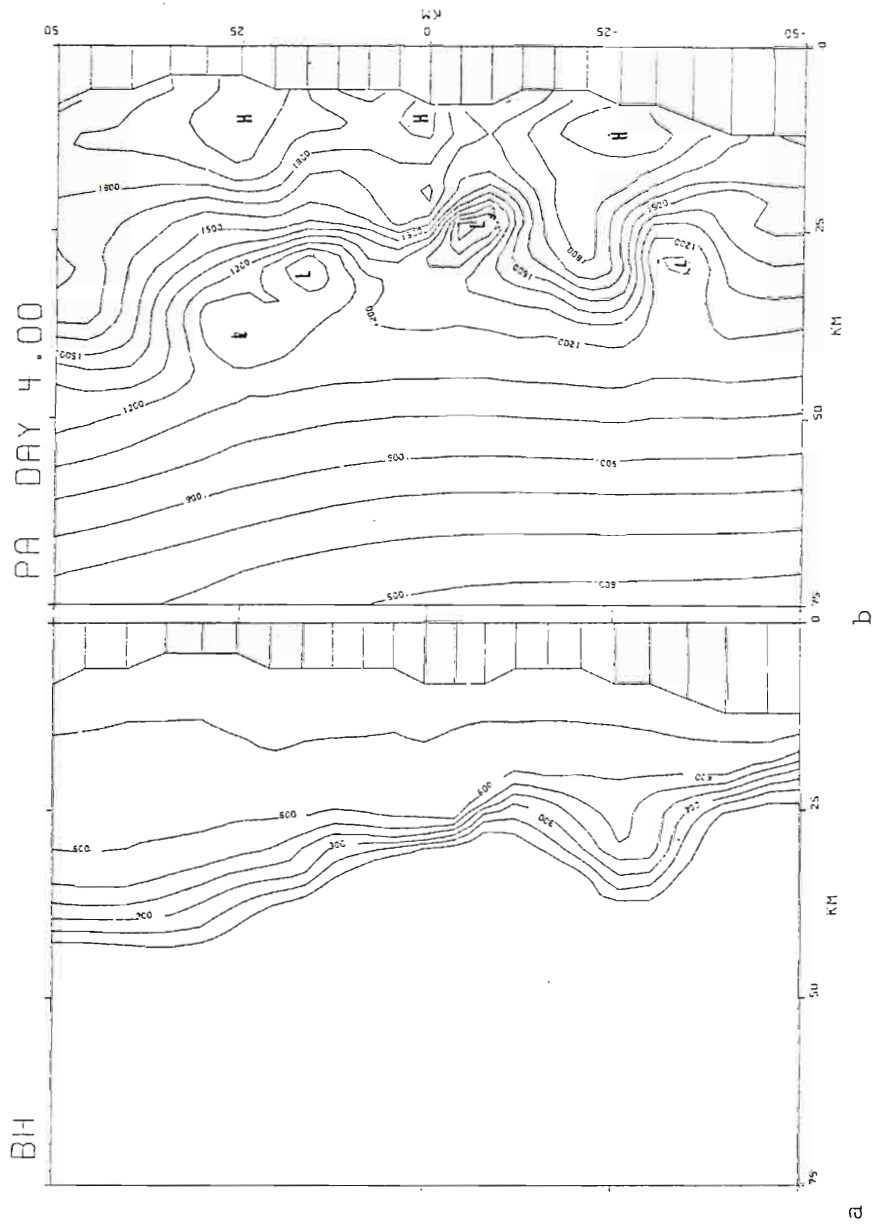Finally in Fig. 17, we have a representation of the vertical

Fig. Fig. 15. Pycnocline height anomaly for model day 4 and bottom topography. A comparison comparison of PA and bottom topography shows the relationship of maxima/minima in PA to bottom bottom topographic features. The contour in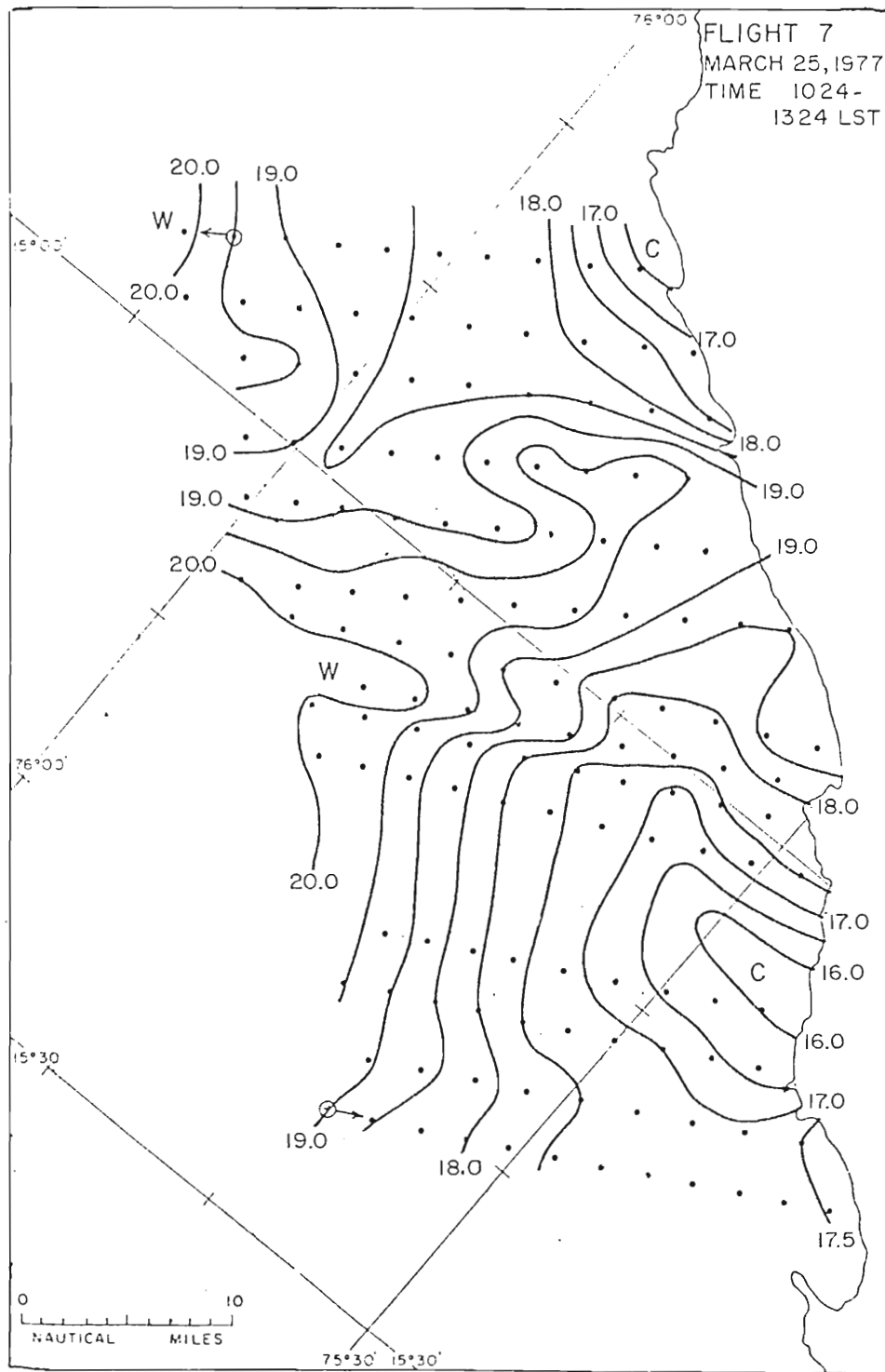terval is 100 m for BH and 100 cm for PA to bottom bottom topographic features. The contour interval is 100 m for BH and 100 cm for PA

Fig. 16. Sea Surface temperature (SST) for 25 March '77 from Moody (1979).

velocity relative to the mean displacement of the interface. This figure shows the vertical movement of the interface due to the propagation of the wave. We can compare this to a plot of the vertical velocity at 20 meters depth at 2 km offshore along the C-line (Fig. 18). This plot was derived from the horizontal current meter observations along the C-line using the variational adjustment technique with the physical constraint of three-dimensional mass continuity presented by O'Brien, Smith and Heburn (1980). We can see a fairly good agreement between the model data and the objectively derived vertical velocities for the period from 24 March through the 31st.

b. THERMODYNAMIC MODEL

As with the hydrodynamic model discussed earlier, the model for this part of the study is also started at 0000Z 22 March 1977. Each case for this part of the study covers a thirty day period. This period was selected since it allows the presentation of the model reaction to at least two complete cycles of the propagating wave forcing with at least one cycle after the initiation of mixing. Also during this period we see (Fig. 8) a series of pulses in the upwelling favorable wind stress with one particular period (day 15 through 20) of strong sustained winds.

The longshore component of the flow, as with the hydrodynamic model, is forced primarily by two factors, the wind stress curl and the externally forced Kelvin waves. The mean poleward flow is the result of the cross-shelf curl of the wind stress as specified in Eq. (53). The variability in the longshore component is induced by the Kelvin wave the cross-shelf curl of the wind stress as specified in Eq. (53). The variability in the longshore component is induced by the Kelvin wave parameterization and the wave interaction with the bottom topography.
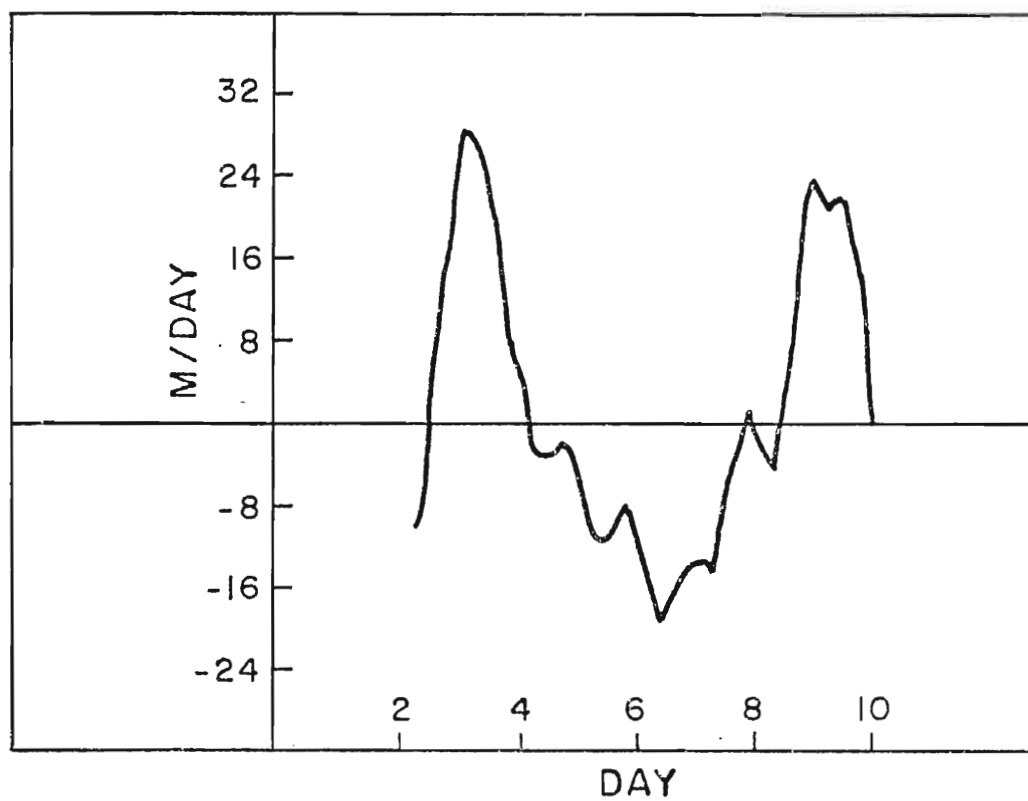
Fig. 17. Vertical velocity relative to mean pycnocline displacement for model days two through ten.
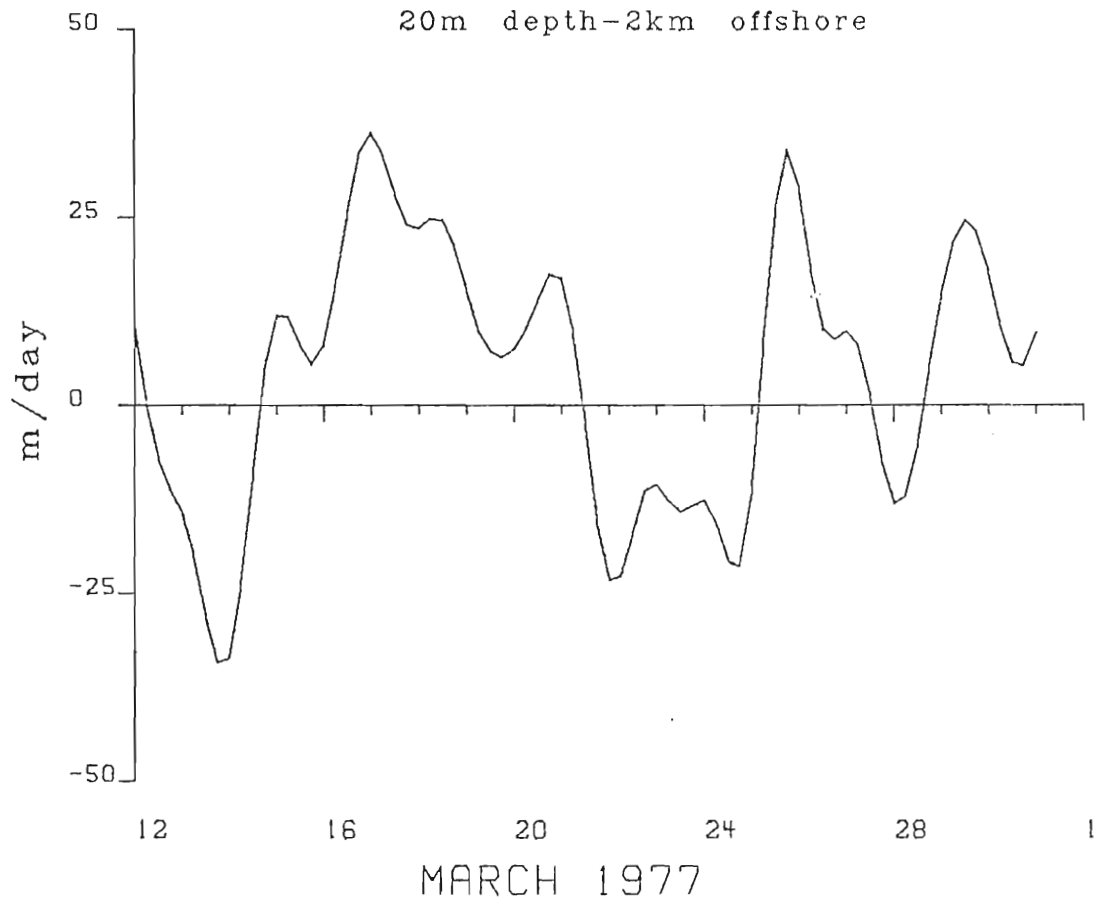
Fig. 18. Vertical Velocity Estimates using objectively adjusted horizontal current meter data from the C-line current meter array and three-dimensional mass continuity.

The cross-shelf component is primarily the result of the inter-
action of the Kelvin wave and the bottom topography, the required on-
shore flow to compensate for the offshore mass transport in the upper
Ekman layer due to the upwelling favorable winds, and secondarily by
the horizontal density gradients.

The interactions between the Kelvin wave and the topography for
the hydrodynamic model was examined in detail in the previous
section. It was shown that, by considering the lower layer to
be a homogeneous fluid with a free upper surface (the interface) which
conserves potential vorticity, the variation in the pycnocline anomally
field (interface displacement) could be directly related to the inter-
action between the Kelvin wave and the bottom topography. Furthermore,
it was shown that the horizontal variations in the lower layer velocity
fields could also be directly related to the Kelvin wave/bottom top-
ography interaction.

By comparing the pycnocline height anomally field (Fig. 12) from
the hydrodynamic model with the upper layer thickness (Fig. 19) from
the thermodynamic model, we see the same features present. This
suggests that we can assume that the same physics, i.e., conservation
of potential vorticity, can be used to explain the intersections
between the propagating waves and the bottom topography.

In the hydrodynamic model, we could directly infer vertical motion
from the movement of the interface. In the thermodynamic model, this
is possible only when the upper layer thickness is greater than the
stabilized mixed layer depth (i.e. when the interface represents a
is possible only when the upper layer thickness is greater than the
stabilized mixed layer depth (i.e. when the interface represents a
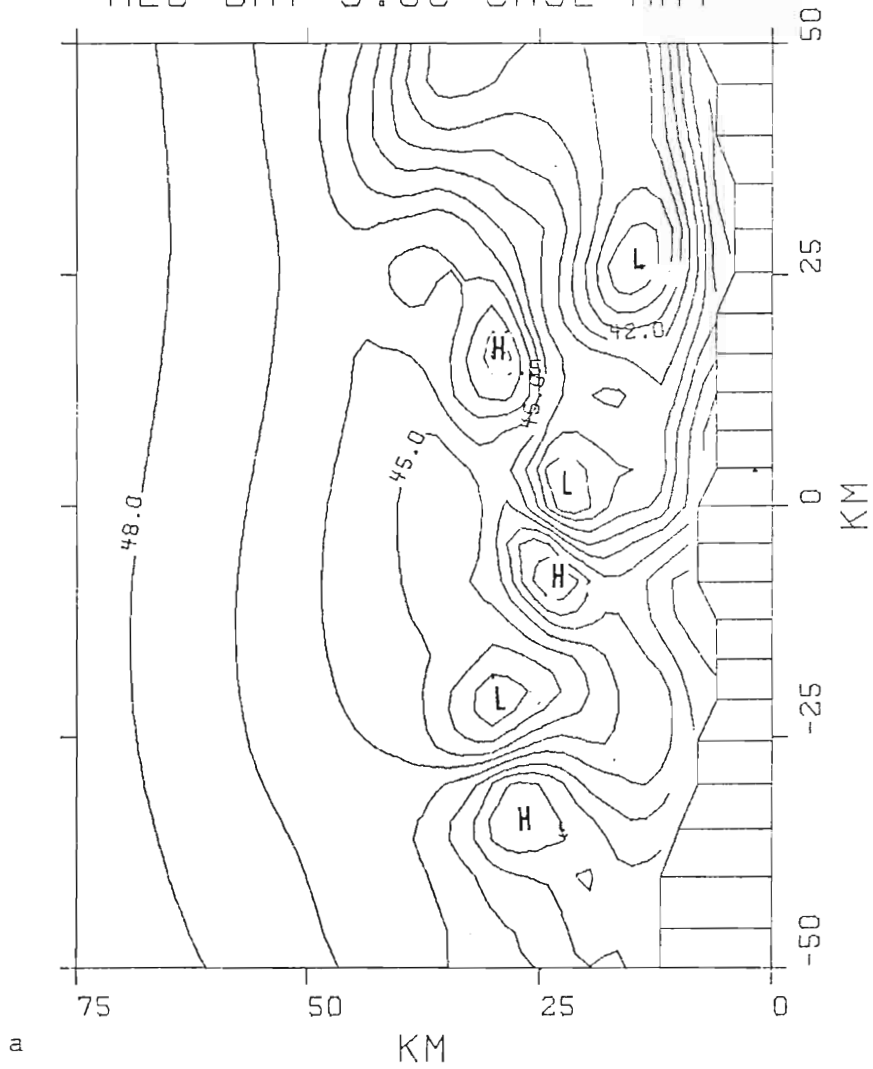material (Lagrangian surface). When the interface ascends into the

MLD DAY 3.00 CASE MH4

a

KM

KM

Fig. 19. The Mixed Layer Depth (MLD) (upper layer thickness)
for days 3, 5, 7 and 9 from the thermodynamic model. Contour interval
is 1 meter.

MLD DAY 5.00 CASE MH4

Fig. 19b.

MLD DAY 7.00 CASE MH4
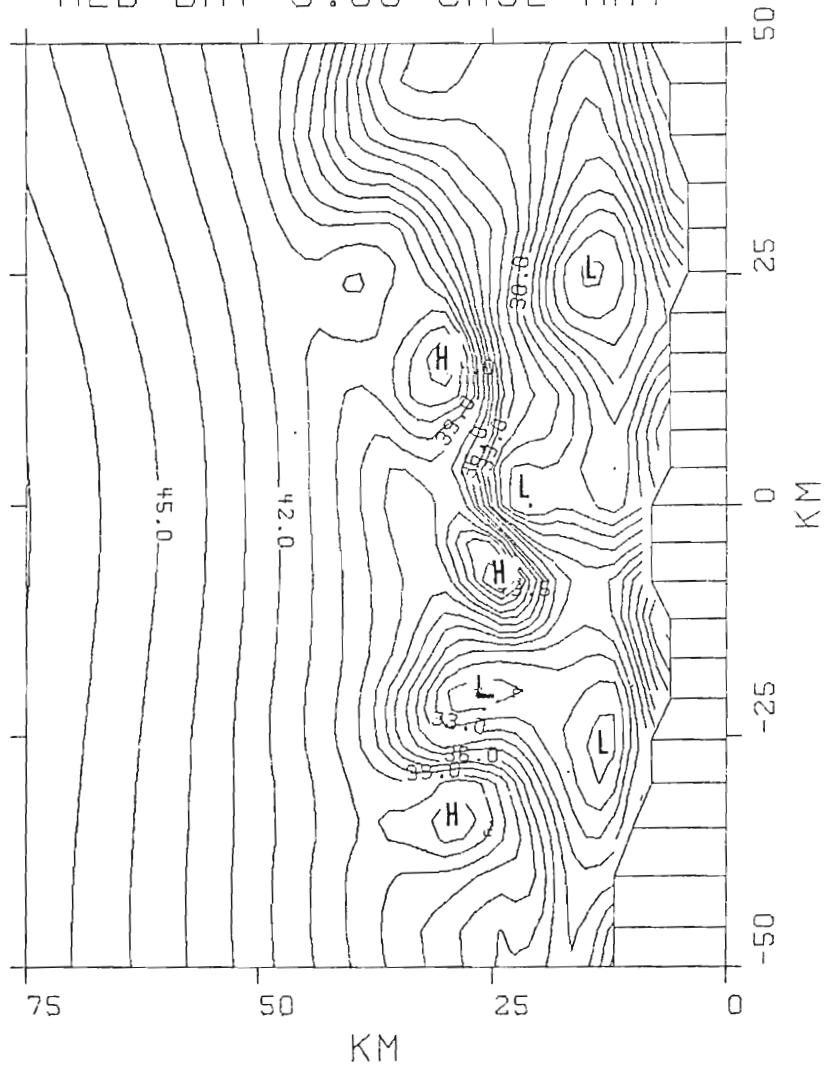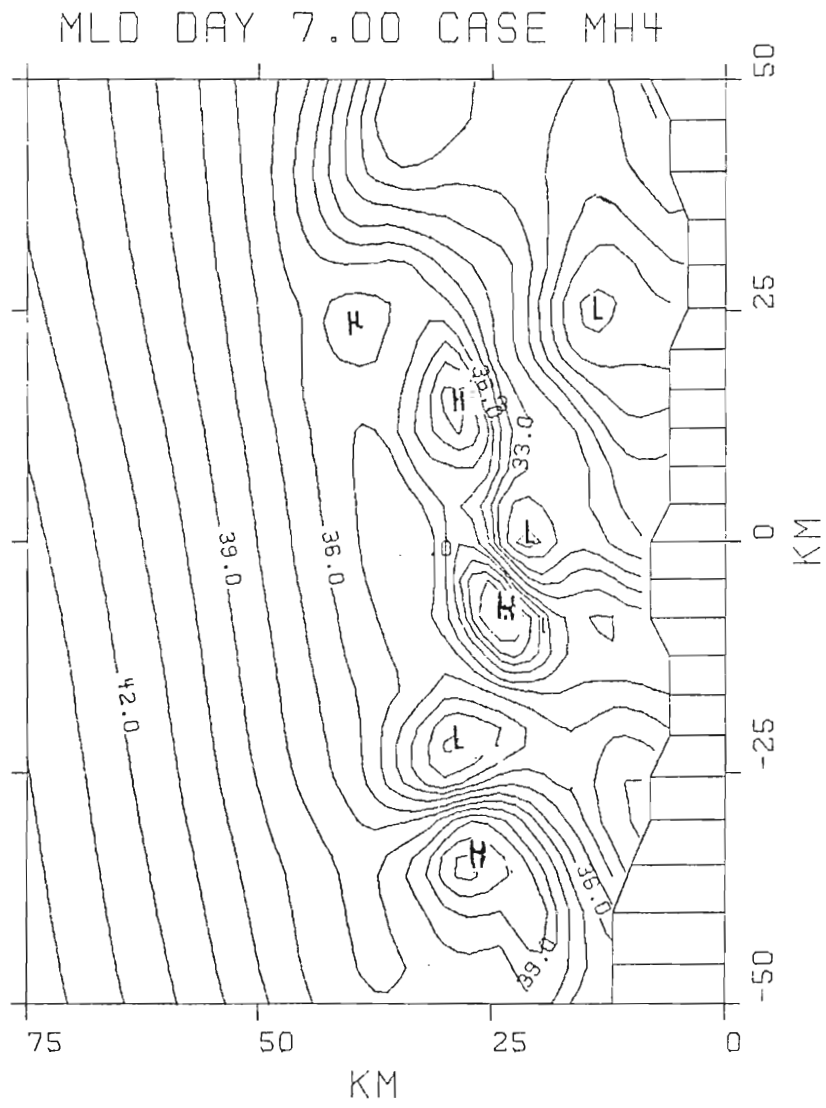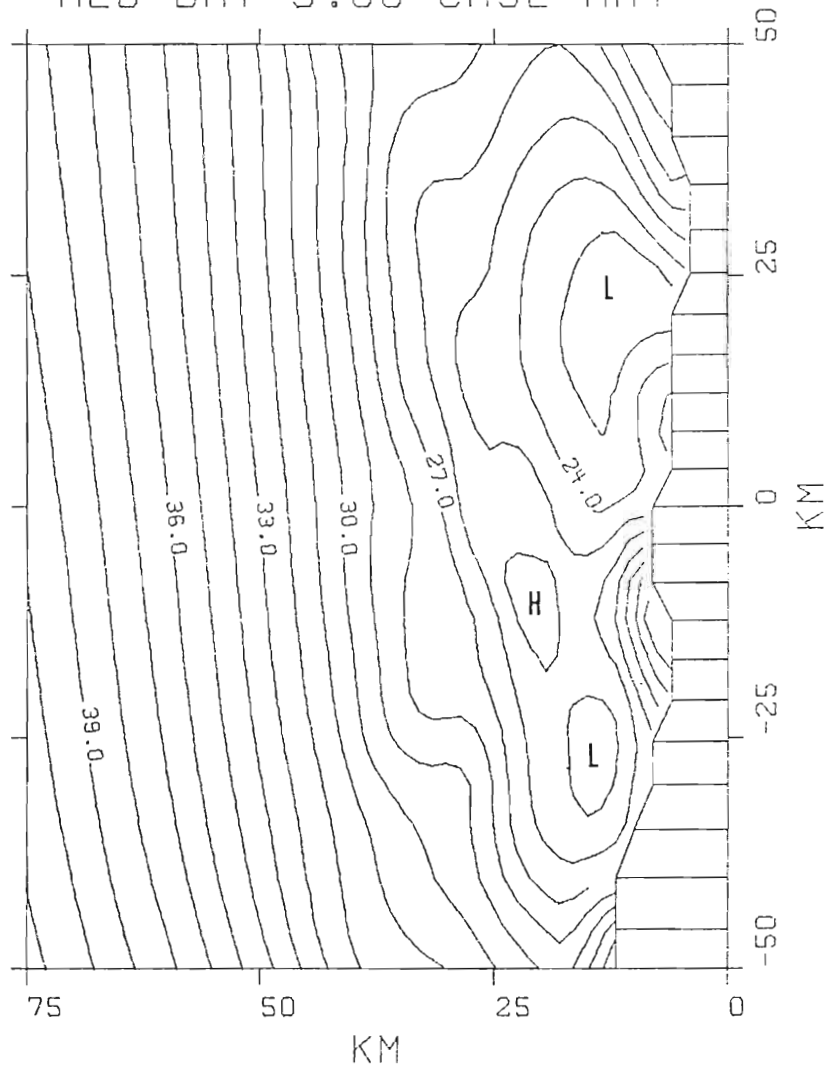
Fig. 19c.

MLD DAY 9.00 CASE MH4

Fig. 19d.

active mixing region, then the vertical motion is given by the mixing parameterization and cannot be directly inferred from the motions of the interface. Therefore, we must use a field other than the upper layer thickness field to identify the areas of enhanced upwelling. We will use the upper layer temperature field, which for a well mixed layer is the same as the sea surface temperature (SST), for this purpose. The SST is obtained from the upper layer density field by using the equation of state for the upper layer;

$$SST = (\rho_0 - \rho_1)/\gamma = T_1 \tag{82}$$

During the first 10 to 11 days, the thermodynamic model behaves the same as the hydrodynamic model. Therefore, the upper layer thickness can be used to identify the upwelling centers. After day 11, the interface ascends into the active mixing region and the sea surface temperature field begins to show more horizontal structure. By day 17, (Fig. 20), we see the formation of a "plume" like structure north of Punta San Ana, in the same location as had been shown in the pycnocline anomaly field. Warm pockets can be also seen in the bays between Punta San Nicolas and Punta Santa Ana, Punta Santa Ana and Cabo Nazca, and Cabo Nazca and Punta Olleros. These warm pockets indicate that there is relatively less upwelling in the areas. This result is also indicated in the pycnocline height anomaly from the hydrodynamic model (see Fig. 12) by the relative minima in this field in the vicinity of indicated in the pycnocline height anomaly from the hydrodynamic model (see Fig. 12) by the relative minima in this field in the vicinity of the bays. The axis of the relative warming region in Fig. 20 is also
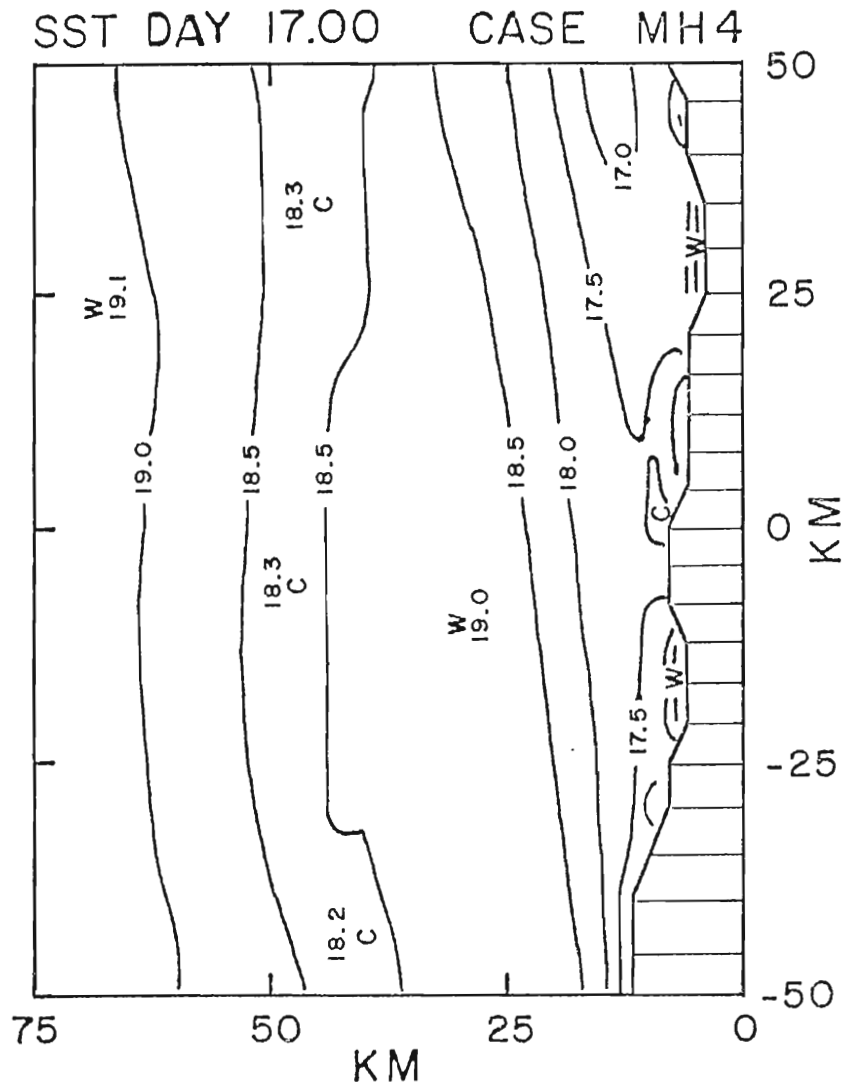
Fig. 20. Sea Surface Temperature (SST) for model day 17. Contour interval is .5°C.

indicated by the axis of the relative minima in the pycnocline anomaly

field (Fig. 12). The locations of these relative minima are directly

related to the bottom topography.

One of the initial assumptions for this model was that heating was

not important. This was based on the comparison of the results from

the heated vs. unheated versions of Thompson's (1974) model. Thompson

found the primary result of heating in his model was to strengthen the

upwelling frontal zone with minimal effect on the flow field. Results

from an unheated version of this model show board scale upwelling

with little horizontal structure. In Fig. 21 we have x-t cross-sections

of the SST field at y = 0, y = 20 km, and y = ± 30 km. In this figure,

we can see after the commencement of mixing that there is a continuous

cooling of the upper layer and, generally, offshore advections of cold

water. Furthermore, the horizontal SST plots for the unheated case

display continuous offshore migration of the isotherms with only slight

longshore variations.

If we add a positive heat flux (an observed feature in this region

during this period) to the model, we then find the expected horizontal

structure. That is, we recover that horizontal structure suggested

by the pycnocline height field of a given situation and by the observa-

tions. Stevenson, Stuart, and Heburn (1980) report that this heat flux

is fairly constant during March and April 1977.

Now in Fig. 22, we have cross-sections for y = 0, ± 10, ± 20, ± 30,

and 40 km. We can see that when a reasonable heating rate (on the order

of .08°C day^{-1} m^{-1}) is added to the system we get a quasi-balance

between the large scale wind driven upwelling and the heating. Then

the fluctuations in the upwelling patterns due to internal wave action,

SST VS T   CASE MH1   Y =-30. KM
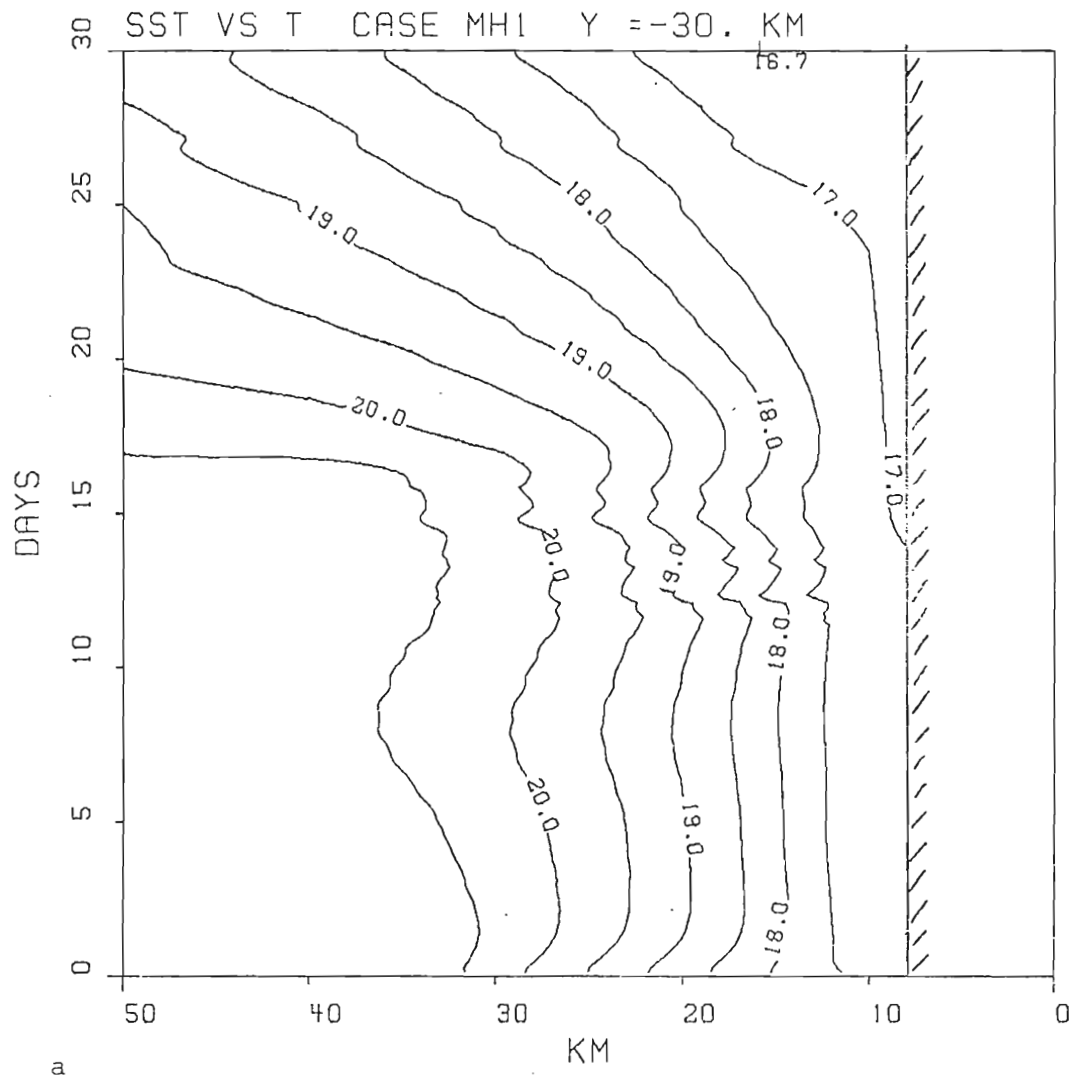
Fig. 21.   Time cross-section (x-t) of the SST field at y = 0, 20, ±30 km for the unheated case.   Contour interval is .5°C.

Fig. 21b.

Fig. 21c.

SST VS T   CASE MH1   Y = 30. KM
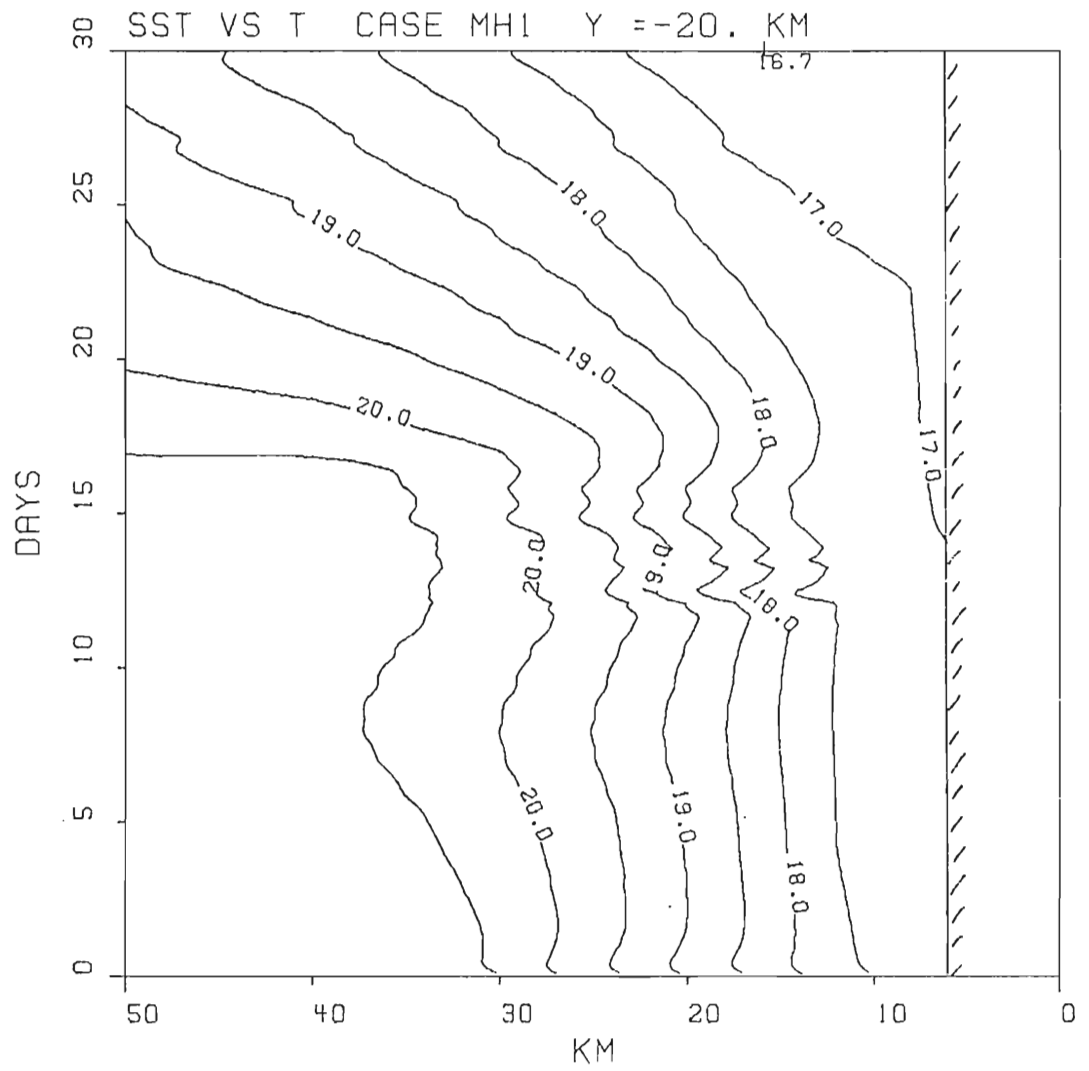
Fig. 21d.

Fig. 22. Time cross-sections (x-t) of the SST field at y = 0, ±10, ±20, ±30 and 40 km for the heated case. Contour interval is .5°C.

Fig. 22b.

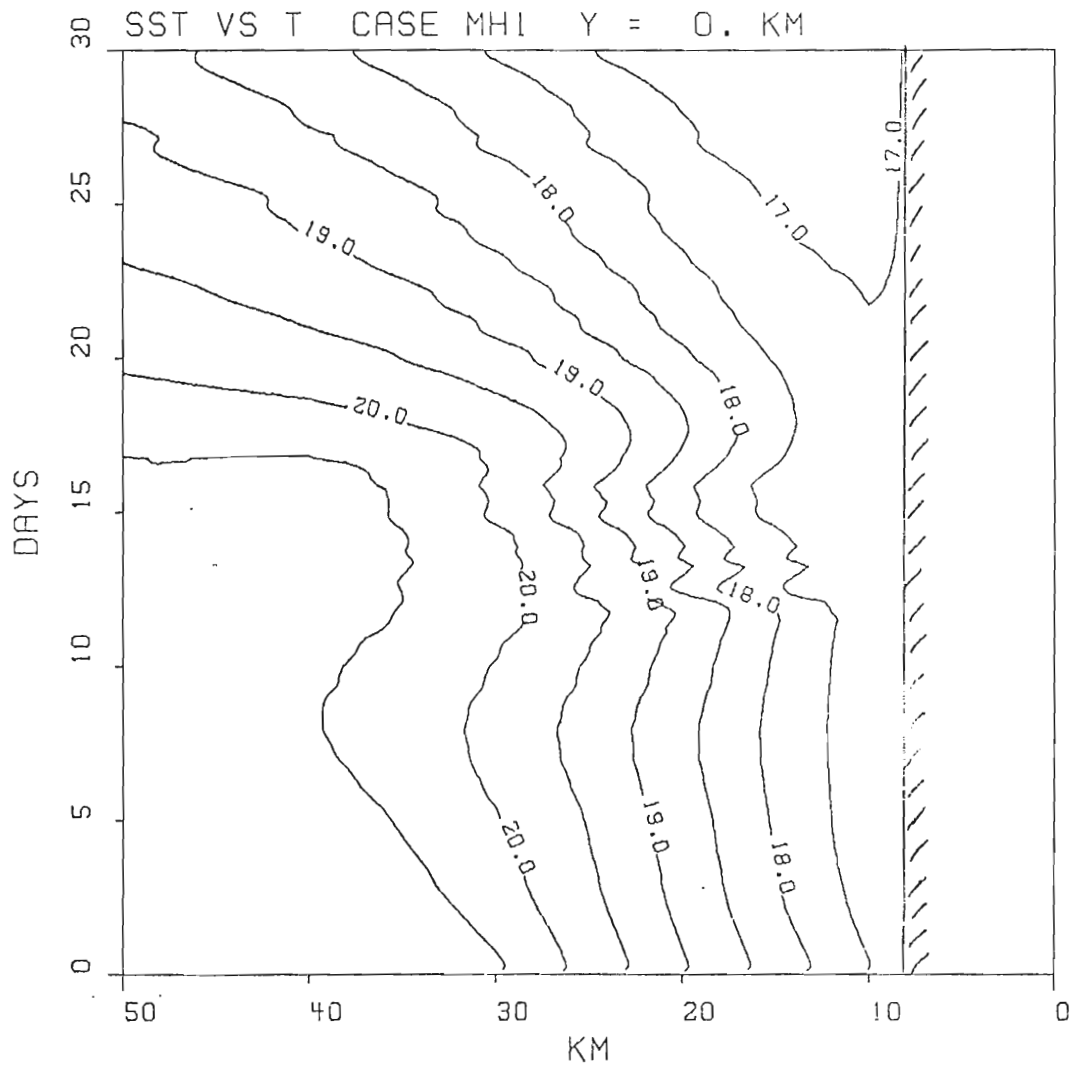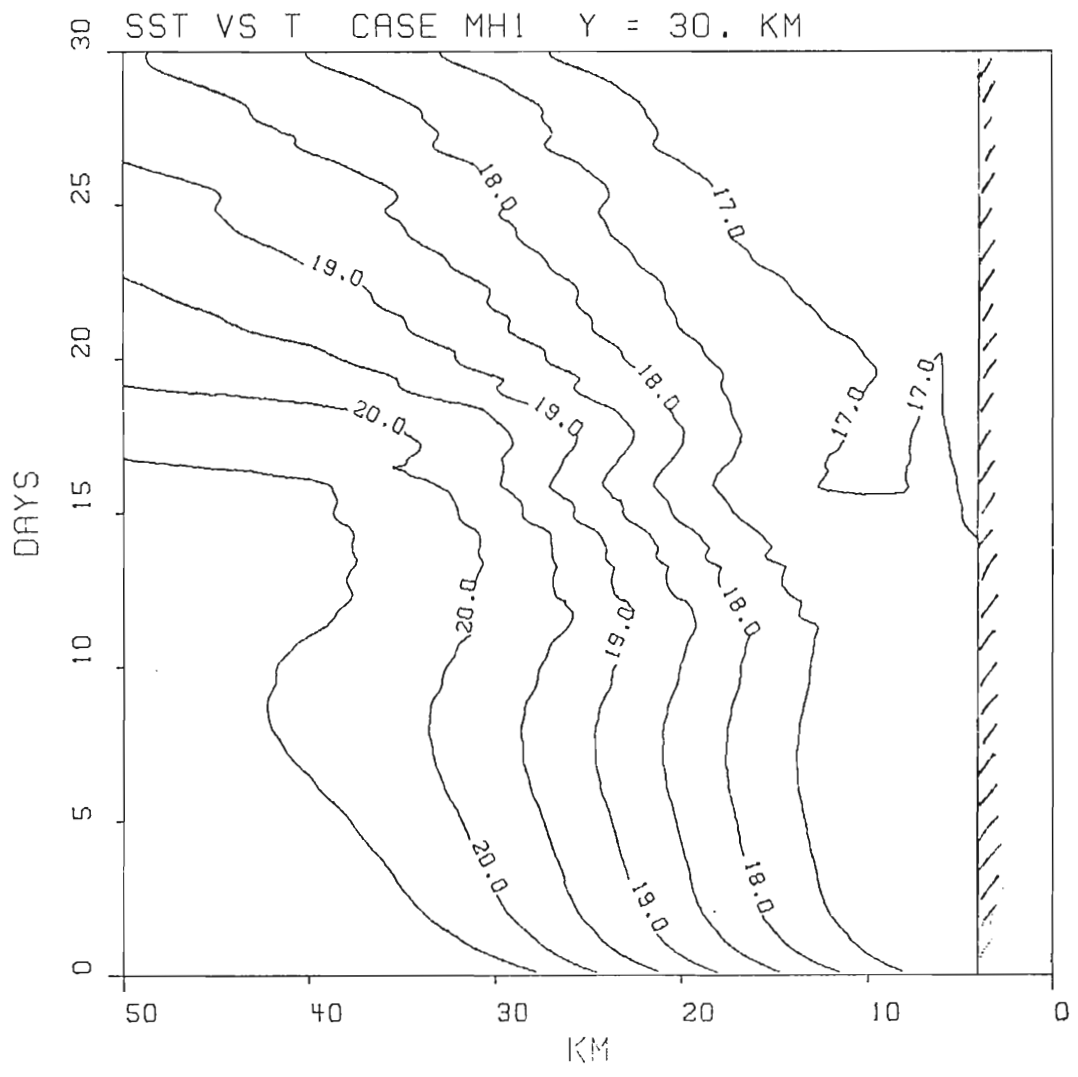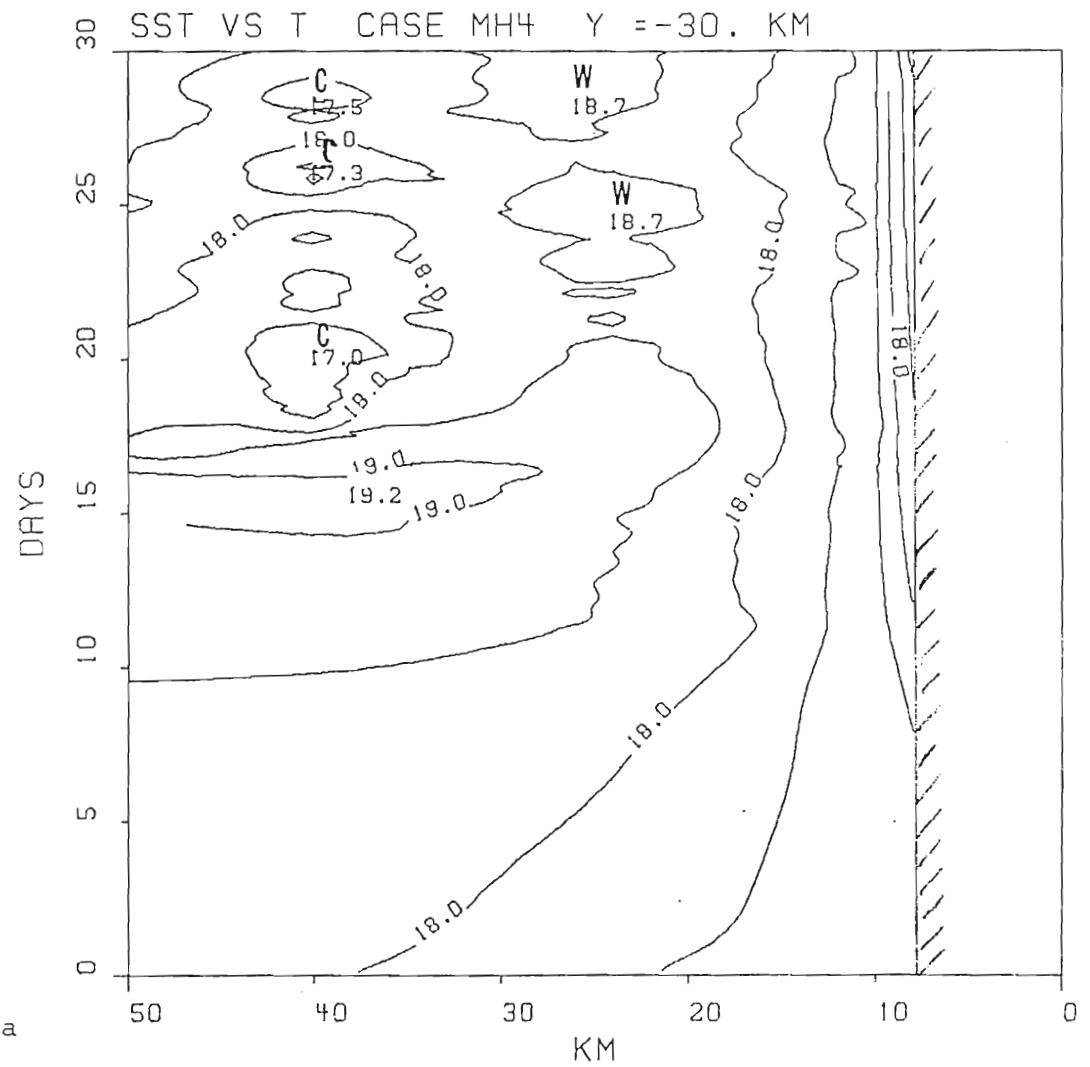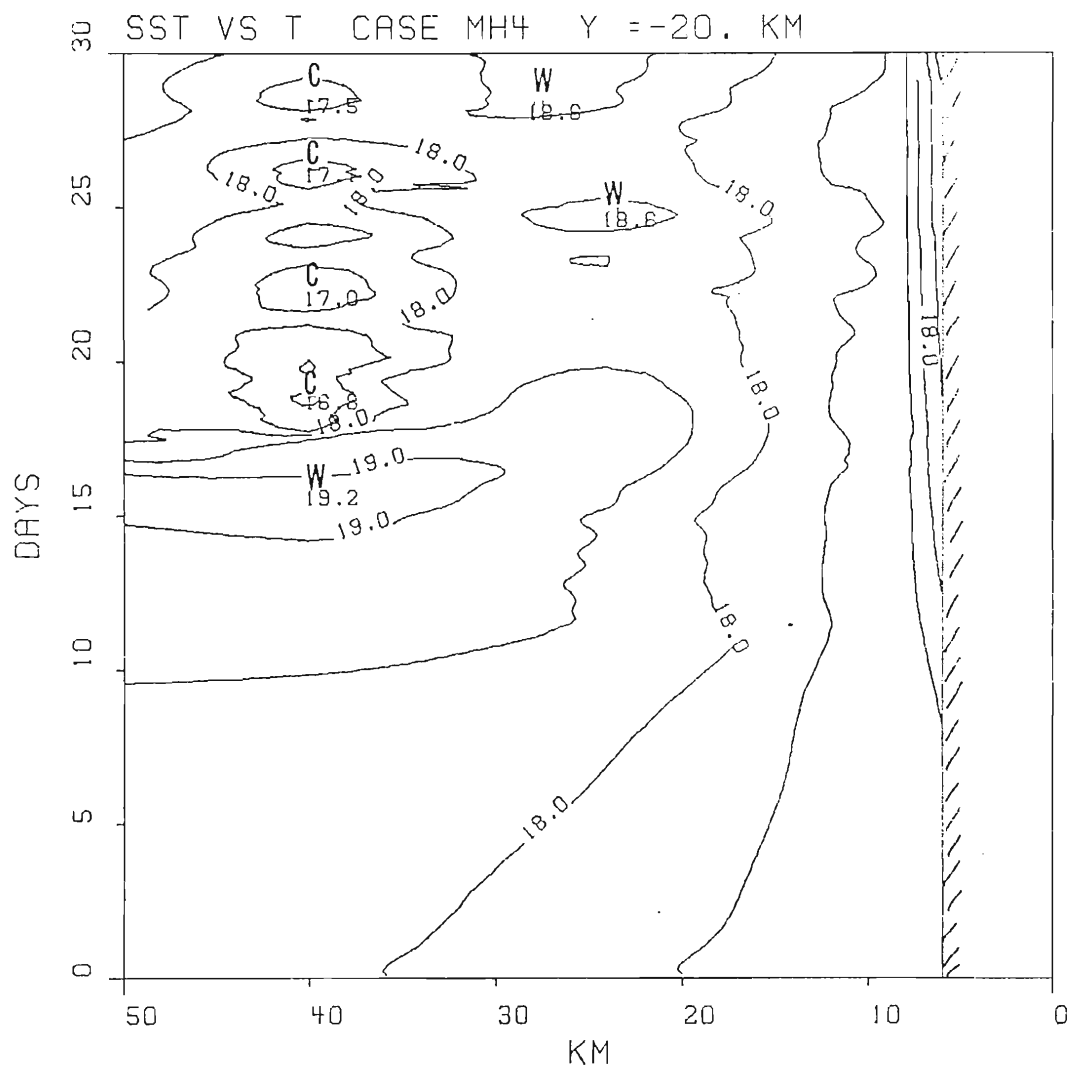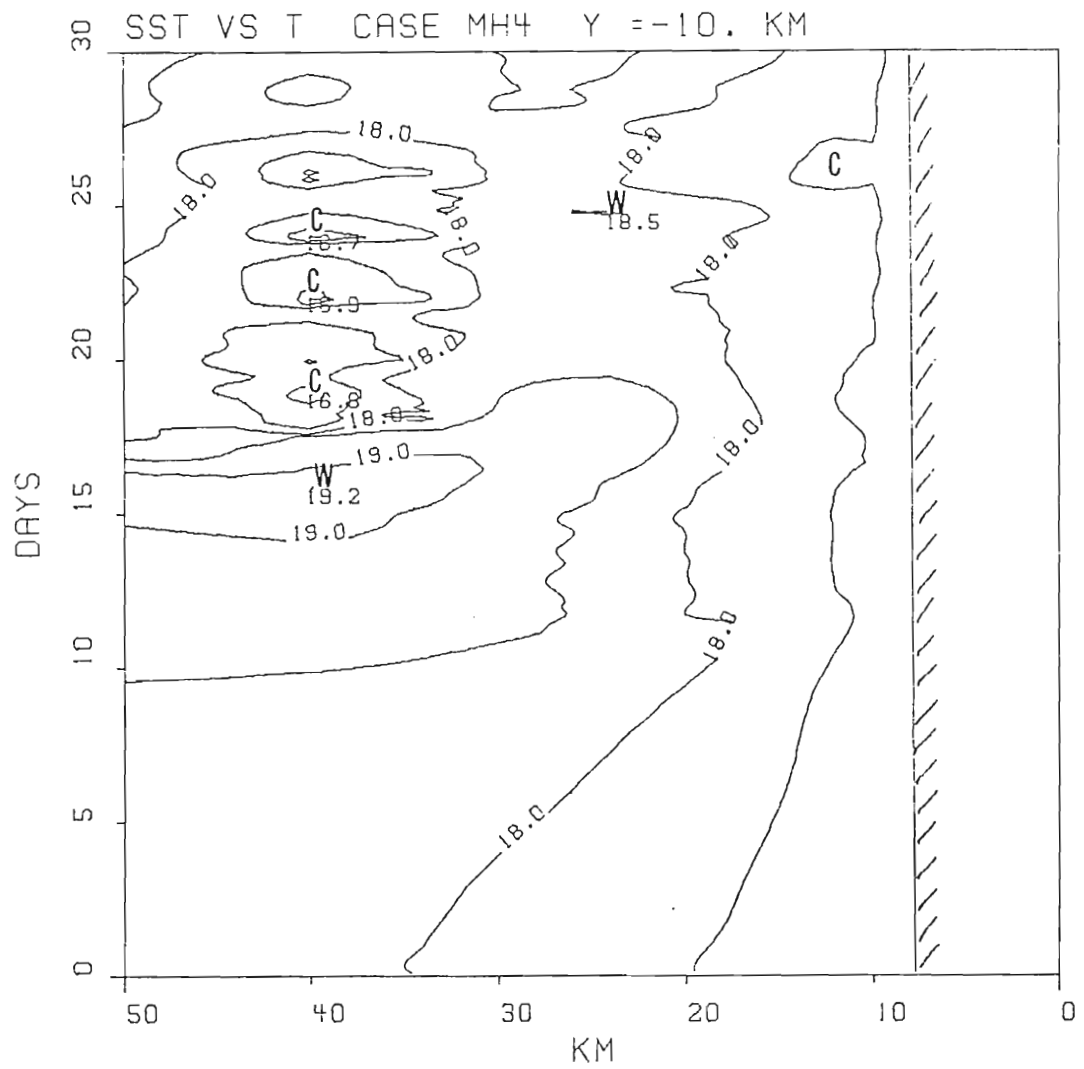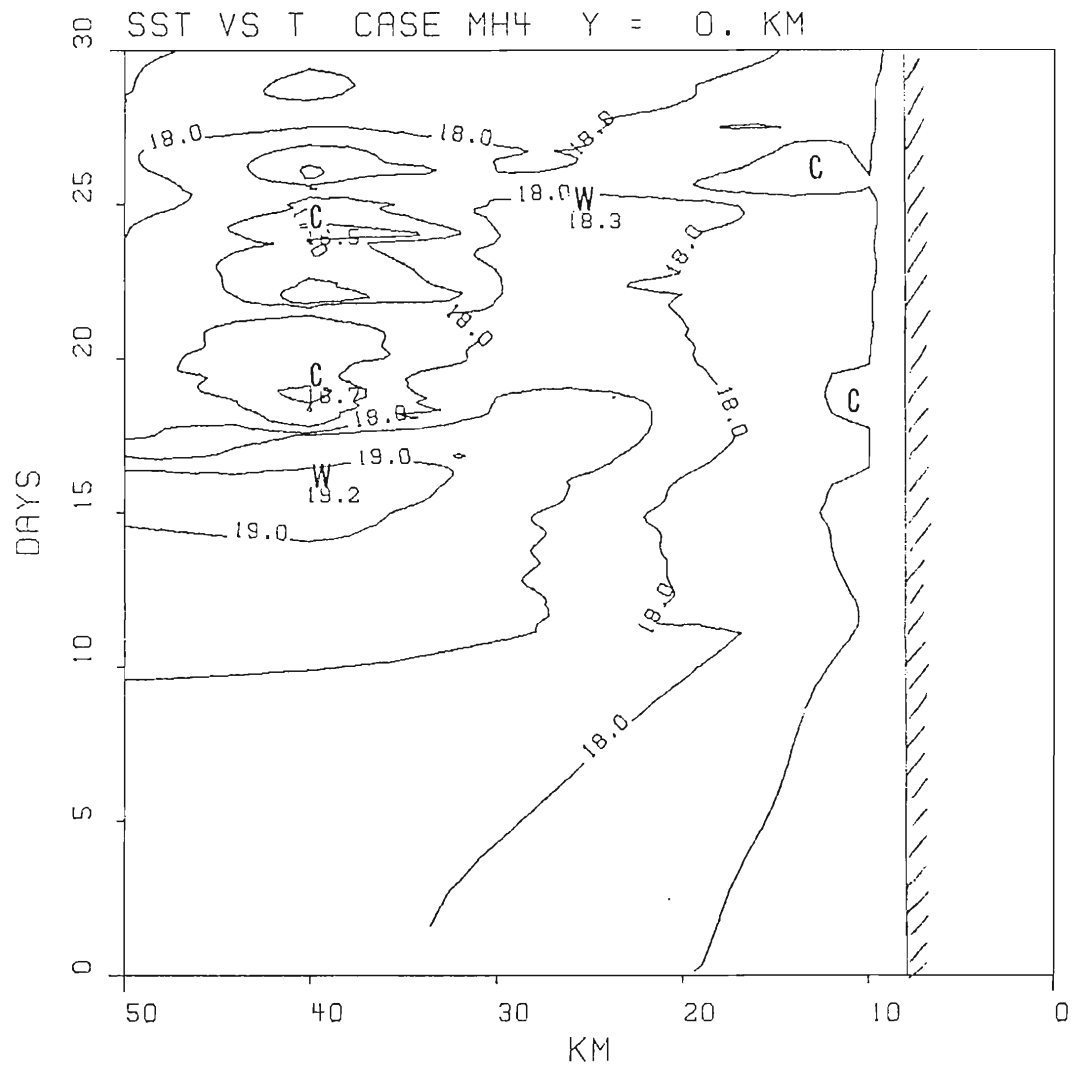Fig. 22c.

Fig. 22d.

Fig. 22e.

SST VS T   CASE MH4   Y = 20. KM
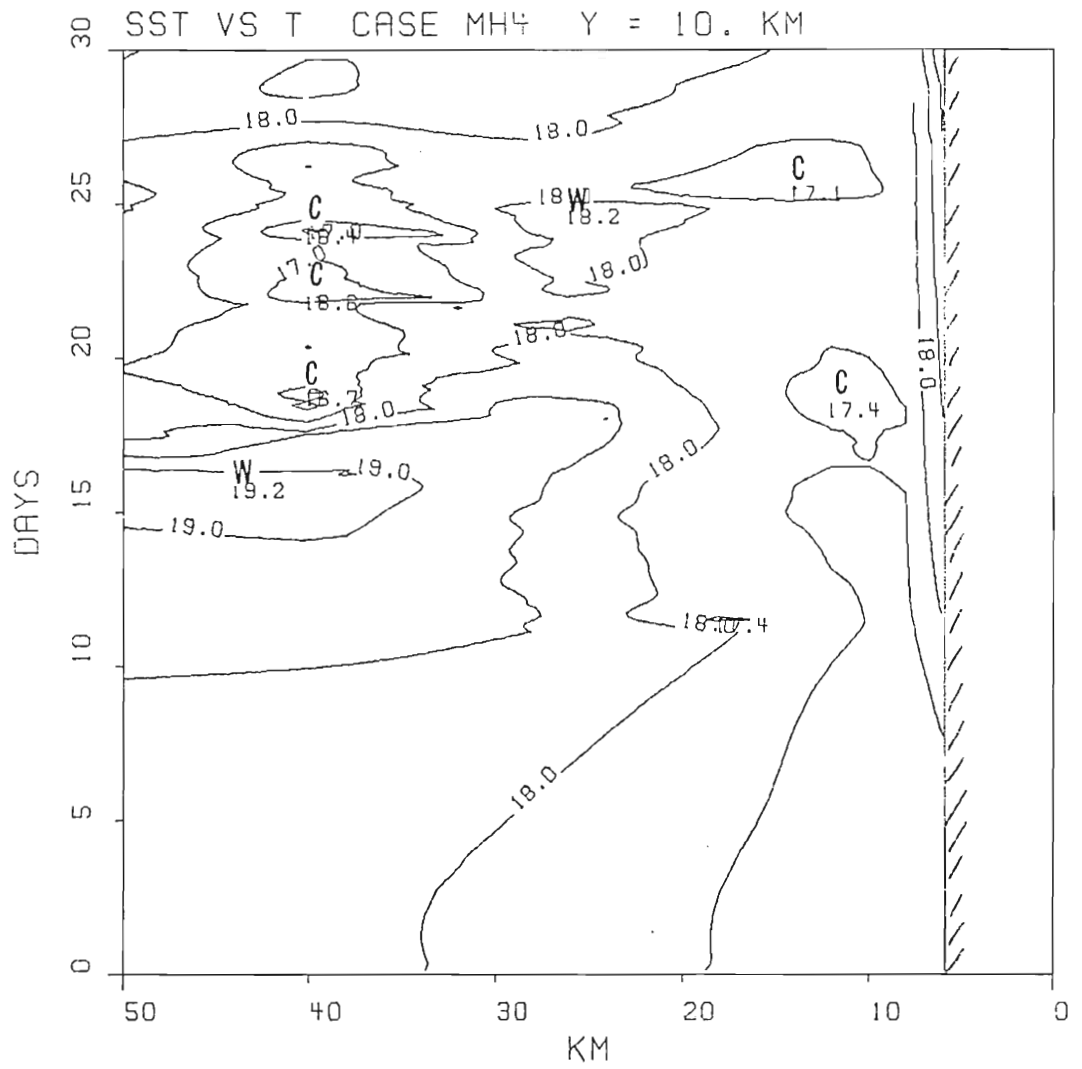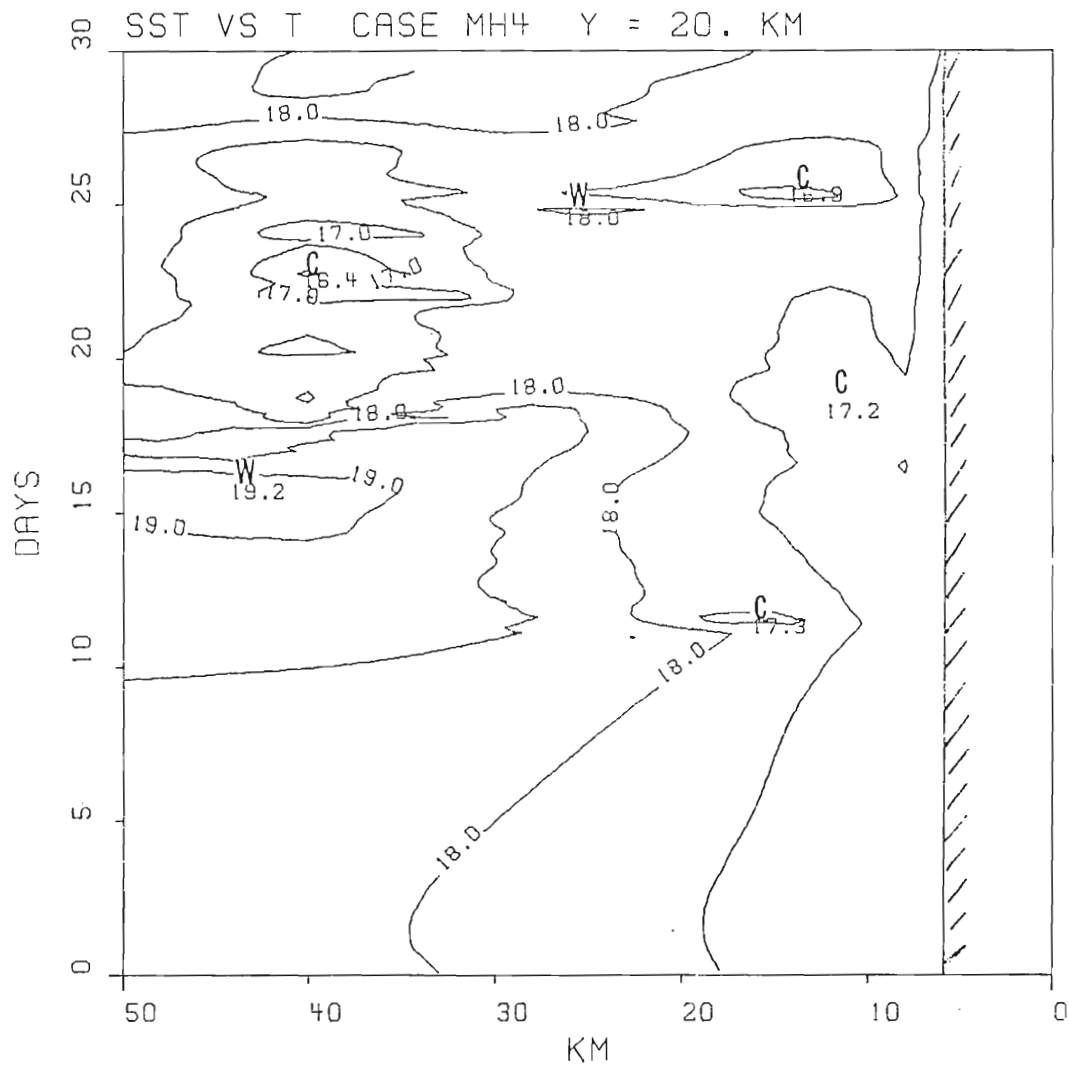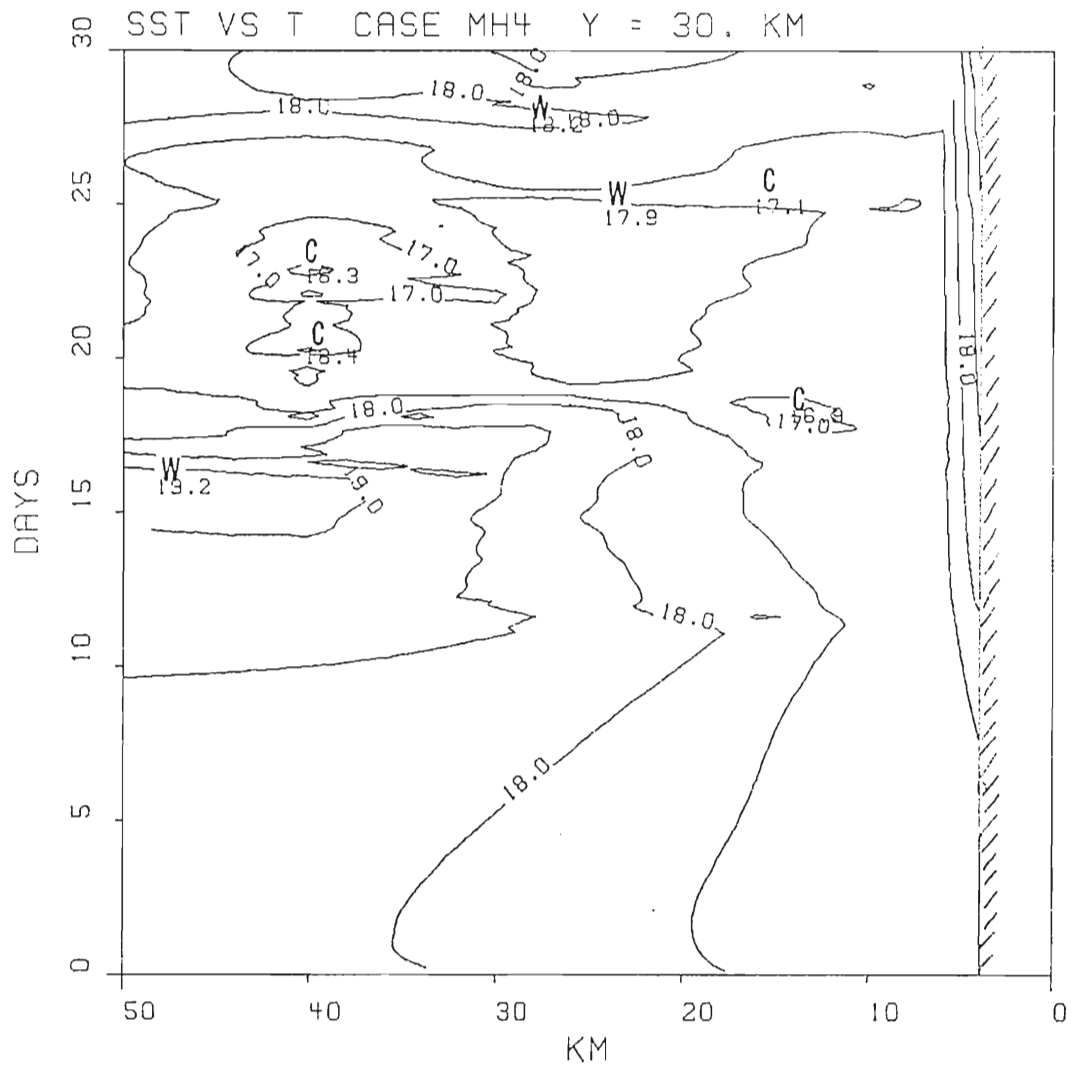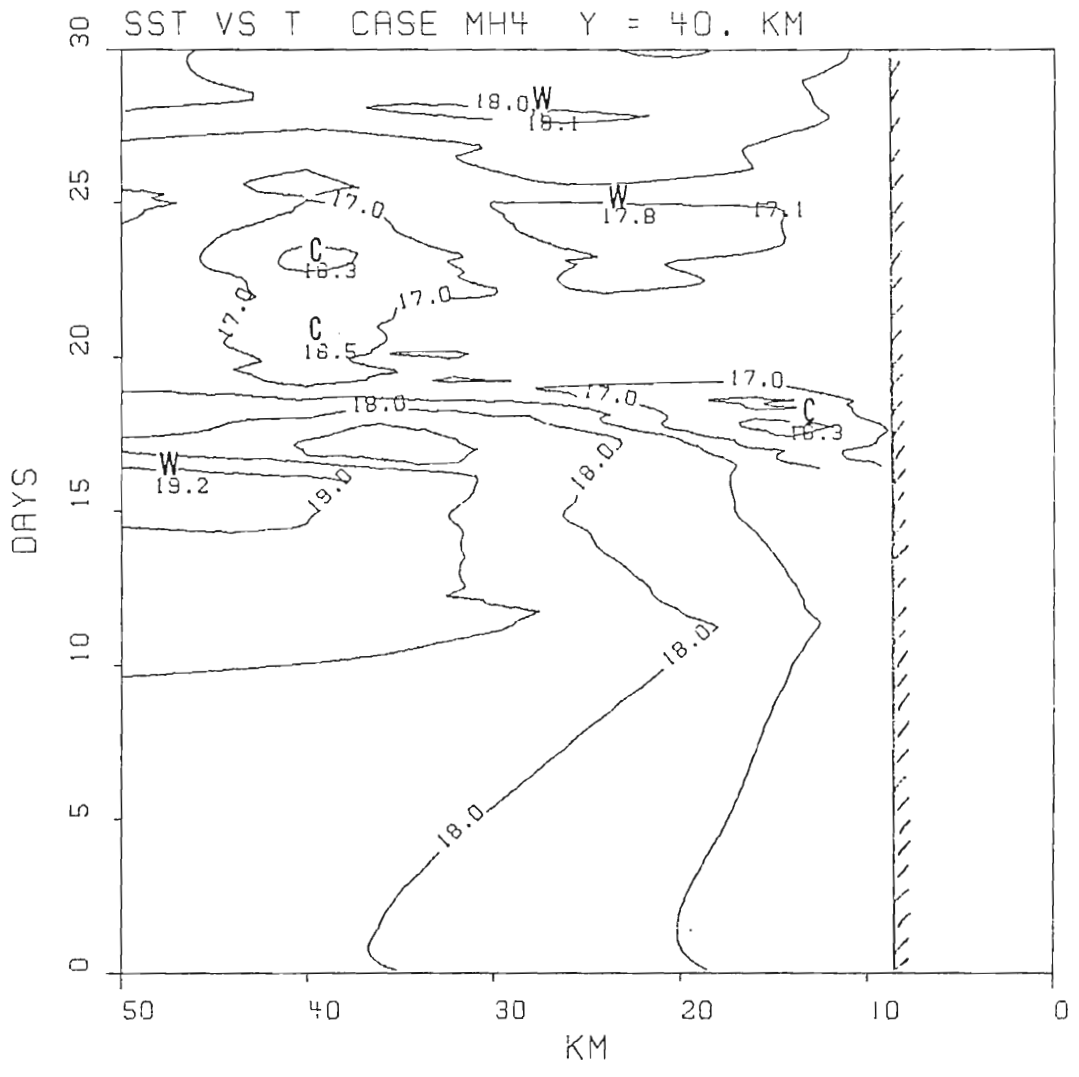
Fig. 22f.

Fig. 22g.

Fig. 22h.

wave/bottom topography interaction, and wind fluctuations becomes apparent.

Although the time periods are different, we see by comparing the y = 0 plot from Fig. 22 to Fig. 23 (from Hoover, 1980) a similar horizontal structure. Both show quasi-periodic fluctuations along the coast and at approximately 30 kms offshore. This quasi-periodic feature at 30 km offshore appears in all the cross-sections.

If we compare the time for the occurrence of the minima in the y = 0 plot with a time series for the long shore undercurrent as measure by the LAGARTA 92M current meter (Fig. 24) we see that the minima generally occur during the retardation of the poleward flow. Now, if we recall that with the passage of a crest of an internal wave we see an equatorward acceleration in the undercurrent and an uplifting of the pycnocline, then we might reasonably assume that fluctuations in the SST in this region are the result of the passage of internal waves. A comparison with the time series (Fig. 8) for the large scale wind stress also shows a relationship between the minima and the peaks in the wind stress thus indicating an interaction between internal waves and wind mixing.

Another feature which we can glean from Fig. 22 is the occurrence of a narrow upwelling zone (approximately 5-10 km) in the southern regions of the model where the shelf is narrow and a broadening of the upwelling zone (approximately 15-20 km) as we progress toward the equator where the shelf becomes wider. Preller and O'Brien (1980) found this same general pattern in their model which used an idealised equator where the shelf becomes wider. Preller and O'Brien (1980) found this same general pattern in their model which used an idealised bottom topography.
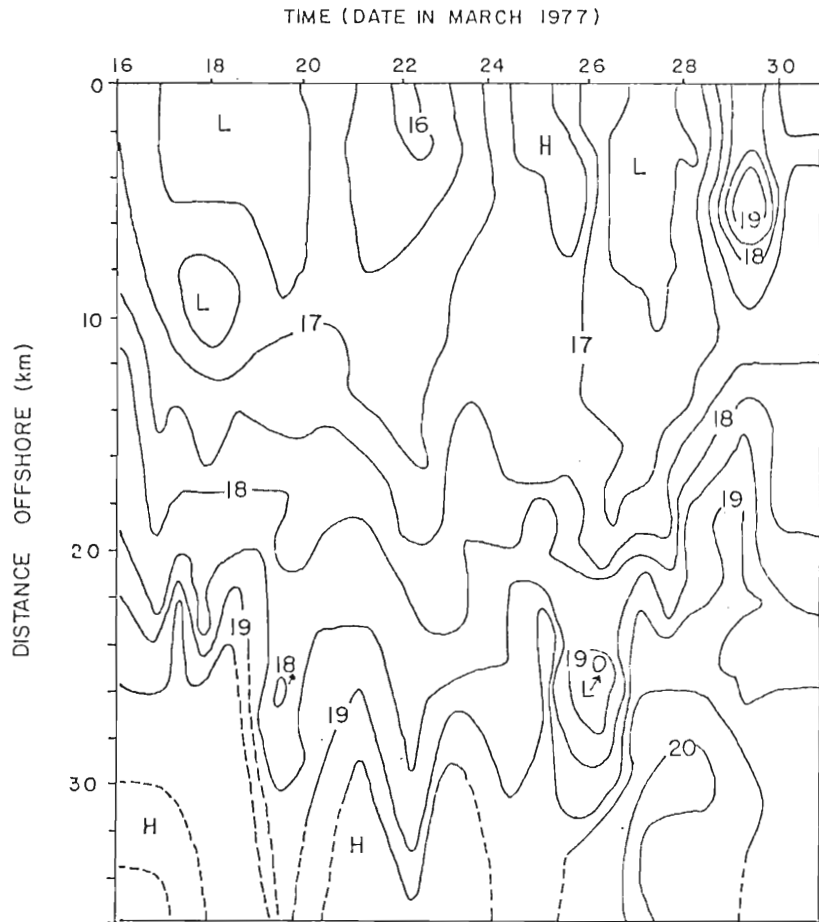
Fig. 23. Surface mixed layer temperature on the C-line from Hoover, 1980.

LAGARTA

DEPTH: 92 M.   CASE: MH06S

U

cm/sec

-40 -30 -20 -10 0 10 20 30 40

a

V

cm/sec

-40 -30 -20 -10 0 10 20 30 40

5   10   15   20   25   30

DAY

LAGARTA

DEPTH: 92 M.   CASE: MH4

U

cm/sec

-40 -30 -20 -10 0 10 20 30 40

b

V

cm/sec

-40 -30 -20 -10 0 10 20 30 40

5   10   15   20   25   30
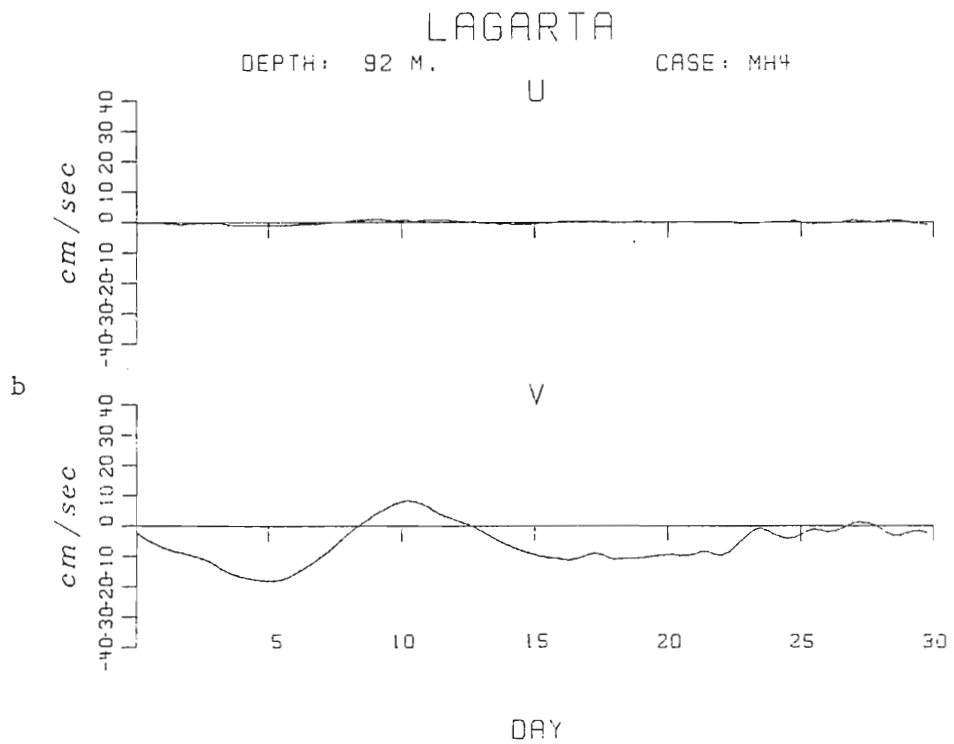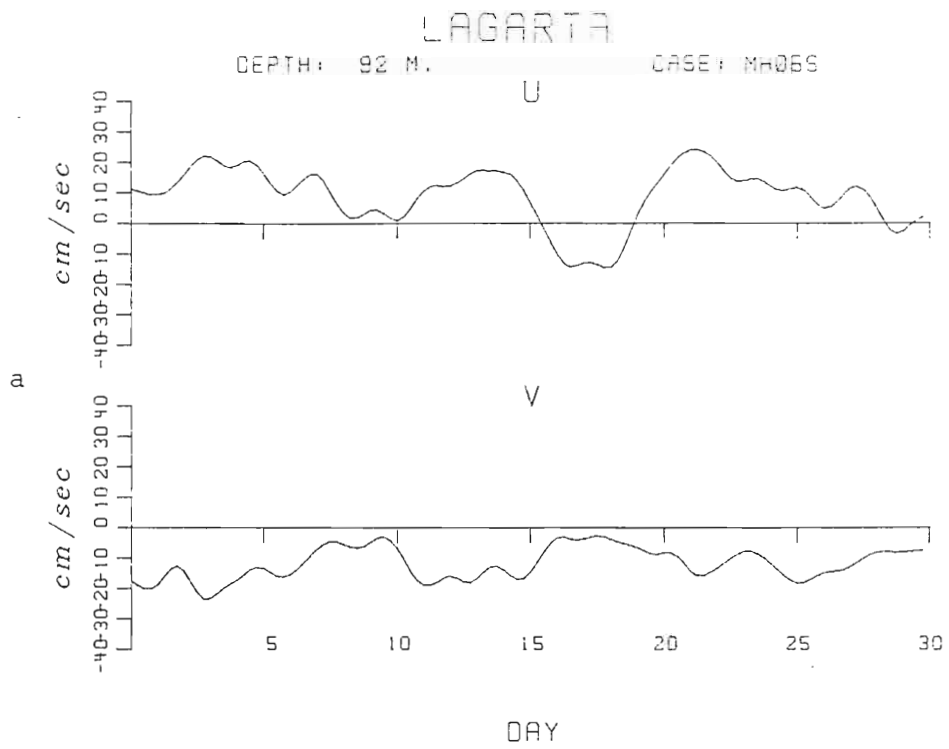
DAY

Fig. 24.   Time series of the longshore (v) and cross-shelf (u)

DAY

Fig. 24.   Time series of the longshore (v) and cross-shelf (u)
velocity.

As with the pycnocline height anomaly, we can see effects of propagating waves in the SST fields. On day 20 (Fig. 25) we have the passage of a trough with its associated enhanced poleward undercurrent (Fig. 26). Here we see the "plume" north of Punta Santa Ana is well defined and thus indicating enhanced upwelling which can be associated, as in the hydrodynamic model, with the interactions of the internal wave and the ridge in the bottom topography located in this region. On day 26 (Fig. 27) we have now the passage of a crest and its associated relaxations of the poleward undercurrent (Fig. 28). Now we see that the "plume" is not as well defined but that we have an axis of colder water extending from the coast at y = 0 and bending equatorward, a large area of warming north of C-line (y = 0) and, also, a region of warming off Punta Santa Ana. In Fig. 29, we have an SST map 26 which shows, basically, the same features, i.e., warming north of the C-line, axis of cold water from coast north of Punta Santa Ana bending equatorward and warming off Punta Santa Ana.

In this and the hydrodynamic model, we have introduced for the first time, a parametrization for the observed fluctuation in the longshore currents. This was accomplished by means of imposing an externally forced Kelvin wave. In Fig. 30 and 31 we have time series of the observed velocity components from the current meters located at PS 12M (12 meters) and MILA V 80M (80 meters) contrasted with simulated current meter data derived from the thermodynamic model. The PS 12M current meter is used to show the comparison in the upper layer and the MILA V 80M to show the comparisons in the lower layer. These two current meter moorings are located at mid-shelf near the layer and the MILA V 80M to show the comparisons in the lower layer. These two current meter moorings are located at mid-shelf near the C-line (see Fig. 6). The PS mooring is a shallow depth mooring
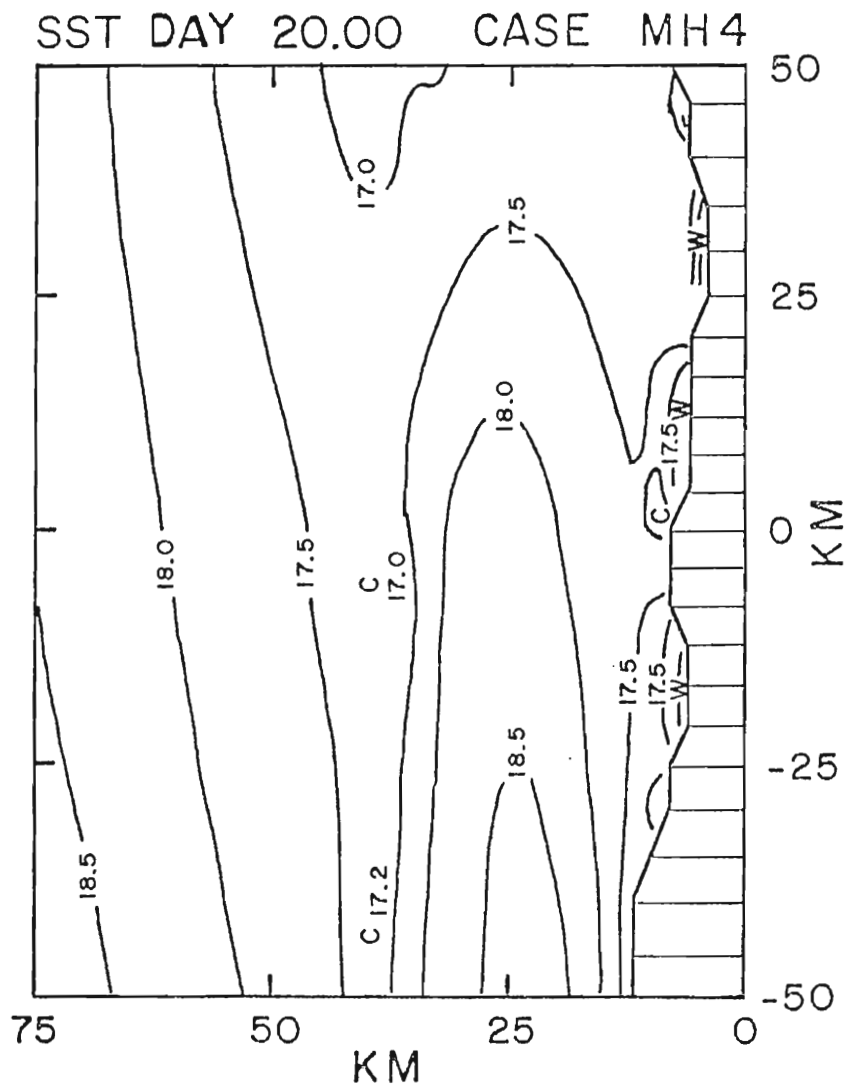
Fig. 25. SST field for day 20 of the heated model. Contour interval is .5°C.
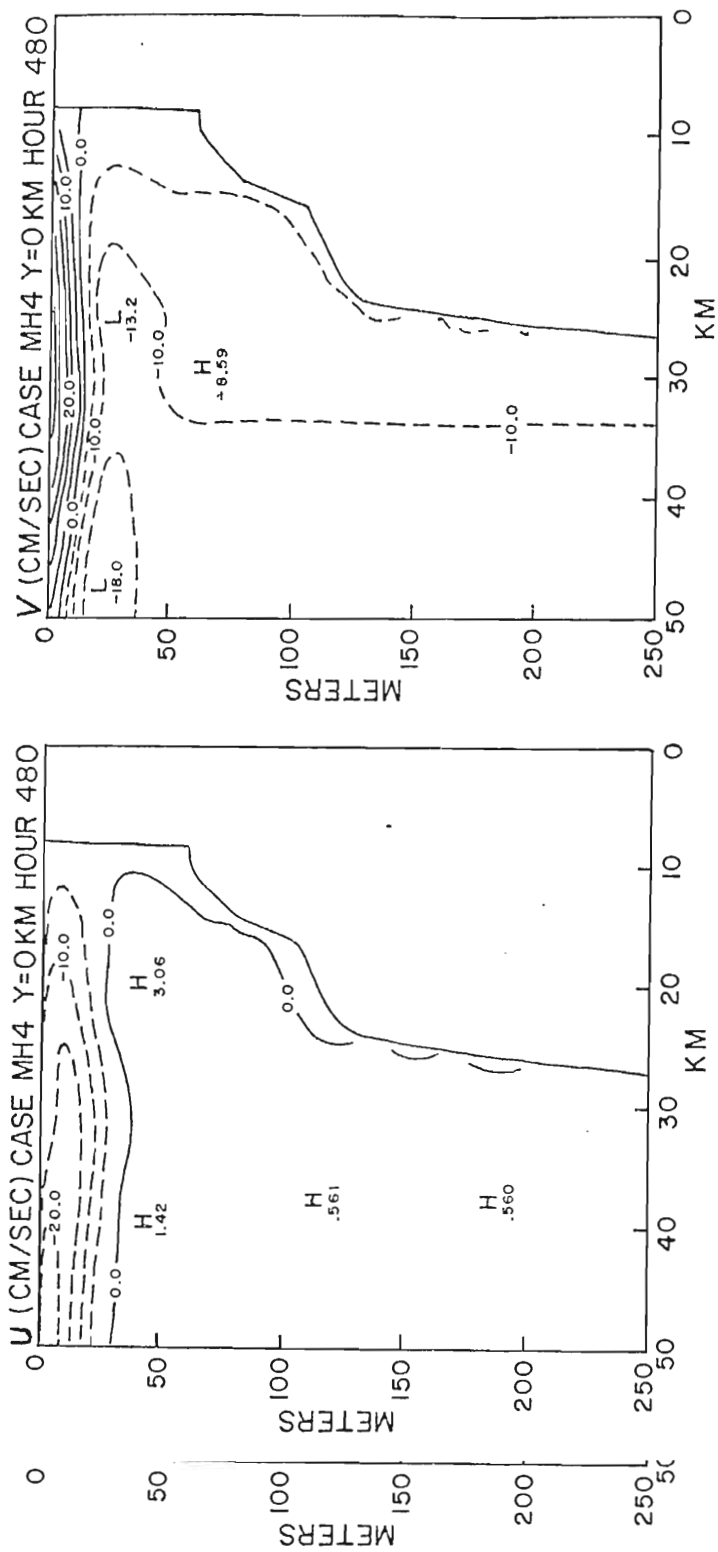
Fig. 26. Longshore (v) and cross-shelf (u) x-z cross-section at y = 0 for model day 20. Contour intour intervals are 5 cm/sec and dashed contours represent negative values.
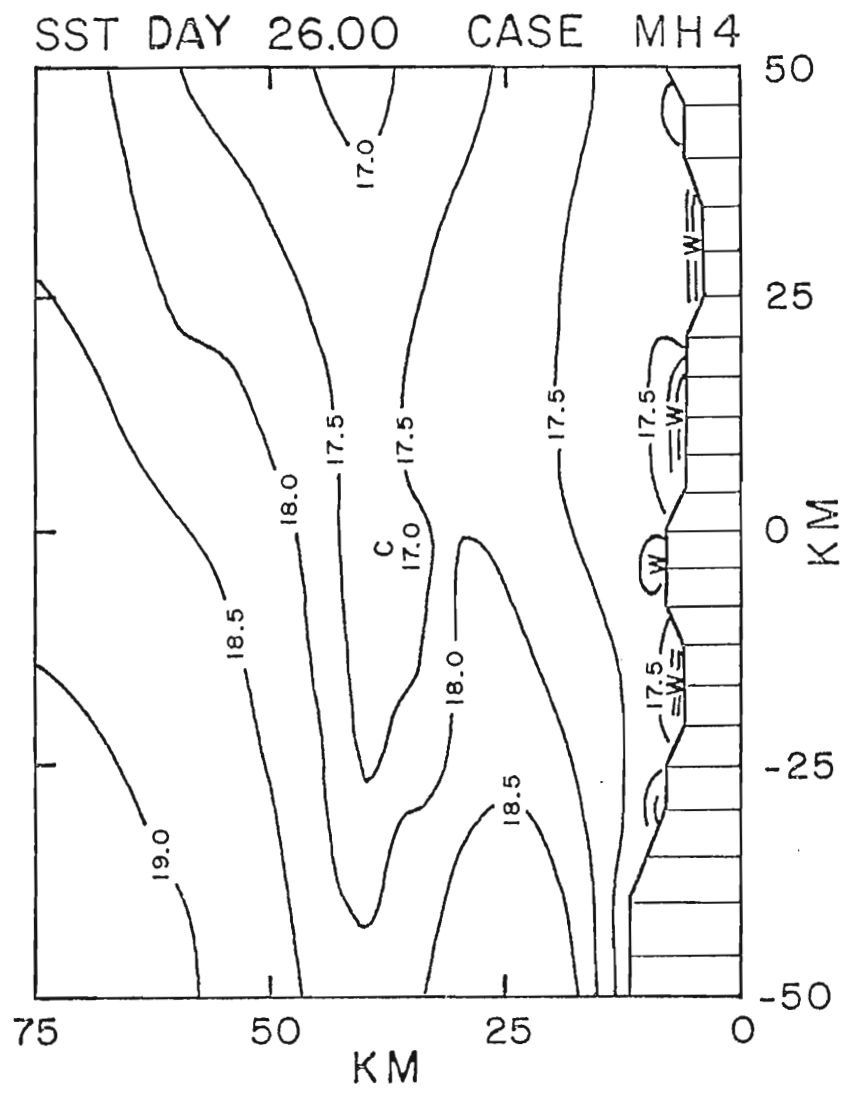
Fig. 27. SST for day 26.
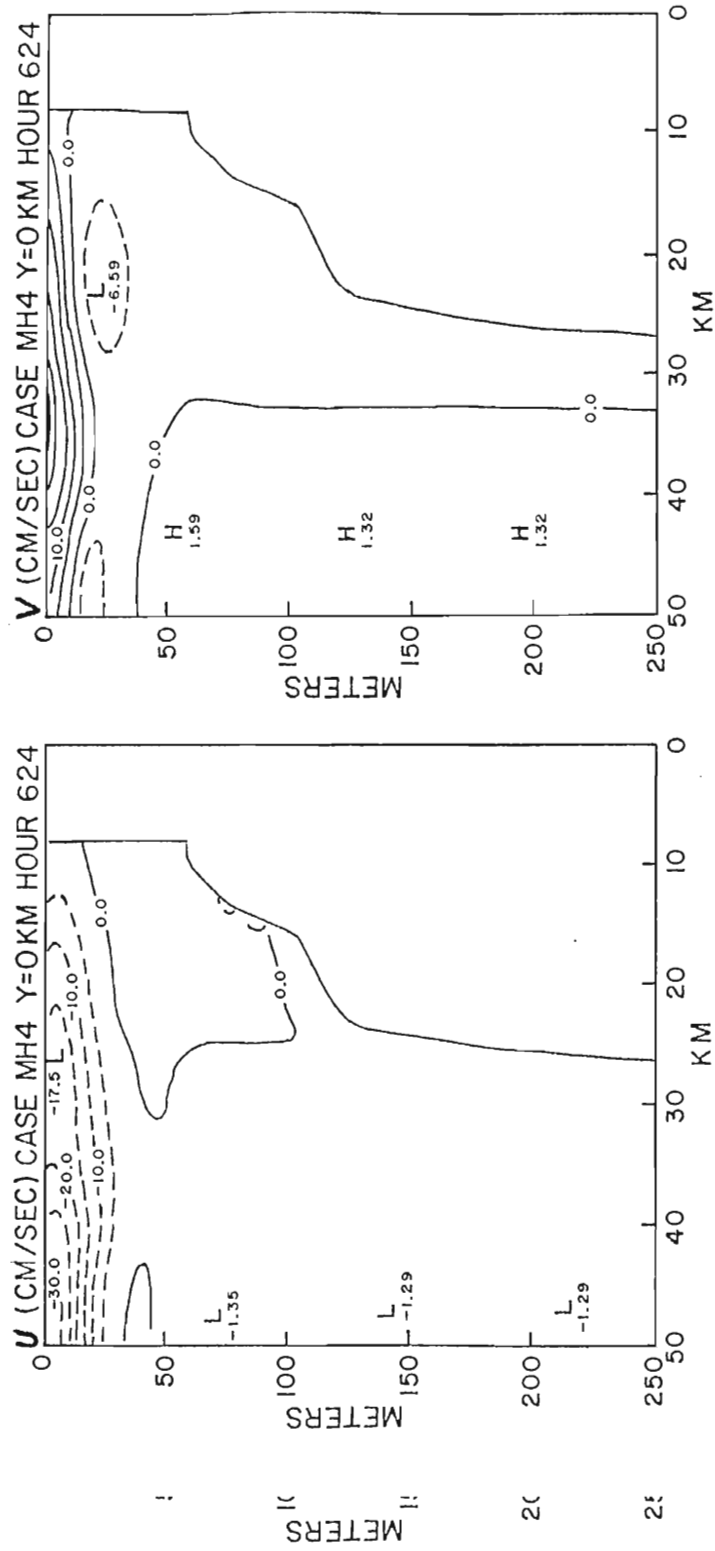
Fig. 28. Cross-shelf (x-z) sections of longshore (v) and cross-shelf (u) velocity components for model day 26.
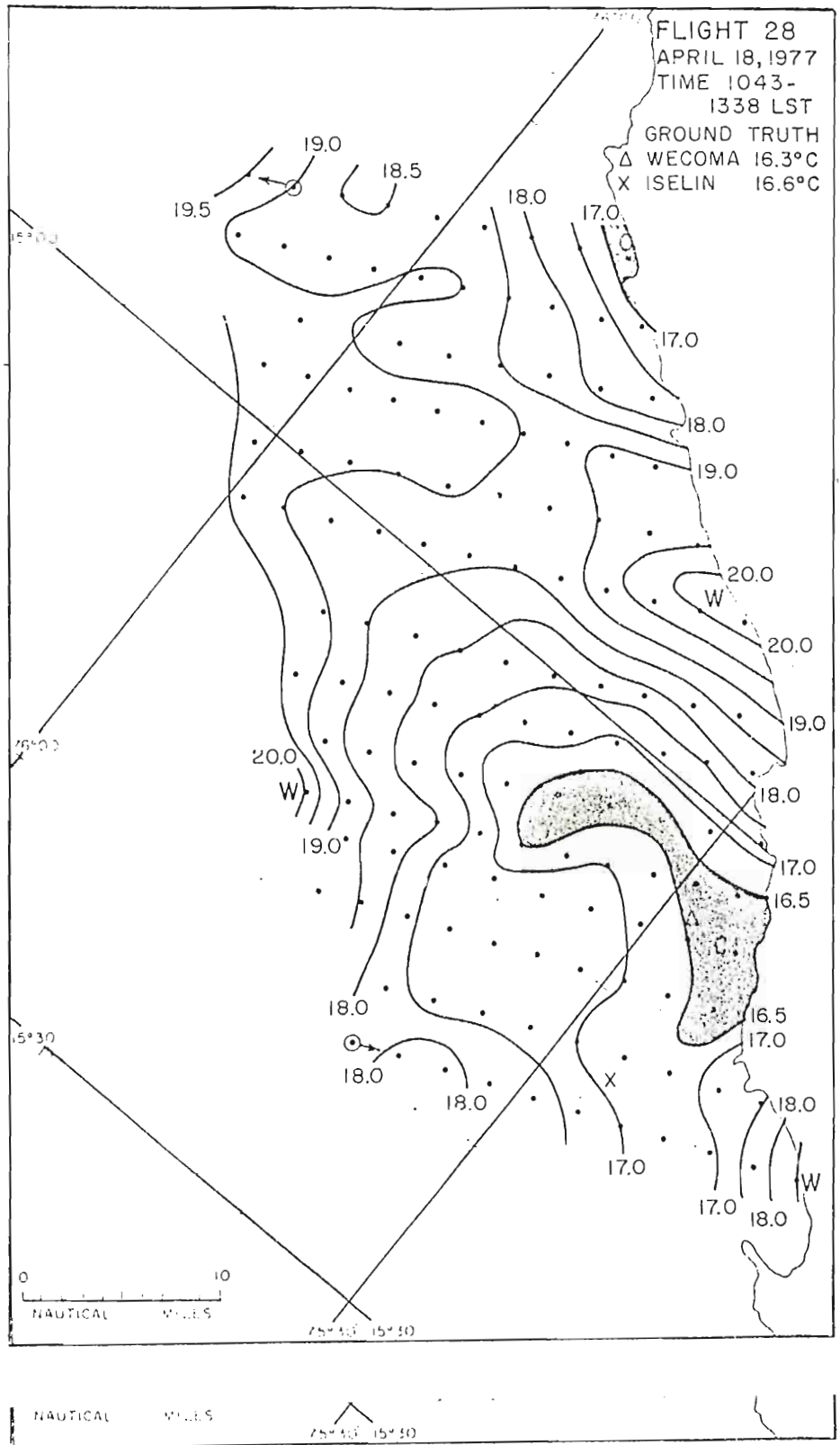
Fig. 29. Sea surface Temperature (SST) for 18 April 1977 from Stuart and Bates, 1977.
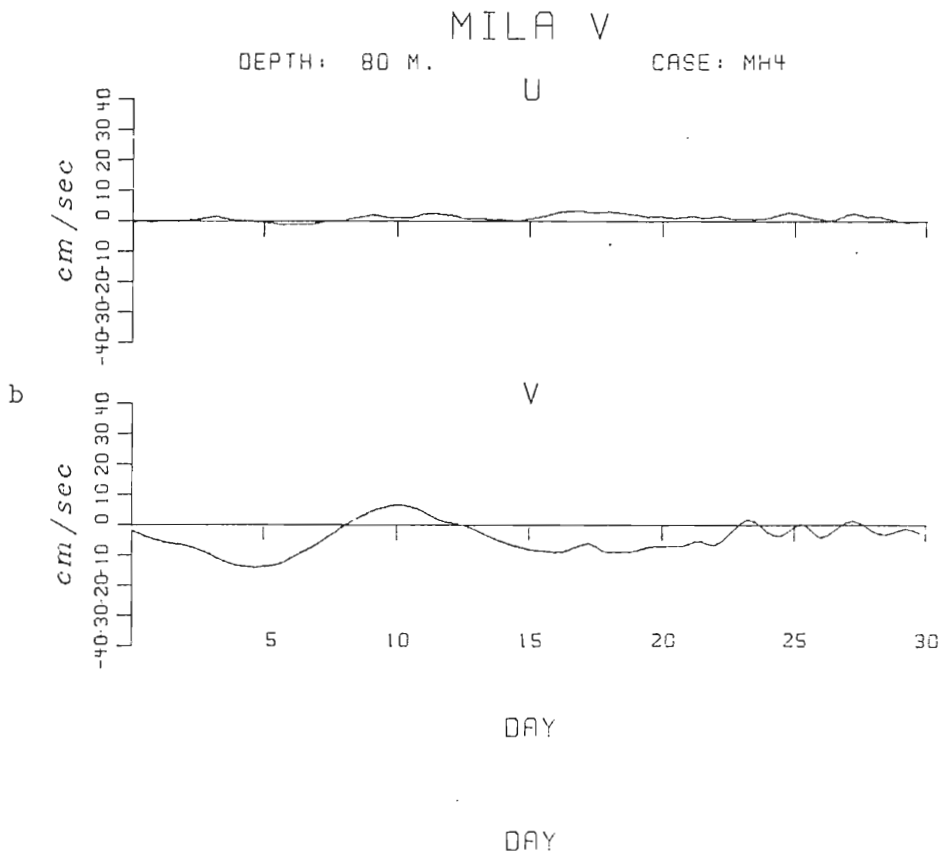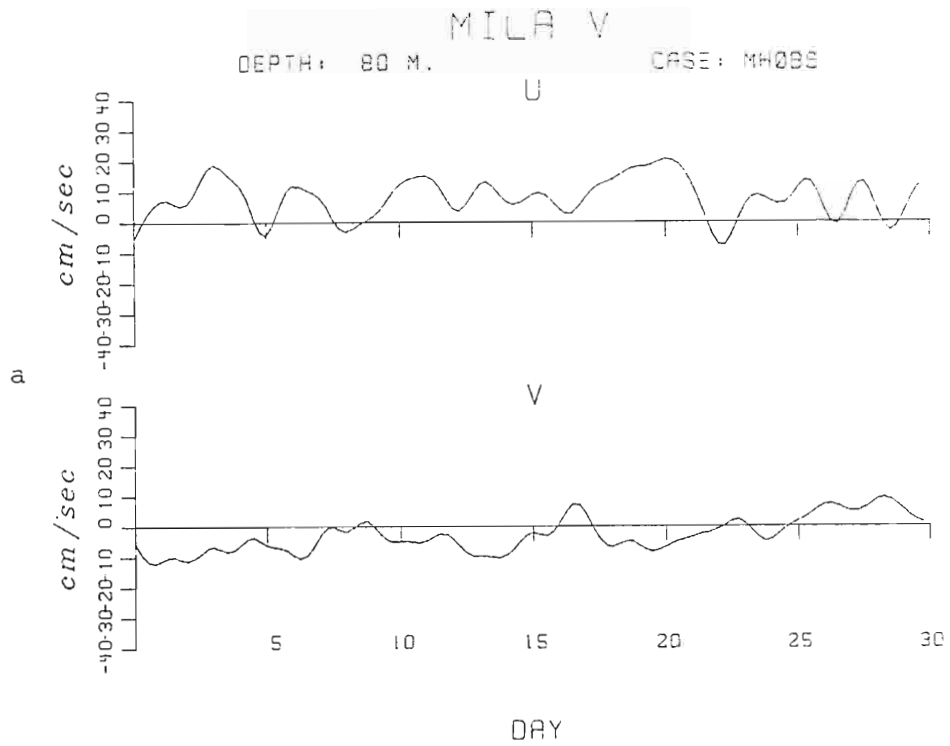
Fig. 30. Time series of Longshore (v) and cross-shelf (u)
velocity components a) observed data, b) model data.

PS

DEPTH: 12 M.   CASE: MHØES

U

V

DAY

PS

DEPTH: 12 M.   CASE: MH4

U

V

DAY

DAY
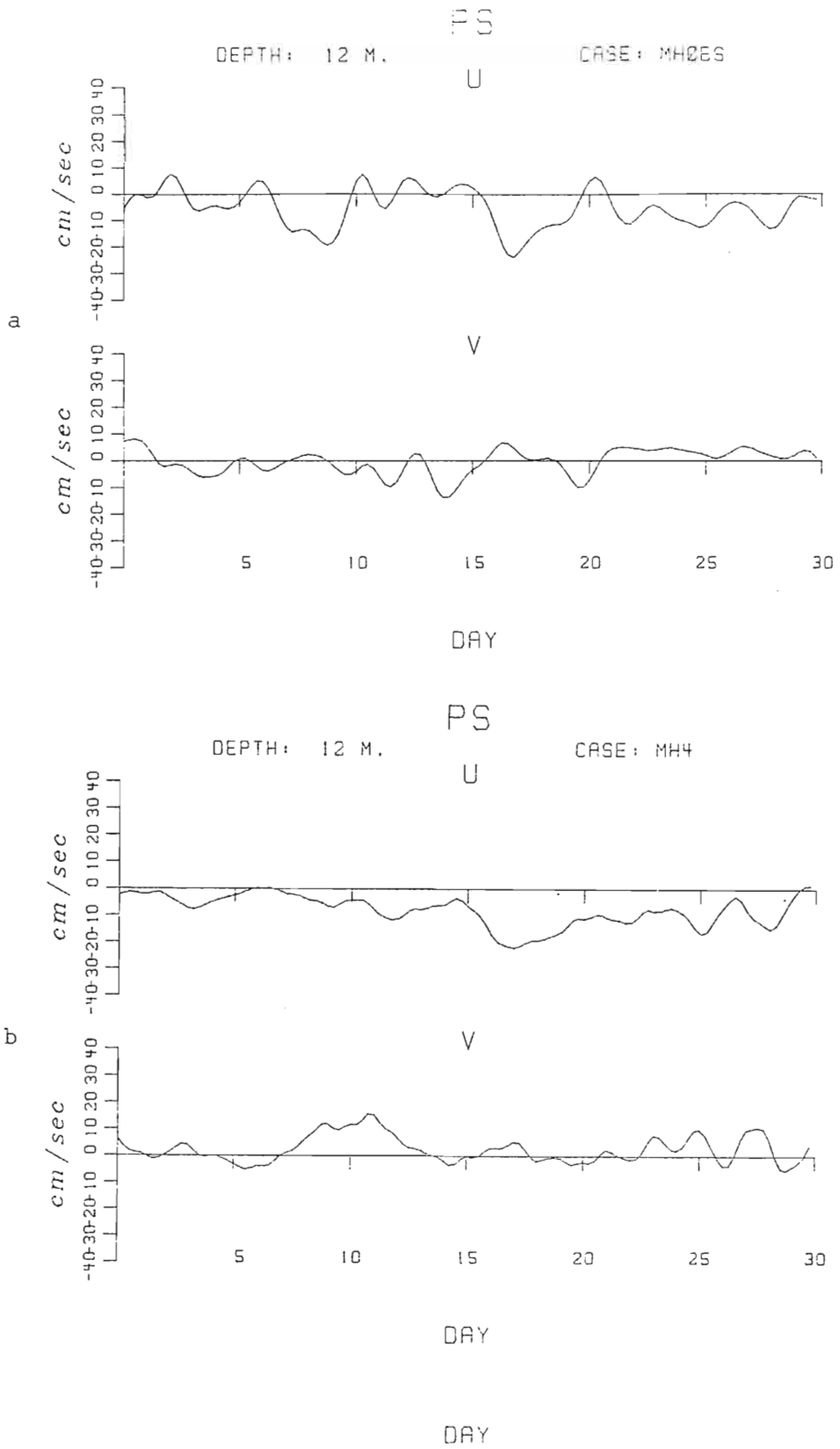
Fig. 31.   Same as fig. 30.

using VACM current meters and the MILA V mooring is a deep depth
mooring using Aanderaa current meters.

In the longshore component (v) for the MILA V 80M current meter,
we see that the long period (approximately 10 days) fluctuations
(those induced by the parameterization scheme) are fairly well repro-
duced. For the Kelvin wave forcing, we would expect the cross-shelf
component (u) to be close to zero which is what we see in the model
data for the lower layer (MILA V 80M). After one look at the MILA V
80M u-component observations and the higher frequency fluctuations in
the v-component, it becomes painfully obvious that there is some other
forcing mechanisms present which the model does not take into account.

Next, we will consider the comparison in the upper layer (PS 12M).
The fluctuation in both the u- and v-components from the model data
in the upper layer show a direct correspondence to the applied wind
stress (Fig. 8). Generally, in comparing the model data to the ob-
servations we see good agreement during the periods of strong wind
stress forcing. Next, if we examine the point of departure between
model data and the observations in the cross-shelf component for the
upper layer (in particular around days 3, 6, 11, 13, 15, 20, 23 and 26)
and compare these to the fluctuations in the observed lower layer
cross-shelf components, we can see a barotropic fluctuation present
in the cross-shelf component. Also, by contrasting the points of
departure between the model data and the observations for both the
upper and lower layer longshore components, we again see a barotropic
oscillation. This suggests that the omitted forcing mechanism is some
upper and lower layer longshore components, we again see a barotropic
oscillation. This suggests that the omitted forcing mechanism is some
sort of barotropic wave form (possibly Continental Shelf waves). This

is an area which will require more study and could possibly lead to an improvement in the parameterization scheme for the externally excited current fluctuations.

One final observation we wish to make concerns the so-called "two-cell" circulation pattern report by Mooers, Collins, and Smith (1976), Johnson and Johnson (1979), and Johnson and Mooers (1980). On day 11 of the model run, we see, in the cross-shelf flow field (Fig. 32), a pattern which resembles the "two-cell" pattern (Fig. 33 from Mooers, Collins, and Smith, 1976). This is a period when the interface is upwarped toward the surface due to the passage of an internal wave crest and when we have equatorward flow (Fig. 32) through the water column in the longshore component. The equatorward flow in the lower layer, which will drive an onshore bottom Ekman layer (Fig. 32) appears to be a necessary requirement for the observation of the "two-cell" pattern. Thus, as Smith (1980) suggests, the "two-cell" circulation pattern is a transient feature which could appear when some mechanism causes an equatorward flow (including an onshore bottom Ekman layer) in the lower layer.
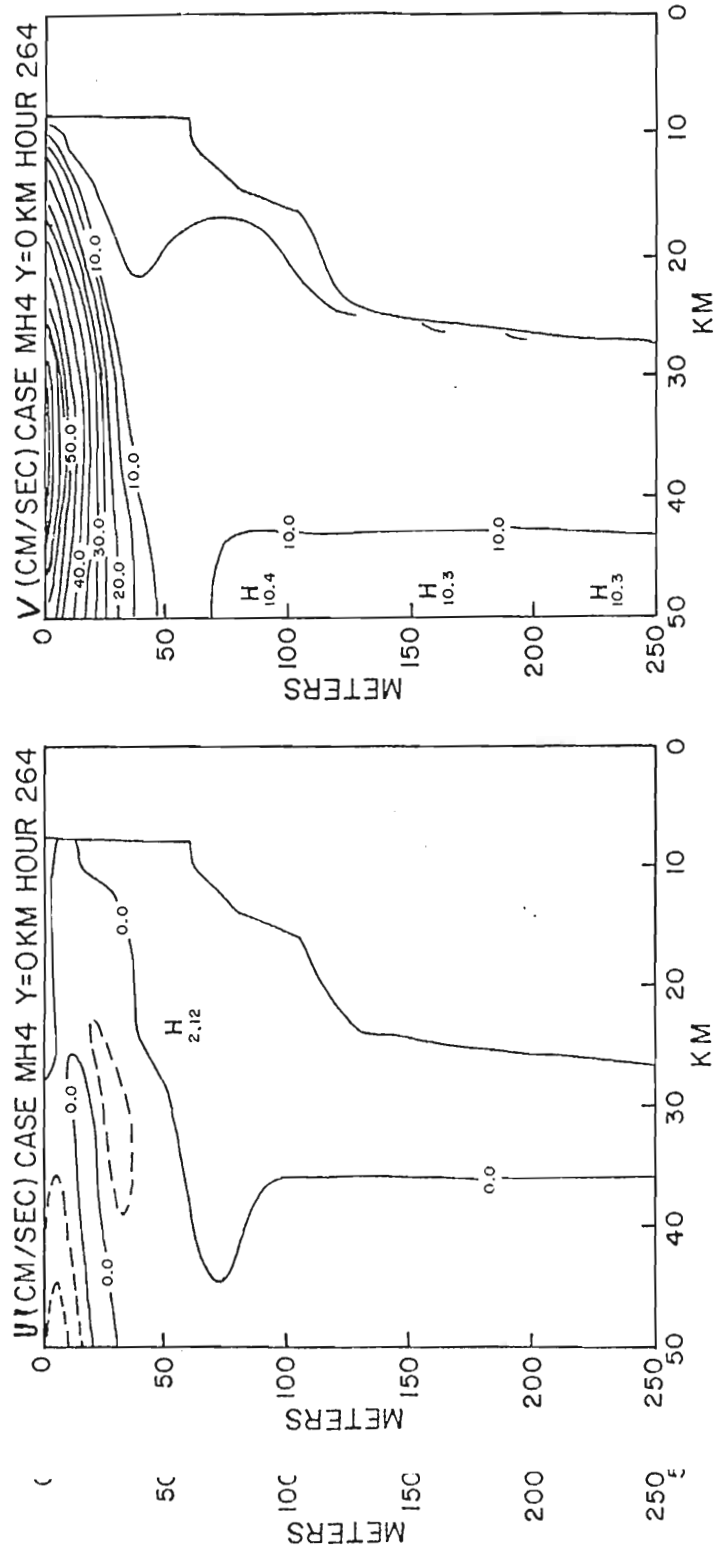
Fig. 32. Cross-shelf (x-z) sections along the C-line (y = 0 in model) of the longshore (v) and cross-shelf (u) velocity components for model day eleven.
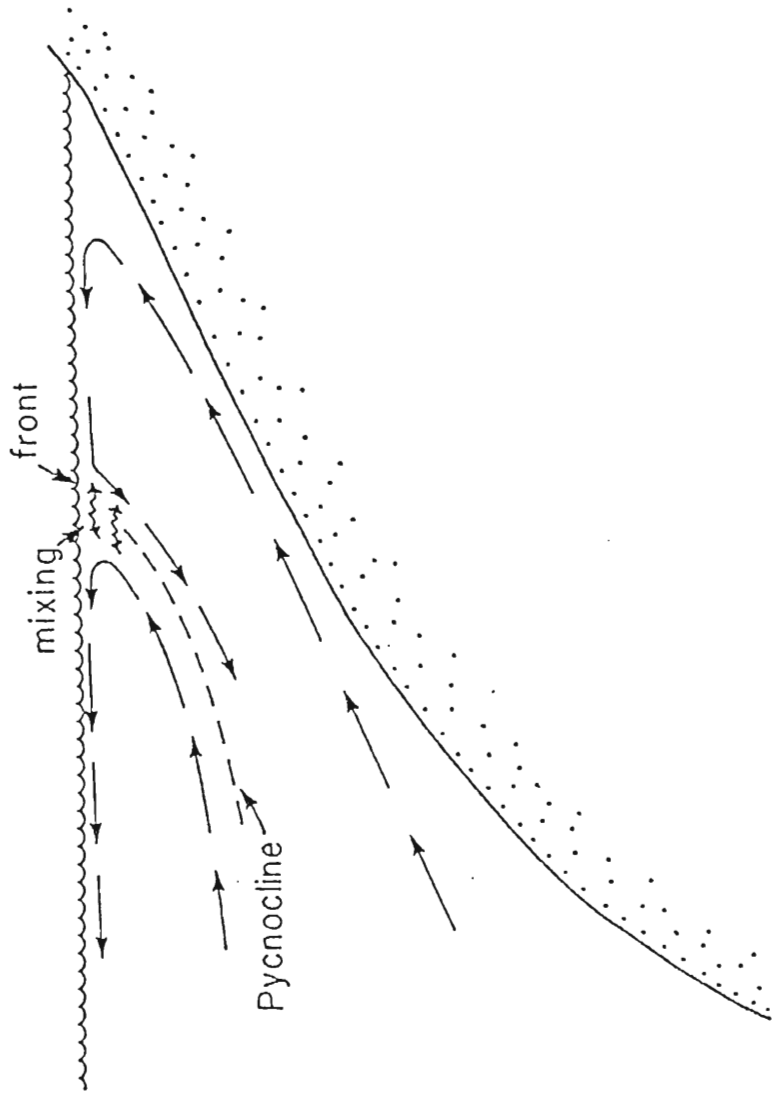
F: Fig. 33.   "Two-cell" upwelling circulation pattern from Mooers, Collins and Smith (1976).

CHAPTER 5

SUMMARY

a. HYDRODYNAMICS MODEL

From this study we can see that the interaction of the under-
currents and bottom topographic features can play a significant role in
determining the locations of the centers of enhanced upwelling.

We have presented a parameterization for the longshore current
fluctuations based on Kelvin wave dynamics which yields realistic
fluctuations and vertical motions.

It is easy to see that the Peruvian upwelling system is very com-
plex but that the primary causes of the upwelling and its variability
are the wind stress and the propagation of Kelvin waves through the
region. Also, the principal of conservation of potential vorti-
city is important in determination of horizontal structure of the
lower layer velocity components and interface displacement.

One severe limitation to the hydrodynamic models is the surfacing
of the interface which limits the length of the time which can be
simulated. Another limitation is the inability to predict sea surface
temperatures which limits the capability for direct comparisons of
model results to more traditional indicators of upwelling.

b. THERMODYNAMIC MODEL.

b. THERMODYNAMIC MODEL.

In this part of the study we have introduced a fluctuating

117

longshore undercurrent into a three-dimensional upwelling model. Furthermore, we have, for the first time, included thermodynamics and mixing into a three-dimensional upwelling model.

In the first part of the study, the hydrodynamic version, it was shown that the interaction of the undercurrent and bottom topography could play a significant role in determining the location of the centers of enhanced upwelling as indicated by the interface displacement. In the second stage, by introducing thermodynamics and interfacial mixing, we have extended the results of the hydrodynamic models. One of the primary benefits of the addition of the mixing parameterization was to permit longer integration periods for the thermodynamic model. We found that one-dimensional wind mixing alone, in an environment which includes horizontal advection of upper layer thickness and fluctuating wind stress magnitude, cannot prevent the surfacing of the interface in a two layer model with a Quasi-Lagrangian vertical coordinate. This was successfully overcome in the present model by switching to an Eulerian vertical coordinate at a predetermined minimum upper layer thickness. The results of this model have shown that the features indicated by the pycnocline height anomally field in the hydrodynamic model can also be observed in the sea surface temperature fields in the thermodynamic model. We have also seen that a positive heat flux was necessary to recover the observed horizontal structure. Without heating we saw that the large scale, wind induced upwelling masked the smaller scale features which

scale, wind induced upwelling masked the smaller scale features which

resulted from the interaction of the propagating internal waves and the bottom topography.

Another important result of this model is, as we have seen, that simple Kelvin wave forcing is not adequate to explain the fluctuations in the cross-shelf component of the undercurrent. The parameterization scheme for the longshore current fluctuations based on Kelvin wave dynamics was evaluated by comparing time series of current meter observations to simulated current meter data derived from the thermodynamic model. It was easy to see that, while the parameterization was a major step in the right directions in simulating the externally forced current fluctuations, it is not the total answer. The parameterization scheme must be revised to include other types of coastal trapped waves (e.g., Continental Shelf waves, Topographic Rossby waves, etc.) besides Kelvin waves.

The aim of this model was to tie together the various aspects of the previous numerical models developed by the Mesoscale Air/Sea Interaction Group at Florida State University in support of the Coastal Upwelling Ecosystem Analysis project. This was a first attempt at using a three-dimensional thermodynamics upwelling model with realistic topography and external forcing, and comparing the results to observational data. While this model has achieved a high degree of qualitative agreement with the observations, it has also pointed out areas of needed improvement. One particular area which must be improved before we can expect to see better quantitative

must be improved before we can expect to see better quantitative

agreement is in the model initialization. As we know from atmospheric modelling experience, accurate initialization of numerical models is a critical requirement for accurate predictability, and has been the study of considerable research. However, unlike his atmospheric counterpart, the ocean modeller does not have a dense synoptic data network available from which he can develop objectively balanced initial states. In the area of oceanic data collection, the JOINT II region is considered to be a heavily sampled area but one current meter array with ten moorings within the model region and airborn SST measurement which cover less than one tenth of the model area are not sufficient to derive an initial state with much more than a guess. Due to the cost of obtaining oceanic data, there will, in the foreseeable future, never be enough data to initialize oceanic models accurately. Thus, alternative methods must be derived for initialization, if we hope to achieve reasonable quantitative predictability in future oceanic models.

APPENDIX A

Numerical Formulation

The numerical formulation for this model has evolved from the previous upwelling models developed by the Mesoscale Air/Sea Interaction Group. O'Brien and Hurlburt (1972) introduced a highly efficient semi-implicit scheme into the upwelling model. This scheme allows a larger maximum time step than the ordinary Courant-Friedrich-Lewy (CFL) condition by treating the terms in the equation which govern the external and internal gravity wave modes (the fastest moving waves) with an implicit time differencing scheme and the remaining terms with an explicit scheme. From this treatment a set of coupled Helmholtz equations for the vertically integrated cross-shelf flow, u_1 and u_2, can be obtained. This set of equations can then be solved iteratively using the tridiagonal variant of Gaussian elimination.

Thompson (1974) introduced and thoroughly tested the discretely telescoping grid used in the x-direction in the model. He found considerable saving in computer time by using this technique versus a fine mesh grid over the entire basin. Also he found less than one percent difference between the two solutions in the upwelling region.

Hurlburt (1974) extended the model to three dimensions and included a variable coastline geometry. The irregular basin geometry limited the effectiveness of using the semi-implicit technique in both horizontal directions in that the advantage gained by using a large the effectiveness of using the semi-implicit technique in both horizontal directions in that the advantage gained by using a large time step was negated by the necessity of using relaxation methods to

solve the coupled two-dimensional Helmholtz equations. Thus Hurlburt used the semi-implicit technique in the x-direction and an explicit method in the y-direction.

To reduce the number of grid points, he used the discretely varying grid in the x-direction and an analytical stretched variable grid in the y-direction. The stretching function used is given by

$$S(a) = c[\alpha a + \sum_{k=1}^{N} \tanh\left(\frac{a-a_k}{\gamma_k}\right) + b \tag{83}$$

where $S(0) = 0$ and $S(1) = 1$ and

$$b = \sum_{k=1}^{N} \tanh\left(\frac{a_k}{\gamma_k}\right) \tag{84}$$

$$c = [\alpha + b + \sum_{k=1}^{N} \tanh\left(\frac{1-a_k}{\gamma_k}\right)]^{-1} \quad . \tag{85}$$

The variables α and γ_k are stretching parameters which can be varied to give the desired variable resolution . Now if we let $q = q(S(a(y)))$ be any dependent variable and normalize, a, by the basin width, $a = y/L_y$, then we find the first and second derivatives in y are given by

$$\frac{dq}{dy} = \frac{1}{L_y} \frac{ds}{da} \frac{dq}{ds} \tag{86}$$

and

$$\frac{d^2q}{dy^2} = \frac{1}{(L_y)^2} \left(\frac{dS}{da}\right)^2 \frac{d^2q}{dS^2} + \frac{1}{(L_y)^2} \frac{d^2S}{da^2} \left(\frac{dq}{dS}\right) \quad . \tag{87}$$

Because of the explicit treatment in the y-direction, the most severe constraint on the maximum allowable time step is given by the linear CFL stability condition;

$$\Delta t \leq MIN\Delta y/[g \cdot MAX \ (H_1 + H_2)]^{1/2} \quad . \tag{88}$$

The diffusive terms are treated implicitly in the x-direction
$$\Delta t \leq MIN\Delta y/[g \cdot MAX \ (H_1 + H_2)]^{1/2} \quad . \tag{88}$$

The diffusive terms are treated implicitly in the x-direction using the Crank-Nicholson (1947) scheme, while the other frictional

terms are lagged in time. Leapfrog time differencing is used for the Coriolis and nonlinear terms. The advection terms are approximated using Scheme F from Grammeltvedt (1969).

REFERENCES

Adamec, D., and J. J. O'Brien, 1978: The seasonal upwelling in the Gulf of Guinea due to remote forcing, J. Phys. Oceanogr., 8, 1050-1060.

Allen, J. S., 1973: Upwelling and coastal jets in a continuously stratified ocean, J. Phys. Oceanogr., 3, 245-257.

Badan-Dangon, A., 1978: Principal components of the velocity field off Northwest Africa, paper presented at the Symposium on the Canary Current: Upwelling and Living Resources, International Council for the Exploration of the Sea, Las Palmas, Canary Islands.

Brink, K. H., J. S. Allen and R. L. Smith, 1978: A study of low frequency fluctuations near the Peru coast, J. Phys. Oceanogr., 8, 1025-1041.

Brink, K. H., W. E. Gilbert and A. Huyer, 1979: Temperature sections along the C-line over the shelf off Cabo Nazca, Peru, from moored current meters, 18 March - 10 May, 1977 and CTD observations, 5 March - 15 May, 1977, CUEA Tech. Rept. 49, 78 pp., School of Oceanography, Oregon State University, Corvallis, Oregon.

Brink, K. H., B. H. Jones, J. VanLeer, C. N. K. Mooers, D. Stuart, M. Stevenson, R. C. Dugdale and G. W. Heburn, 1980: Physical and biological structure and variability in an upwelling center off Peru near 15°S during March 1977, to appear in IDOE International Symposium on Coastal Upwelling.

Brink, K. H., R. L. Smith and D. Halpern, 1978: A compendium of time series measurements from moored instrumentation during the MAM '77 phase of JOINT - II, CUEA Technical Report 45, School of Oceanography, Oregon State University, 72 pp.

Charney, J. G., 1955: The generation of oceanic currents by wind, J. Marine Res., 14, 477-498.

Clancy, R. M., J. D. Thompson, H. E. Hurlburt and J. D. Lee, 1979: A model of mesoscale air-sea interaction in a sea breeze-coastal upwelling regime, Monthly Weather Review, 107, 1476-1505.

Clancy, R. M., J. D. Thompson, H. E. Hurlburt and J. D. Lee, 1979: A model of mesoscale air-sea interaction in a sea breeze-coastal upwelling regime, Monthly Weather Review, 107, 1476-1505.

Crank, J., and P. Nicholson, 1947: A practical method for numerical evaluation of solutions of partial differential equations of heat-conduction type, Proc. Camb. Philos. Soc., 43, 50-67.

Denman, K. L., and M. Miyake, 1973: Upper layer modification at ocean station PAPA: Observation and simulation, J. Phys. Oceanogr., 3, 185-196.

Denman, K. L., 1973: A time-dependent model of the upper ocean. J. Phys. Oceanogr., 3, 173-184.

deSzoeke, R. A., and P. B. Rhines, 1976: Asymptotic regimes in mixed layer deepening, J. Mar. Res., 34, 111-116.

Ekman, V. W., 1905: On the influence of the earth's rotation on ocean currents, Arkiv. Mat. Astron. Fysik, 12, 1-52. (Reprinted in Royal Swedish Acad. of Sci., 1963)

Garvine, R. W., 1971: A simple model of coastal upwelling dynamics, J. Phys. Oceanogr., 1, 169-179.

Gill, A. E., and A. J. Clarke, 1974: Wind-induced upwelling, coastal currents and sea-level changes, Deep Sea Res., 21, 325-345.

Grammeltvedt, A., 1969: A survey of finite-difference schemes for the primitive equations for a barotropic fluid, Mon. Wea. Rev., 97, 384-404.

Greenspan, H. P., 1968: The theory of rotating fluids. Cambridge Monographs on Mechanics and Applied Mathematics, Cambridge University Press, 327 pp.

Hartline, B. K., 1980: Coastal upwelling: Physical factors feed fish, Science, 208, 38-40.

Heburn, G. W., and J. J. O'Brien, 1980: Numerical study of the influence of longshore current fluctuations on coastal upwelling off Peru, (to be submitted to J. Phys. Oceanogr.)

Hidaka, K., 1954: A contribution to the theory of upwelling and coastal currents. Trans. Amer. Geophys. Union, 35, 431-444.

Hoover, S. T., 1980: Mixed layer variability in the upwelling region off Peru - March 1977, M.S. Thesis, University of Delaware, pp. 115.

Hurlburt, H. E., 1974: The influence of coastline geometry and bottom topography on the eastern ocean circulation, Ph.D. Dissertation, Florida State University, Tallahassee, pp. 103.

Hurlburt, H. E., J. C. Kindle, and J. J. O'Brien, 1976: A numerical simulation of the onset of El Niño, J. Phys. Oceanogr., 6, 621-631.

Hurlburt, H. E., and J. D. Thompson, 1973: Coastal upwelling on a
Hurlburt, H. E., J. C. Kindle, and J. J. O'Brien, 1976: A numerical simulation of the onset of El Niño, J. Phys. Oceanogr., 6, 621-631.

Hurlburt, H. E., and J. D. Thompson, 1973: Coastal upwelling on a β-plane, J. Phys. Oceanogr., 3, 16-32.

Huyer, A., R. L. Smith and E. J. C. Sobey, 1978: Seasonal differences in low-frequency current fluctuations over the Oregon continental shelf, J. Geophys. Res., 83, 5071-5089.

Johnson, D. R., and W. R. Johnson, 1979: Vertical and cross-shelf flow in the coastal upwelling region off Oregon, Deep-Sea Res., 26, 399-408.

Johnson, D. R., and C. N. K. Mooers, 1979: Double-cell circulation during coastal upwelling, submitted to Deep-Sea Res.

Kato, H., and O. M. Phillips, 1969: On the penetration of a turbulent layer into a stratified fluid, J. Fluid Mech., 37, 643-655.

Kindle, J. C., 1979: Equatorial Pacific Ocean variability -- seasonal and El Niño time scales, Ph.D. dissertation, Florida State University, 134 pp.

Kindle, J. C., and J. J. O'Brien, 1974: On upwelling along a zonally-orientated coastline, J. Phys. Oceanogr., 4, 125-130.

Kraus, E., and J. S. Turner, 1967: A one-dimensional model of the seasonal thermocline II. The general theory and its consequences, Tellus, 19, 98-106.

Kwizak, M., and A. Robert, 1971: A semi-implicit scheme for grid point atmospheric models of the primitive equations, Mon. Wea. Rev., 99, 32-36.

Martin, P. M., and J. D. Thompson, 1977: Formulation and testing of a layer-compatible upper ocean mixed-layer model, (submitted to J. Phys. Oceanogr.)

McCreary, J., 1976: Eastern tropical response to changing wind systems: with application to El Niño, J. Phys. Oceanogr., 6, 632-645.

Mellor, G. L., and T. Yamada, 1974: A hierarchy of turbulence closure models for planetary boundary layers, J. Atmos. Sci., 31, 1791-1806.

Mittelstaedt, E., R. D. Pillsbury and R. L. Smith, 1975: Flow patterns in the Northwest African upwelling area, Deutchen Hydrographischem Zeitschrift, 28, 145-167.

Moody, G. L., 1979: Aircraft derived low level winds and upwelling off the Peruvian coast during March, April and May, 1977, CUEA Technical Report 56, Department of Meteorology, Florida State University, Tallahassee, Florida, 110 pp.

Mooers, C. N. K., C. A. Collins, and R. L. Smith, 1976: The dynamic structure of the frontal zone in the coastal upwelling region off Oregon, J. Phys. Oceanogr., 6, 3-21.

Moore, D. W., 1968: Planetary-gravity waves in an equatorial ocean, Ph.D. Thesis, Harvard University.

Moore, D. W., and S. G. H. Philander, 1977: Modeling of the tropical oceanic circulation, The Sea, Vol. 6, E. Goldberg, et al., Eds., Wiley-Interscience, 319-361.

Niiler, P. P., 1975: Deepening of the wind-mixed layer, J. Mar. Res., 33, 405-422.

O'Brien, J. J., R. M. Clancy, A. J. Clarke, M. Crepon, R. Elsberry, T. Gammelsrød, M. MacVean, L. P. Røed and J. D. Thompson, 1977: Upwelling in the ocean: Two and three-dimensional models of upper ocean dynamics and variability. Modelling and prediction of the upper layers of the ocean, Ed. by E. Kraus, Pergamon Press, New York, 178-228.

O'Brien, J. J., G. W. Heburn, M. Peffley, R. Preller and J. D. Thompson, 1980: Peru upwelling models, Chapter 7 section 7.1 in Productivity of upwelling ecosystems M. E. Vinogradov and R. T. Barber, Editors (in press).

O'Brien, J. J., and H. E. Hurlburt, 1972: A numerical model of coastal upwelling. J. Phys. Oceanogr., 2, 14-26.

O'Brien, J. J., R. L. Smith and G. W. Heburn, 1980: Determination of vertical velocity on the continental shelf, (to be submitted to J. Phys. Oceanogr.)

Pedlosky, J., 1974: On coastal jets and upwelling in bounded basins, J. Phys. Oceanogr., 4, 3-18.

Pedlosky, J., 1978a: An inertial model of steady coastal upwelling, J. Phys. Oceanogr., 8, 171-177.

Pedlosky, J., 1978b: A nonlinear model of the onset of upwelling, J. Phys. Oceanogr., 8, 178-187.

Pedlosky, J., 1979: Geophysical Fluid Dynamics, Springer-Verlag, New York, N. Y., 624 pp.

Peffley, M., and J. J. O'Brien, 1976: A three-dimensional simulation of coastal upwelling off Oregon, J. Phys. Oceanogr., 6, 164-180.

Pietrafesa, L., 1973: Steady baroclinic circulation on a continental
Peffley, M., and J. J. O'Brien, 1976: A three-dimensional simulation of coastal upwelling off Oregon, J. Phys. Oceanogr., 6, 164-180.

Pietrafesa, L., 1973: Steady baroclinic circulation on a continental shelf, Ph.D. Dissertation, University of Washington, Seattle.

Pollard, R. T., and R. C. Millard, 1970: Comparison between observed and simulated wind generated inertial oscillations, Deep Sea Res., 17, 813-821.

Pollard, R. T., P. B. Rhines and R. O. R. Y. Thompson, 1973: The deepening of the wind-mixed layer, J. Geophys. Fluid Mech., 4, 381-404.

Preller, R., and J. J. O'Brien, 1977: Peruvian bottom topography and coastline map, available from Mesoscale Air-Sea Interaction Group, Florida State University, Tallahassee, Florida, 80 pp.

Preller, R., and J. J. O'Brien, 1980: The influence of bottom topography on upwelling off Peru, J. Phys. Oceanogr., (in press).

Rhines, R., 1970: Edge-, bottom-, and Rossby waves in a rotating, stratified fluid, Geophys. Fluid Dyn., 1, 273-302.

Ryther, J. H., 1969: Photosynthesis and fish production in the sea, Science, 166, 72-76.

Saito, Y., 1956: The theory of the transient state concerning upwelling and coastal current, Trans. Amer. Geophys. Union, 37, 38-42.

Smith, R. L., 1968: Upwelling, Oceanogr. Mar. Biol. Ann. Rev., 6, 11-47.

Smith, R. L., 1974: A description of current, wind, and sea level variations during coastal upwelling off the Oregon coast, July - August, 1972, J. Geophys. Res., 79, 435-443.

Smith, R. L., 1978: Poleward propagating perturbations in currents and sea level along the Peru coast, J. Geophys. Res., 83, 6083-6092.

Smith, R. L., 1980: A comparison of the structure and variability of the flow field in the three coastal upwelling regions: Oregon, Northwest Africa and Peru, submitted to IDOE International Symposium on Coastal Upwelling.

Spiegel, E. A., and G. Veronis, 1960: On the Boussinesq approximation for a compressible fluid, J. Astrophys., 131, 442-447.

Stevenson, M. R., D. W. Stuart and G. W. Heburn, 1980: Short term variations observed in the circulation, heat content and surface mixed layer of an upwelling plume off Cabo Nazca, Peru, submitted to IDOE International Symposium on Coastal Upwelling.

Stuart, D. W., and J. J. Bates, 1977: Aircraft sea surface temperature mixed layer of an upwelling plume off Cabo Nazca, Peru, submitted to IDOE International Symposium on Coastal Upwelling.

Stuart, D. W., and J. J. Bates, 1977: Aircraft sea surface temperature data - JOINT II 1977, CUEA Data Report 42, Department of Meteorology, Florida State University, Tallahassee, Florida, 39 pp.

Suginohara, N., 1980: Quasigeostrophic waves in a stratified ocean with bottom topography, (submitted to J. Phys. Oceanogr.)

Sverdrup, H. U., 1938: On the processes of upwelling, J. Mar. Res., 1(2), 155-164.

Sverdrup, H. U., and R. H. Fleming, 1941: The water off the coast of southern California, Bulletin Scripps Inst. Oceanogr., 4, 261-378.

Thompson, J. D., 1974: The coastal upwelling cycle on a Beta-plane: Hydrodynamic and thermodynamics. Tech. Report, Mesoscale Air-Sea Interaction Group, Florida State University, 141 pages.

Thompson, J. D., 1978: Role of mixing in the dynamics of upwelling systems, Upwelling Ecosystems, Ed. M. Tomczak and F. Boje, Springer-Verlag, New York, 203-221.

Thompson, J. D., and J. J. O'Brien, 1973: Time-dependent coastal upwelling, J. Phys. Oceanogr., 3, 33-46.

Thorade, H., 1909: Die Kalifornischen Meeresströmungen, Ann. Hydrogr. Bul., 37, 17-34, 63-76.

Turner, J. S., 1973: Buoyancy effects in fluids, Cambridge monographs on mechanics and applied mathematics, Cambridge Univ. Press, 367 pp.

Wang, D-P, and C. N. K. Mooers, 1976: Coastal-trapped waves in a continuously stratified ocean, J. Phys. Oceanogr., 6, 853-863.

Watson, A. I., 1978: A study of the low-level mesoscale winds observed off the Peruvian coast during March and April, 1976, CUEA Technical Report 41, Department of Meteorology, Florida State University, Tallahassee, Florida, 120 pp.

Wyrtki, K., 1975: El Niño - the dynamics response of the equatorial Pacific Ocean to atmospheric forcing, J. Phys. Oceanogr., 5, 572-584.

Yoshida, K., 1967: Circulation in the eastern tropical oceans with special references to upwelling and undercurrents, Japan J. Geophys., 4, 1-75.

Zilitinkevich, S. S., D. V. Chalikov, Yu. D. Resnyansky, 1979: Modelling the oceanic upper layer, Oceanol. Acta., 2, 2, 219-240.

VITA

George W. Heburn was born August 27, 1942 in Fort Benning, Georgia. In December, 1965, he graduated with a Bachelor of Aerospace Engineering from the Georgia Institute of Technology, Atlanta, Georgia. He was awarded a Master of Science (with distinction) in Meteorology from the Naval Postgraduate School, Monterey, California in March, 1972. He began his doctoral study in the Department of Meteorology at Florida State University in the fall of 1976.